Energy Efficiency of Electric Vehicles and Recharging Technologies under Consideration of Usage Profiles

by

Guido Wager

MSc

THE UNIVERSITY OF WESTERN AUSTRALIA

This thesis is presented for the degree of

Doctor of Philosophy

of

The University of Western Australia

School of Electrical, Electronic and Computer Engineering

August 2017

DECLARATION FOR THESIS CONTAINING PUBLISHED WORK AND/OR WORK PREPARED FOR PUBLICATION

This thesis contains **published work and/or work prepared for publication, which has been co-authored**. The bibliographical details of the work and where it appears in the thesis are outlined below.

Wager G, Bräunl T, Whale J, Performance Evaluation of Regenerative Braking Systems
Proceedings of the Institution of Mechanical Engineers Part D: Journal of Automobile Engineering, accepted and in press (Chapter 3)
The estimated percentage contribution of the candidate is 80%.

Wager G, Bräunl T, Whale J, McHenry M, Enhanced EV and ICE vehicle energy efficiency through drive cycle synchronisation of deferred auxiliary loads, *International Journal of Electric and Hybrid Vehicles*, Volume 6, Issue 3 (2014) pp. 179 –194.
The estimated percentage contribution of the candidate is 80%.

Wager G, Bräunl T, Whale J, Smart Accelerating and Braking Achieving Higher Energy Efficiencies in Electric Vehicles
International Journal of Electric and Hybrid Vehicles, under review, (Chapter 5)
The estimated percentage contribution of the candidate is 80%.

Wager G, Bräunl T, Whale J, Battery cell balance of electric vehicles under fast-DC charging, *International Journal of Electric and Hybrid Vehicles*, Volume 8, Issue 4 (2016) pp. 351 –361 (Chapter 6)
The estimated percentage contribution of the candidate is 80%.

Wager G, Bräunl T, Whale J, Driving electric vehicles at highway speeds: The effect of higher driving speeds on energy consumption and driving range for electric vehicles in Australia, *Renewable and Sustainable Energy Reviews*, Volume 63, 2016, Pages 158-165 (Chapter 7)

The estimated percentage contribution of the candidate is 80%.

Guido Wager		31/08/17
Print Name	Signature	Date
Thomas Braunl		11/08/2017
Print Name	Signature	Date
Jonathan Whale		
Print Name	Signature	Date
Mark P. McHenry		10/8/2017
Print Name	Signature	Date

Abstract

The work performed in this thesis concentrates on studying factors that affect energy efficiencies of electric vehicles (EVs). The studies outlined in the thesis are structured in five sections.

The first study investigates energy recovery on a modified EV driving a typical city stop-and-go scenario. It revealed that by changing the control strategy for large auxiliary loads, such as air conditioner and heaters, sufficient kinetic energy can be recovered and used to maintain comfortable passenger compartment temperature. Implementing this strategy has the potential to increase battery lifespan.

The second study investigates performance tests on regenerative brake system (RBS). The results showed that the energy recovery system increases the driving range. The results further showed that driving an EV with an energy recovery system also reduces brake maintenance cost.

The third study investigates efficient acceleration and deceleration of an EV. The results showed significant improvements in efficiency of the EV through applying high loads to the vehicle. It was also found that under certain high acceleration rates, energy losses increased, which outweighed the benefits of loading an EV motor to its efficient operating regions.

The fourth study investigates the relatively new fast-DC charging technology and how it affects an EV's battery systems. The experiment showed that the vehicle's battery management systems were capable of successfully balancing individual cells and hence, maintaining the batteries' charge capacity. The findings suggest that fast-DC charging technology is a feasible option to allow EVs to travel large distances in a day.

The fifth study furthered investigations on the fast-DC charger by researching how fast-DC charging affects the vehicles' range under high-speed travelling. To simulate higher driving speeds, strong head winds or large auxiliary loads, the various components of traction power demand of the cars' batteries were modelled mathematically and the energy consumption of the cars were calculated to estimate the drivable range at these high speeds and loads. The results show a significantly reduced range under conditions relevant for highway driving and a significant deviation from the driving ranges published by EV manufacturers. To prevent

stranded cars and a possible negative perception of EVs, drivers and charging infrastructure planners need to be aware of how EV energy and recharging demands can significantly change under different loads and driving patterns.

Table of Contents

Acknowledgements

Special thank to Professor Thomas Braunl encouraging me to enrol in the PhD research project, Dr. Jonathan Whale and Adj. Professor David Harries in co-supervising the research and my partner Dr. Evelyne Deplazes for the encouragement and great support.

I would also like to extend my sincere thanks to the following people for their advice

Mark McHenry
John Breen
Mike Turner
Many Palacios
Nick Sergison
Orbital Engine Corporation in Balcatta

I would like to thank EV-Works, the Nissan Motor Company in Welshpool WA and the UWA Facility Management for lending the test vehicles, and the donors of the fast-DC charging station for our experiments. I also would like to thank Orbital Engine Corporation in Balcatta for the use of their chassis dynamometer facilities.

This research was supported by an Australian Government Research Training Program (RTP) Scholarship.

Guido Wager
September 2017

Statement of Candidate Contribution

I, Guido Wager, certify that this thesis is composed of my original work, to the best of my knowledge and belief and contains no material previously published or written by another person except where due reference has been made in the text.

Signature: 

Guido Wager

05. September 2017

Publications Arising from this Thesis

Journal papers

1. Wager G, Bräunl T, Whale J, Performance Evaluation of Regenerative Braking Systems *Proceedings of the Institution of Mechanical Engineers Part D: Journal of Automobile Engineering*, in press

2. Wager G, Bräunl T, Whale J, McHenry M, Enhanced EV and ICE vehicle energy efficiency through drive cycle synchronisation of deferred auxiliary loads, *International Journal of Electric and Hybrid Vehicles*, Volume 6, Issue 3 (2014) pp. 179 –194.

3. Wager G, Bräunl T, Whale J, Smart Accelerating and Braking Achieving Higher Energy Efficiencies in Electric Vehicles
International Journal of Electric and Hybrid Vehicles, under review

4. Wager G, Bräunl T, Whale J, Battery cell balance of electric vehicles under fast-DC charging, *International Journal of Electric and Hybrid Vehicles*, Volume 8, Issue 4 (2016) pp. 351 –361

5. Wager G, Bräunl T, Whale J, Driving electric vehicles at highway speeds: The effect of higher driving speeds on energy consumption and driving range for electric vehicles in Australia, *Renewable and Sustainable Energy Reviews*, Volume 63, 2016, Pages 158-165

List of Figures

List of Tables

List of Symbols

AF	Projected frontal area of the vehicle [m^2]
C_D	Drag coefficient (depends on the vehicle's shape) [-]
C_{RR}	Tyre rolling resistance coefficient (depends on the specific tyres used) [-]
E_{cons}	Energy consumption [Wh]
Ek	Kinetic energy [J]
E_{regen}	Recovered electrical energy [Wh]
g	Physical constant for the gravitational force [m/s^2]
I	Electrical current [A]
m	Vehicle mass [kg]
N	Number of samplings (for a sample rate of 1 second) [-]
P	Power [W]
P_{aux}	Auxiliary energy [W]
$P_{tractive}$	Traction power demand [W]
r	Rotational inertia compensation factor [-]
t_{inc}	Time increment [s]
V	Voltage [V]
V_i	Vehicle velocity at the current y time increment [m/s]
V_{i-1}	Vehicle velocity at the previous time increment [m/s]
η_{dtrain}	Drive train efficiency [%]
η_{regen}	$_{RBS}$ electrical recovery efficiency [%]
θ	Road gradient (degrees from horizontal) [°]
ρ	Density of air [kg/m^3]

Chapter 1

Introduction

1.1 Background

The development of the motor vehicle started more than 100 years ago and had an almost unprecedented impact on our modern world. Our current transportation technology provides freedom for human beings all over the world. Unfortunately, the rapid uptake of motor vehicles has also caused many problems. Some of the main concerns include the dependency on fossil fuels and its inherent economic vulnerability to oil price shocks. A further major impact from operating motor vehicles on fossil fuels is air pollution with its proven negative impact on economy and the wellbeing of the society. Although combustion engines clean-car technology has improved continuously over the years, air quality still needs improvements [1] [2]. The automotive industry offers many different types of electric vehicles (EVs), which have the potential to operate more cost effectively than combustion engine cars and with zero emissions, if the EVs are manufactured and charged using electricity generated from purely renewable energy sources. The shift from generating electricity from fossil fuels towards renewable energy will significantly reduce emissions and dependency on fossil fuels, which reduces the risk of economic vulnerability. Although EV sales numbers are steadily increasing, there are currently very few EVs on the roads. This is due to a number of reasons including relatively high upfront costs, concealed actual ICE vehicle costs, general user sceptics, concerns about limited vehicle drivable range, unawareness of the technology, and the

absence of public charging infrastructure. The research project in this report aimed to address some of these issues and remove barriers currently hindering a rapid EV market uptake.

Transportation and energy supply in our developed world are complex systems and main arteries of our current world economy. A permanent flow is vital and a sudden blockage would affect the economy and human wellbeing.

The invention and subsequent development of the motor vehicle as the main form of transportation may be one of the biggest achievements of modern technology. However, the mass production and rapid uptake of motor vehicles produces side effects, so called negative externalities. A main concern is air pollution caused by the use of fossil fuels, the source of energy in almost all of the estimated one billion motor vehicles currently operating around the world [3]. Another current contentious issue of transport is its heavy dependency of these fossil fuels. Although EVs are a feasible solution to reduce current transport energy issues in the mainstream use, market introduction and adoption of electric vehicles faces many engineering, political, economic, electricity generation and distribution challenges. The studies of this thesis focus solely on the vehicle engineering issues and challenges.

This introduction outlines current transport air pollution issues with its associated damage and costs diffused to society. It briefly outlines energy security risks and then explains how EVs operate and how they have the potential to solve air quality issues and reduce the risk of economic vulnerability to peak oil. It discusses EV mainstream market uptake barriers, in particular the vehicle engineering issues of limited range, efficiency and recharging. It then states how these issues have been identified and researched by the author.

1.2 Air Pollution—a Costly and Potentially Deadly Game

The majority of the current 7.5 billion people on the planet live in large cities. Figure 1-1 shows an overview of the current situation. It shows the world's largest cities with populations over 10 million. In such large cities, the demand for transport has led to prohibitive increases in traffic density and its associated increase in demand of fossil fuel, noise and tailpipe emissions. Every single car driving on hydrocarbon based fuels (HC), with an internal combustion engine (ICE) produces potentially deadly [4] [5] and environmental damaging pollutants [6].

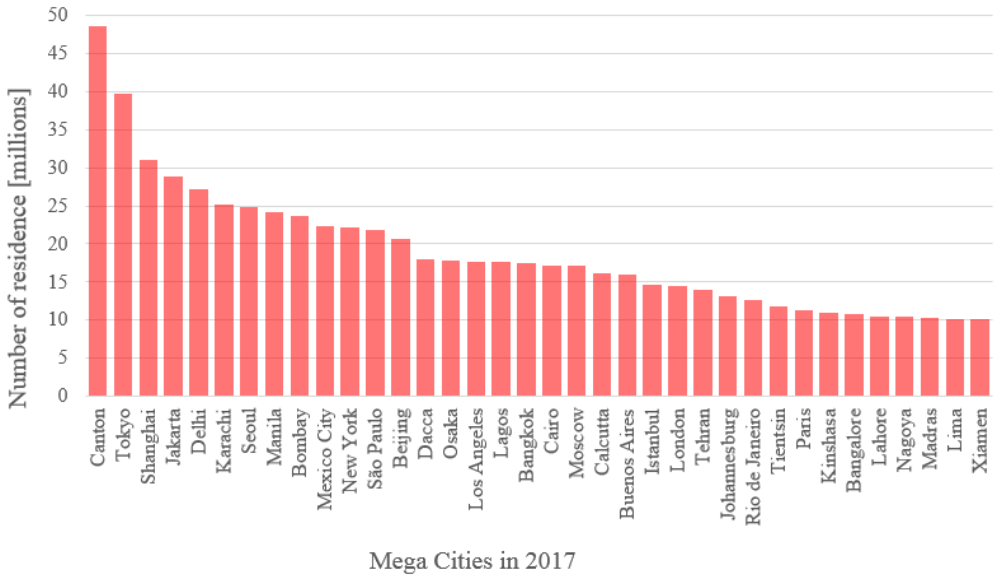

Figure 1-1 Number of residences in the worlds mega cities in 2014. Data extracted from [7]

Figure 1-2 shows how and where ICE vehicles produce dangerous exhaust gas emissions and evaporative emissions from the release of fuel vapours. Fuel vapours develop even if a car is not running. Although some of these vapours are captured in a evaporative emissions carbon canister, at some stage it is saturated and fuel vapours, volatile organic compounds (VOCs) as HC [8], are released into the atmosphere.

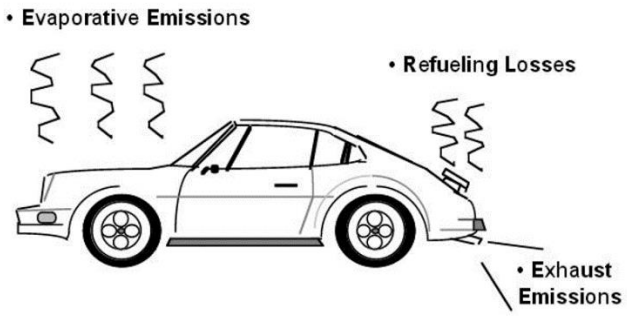

Figure 1-2 Emission sources on combustion engine motor vehicle [9]

The major components of exhaust gas emissions include carbon monoxide (CO), unburned HC and nitrogen oxides NOx. CO and HC are products from incomplete combustion. CO is toxic for humans and animals. If CO is inhaled at a certain concentration, it can lead to death. Depending on the nature of unburnt HC they can have a carcinogenic or direct toxic effect on humans [10]. NO_x develop in the reaction between oxygen from the ambient air and nitrogen from burned fuel. NO_x can have adverse health impacts on living cells and in ambient air NOx is responsible for smog and damaging acid rain[6, 9]. Ozone is another pollutant that occurs as the consequence of exhaust emissions, but is not directly caused by burning fossil fuels. Ozone is a product of the photochemical reaction between O_2 and NO_2 in the atmosphere. Even in low concentration, exposure to ozone can be very dangerous especially for small children, the elderly and people suffering from asthma [6, 11] .
Besides motor vehicle emissions in gaseous form, particulate matter (PM) are dangerous by-products of burning fossil fuels [12]. Depending on the particle size, PM have the potential to penetrate deep into the lung tissue and cause health issues such as cardiovascular disease, increased respiratory symptoms, decreased lung function or even increased respiratory morbidity. Such negative impacts from airborne PM can be observed even on PM levels below US air quality standards. As a consequence, people affected by PM levels are restricted in their everyday activities. Furthermore, increased hospitalization will increase costs on public health systems [5].

How seriously urban air pollution affects our everyday live was estimated by Yim and Barret [13]. The study reported that burning fossil fuels in the United Kingdom and on the European mainland might be responsible for 13,000 premature deaths per year. Concerns may arise further by the fact that the number from premature death far outweighs the annual road fatalities (1.901) [14].

Beside causing increased premature mortality and immense costs and loss to society, air pollution may also cause associated diseases. For example several studies found a possible link between diabetes and air pollution, especially to PM smaller than 2.5 µm [15, 16].

Even in Australia with its relative low population density [7], vehicle emissions are a problem [17] [10]. Operating vehicles on fossil fuel is costly and a potential health issue or even deadly for Australians living in urban areas. A study by R. Simpson [18] found an association between air pollution and short-term mortality in Brisbane, Melbourne, Perth and Sydney. A small increase in PM 2.5 increases the daily total number of deaths by 1%. In 2007, the Commonwealth Scientific and Industrial Research Organisation (CSIRO) and Orbital Engines conducted a $3.9 million project [19] to investigate the health impact from vehicle emissions and the potential health benefits by replacing unleaded petrol with ethanol blends. By adding 50% ethanol to the motor vehicle fuel (E10) of Australia's ethanol compatible vehicles fleet, human lives and 39 million AUD could have been saved per annum [20]. It needs to be emphasised that the study did not investigated the high particulate emissions from diesel and modern direct injection engines [21]. Furthermore, the study did not include the recent change in technology and uptake of new powerful passenger car diesel engines with its associated increase in diesel emissions. With an additional reduction of diesel and direct fuel injected tailpipe emissions, it can be assumed the health and cost benefit would increase even further. This detailed study by CSIRO and Orbital has shown that even in Australia, tailpipe emissions result in cost to the health system, health issues and premature death on society.

Unlike countries, free air does not have boundaries. Air pollution travels around the globe many thousands of kilometres. A major by-product of burning fossil fuels is carbon dioxide CO_2. It is not directly harmful to humans but as a major greenhouse gas it has the potential for global warming with its associated risks [9]. Motor vehicles contribute significantly to the CO_2 production. The International Energy Agency (IEA) states that in 2014 combustion from transport counts for about 23% of the total global CO_2 production[22]. To overcome issues associated with vehicle tailpipe emissions, EVs have the potential to lower emissions provided the electricity is generated from renewable energy sources.

In summary, millions of motor vehicles operating in concentrated areas produce dangerous and environmentally damaging pollutants. Consequently, people living in cities and suburban areas suffer from diseases and the pollution may lead to their premature deaths. In addition, society is burdened with the costs of pollution and the negative impacts on the economy [17].

.

1.3 Economic Vulnerability to Peak Oil and Alternative Energy Sources

The economic dependency on oil in most countries implies the risk of being vulnerable to 'peak oil' and oil price shocks. The term 'peak oil' can be defined as the maximum possible oil production rate. It is the point where the demand for oil is larger than the oil industry can supply. Predictions of when peak oil happens are controversial. It depends mainly on demand growth and the successful explorations of new oil fields. Despite its potential dangers apparently there is little known about how this phenomenon impacts economies. According to one study the entire U.S. economy could be at risk from reductions in supply after peak oil [23]. It can be assumed that Australia would be at a similar risk from peak oil as the US.

Electric passenger cars, buses and light trucks have the potential to lower the demand on oil reducing the potential risks associated with peak oil. EVs can be operated without the strong dependency of fossil fuels. EVs' traction batteries can be charged with electricity generated from any energy source. Australia's renewable energy resources such as solar, wind, hydro, geothermal etc. have the potential to charge EVs and contribute to lowering our dependency on fossil fuels.

1.4 Research Goals and Thesis Organisation

This study aimed to address some of the barriers to EVs outlined in section 1.1. The research focused on the question: What technical improvements can be made to increase efficiency and hence the range of EV's?

This presented study aimed to investigate the potential for improvements in vehicle energy efficiency and recharging technologies. For this, vehicle performance data was collected using purpose built and programmed instrumentation systems. The resulting data helped to identified inefficiencies and enabled the development and implementation of new control strategies.

By increasing knowledge in this area, this research has the potential to increase EV overall efficiency, drivable range, EV popularity, increase market acceptance, increase air quality and

hence reduce the negative health impact and cost put on society currently produced by motor vehicles.
The remainder of this chapter describes the research goals and thesis organisation.

This thesis comprises eight chapters. The seven chapters following this introductory chapter are arranged as follows:

Chapter 2 provides some introductory notes on the issues of the current transport paradigm. A brief literature review on the state-of-art with respect to EV and ICE vehicles and associated issues are also covered.

Chapter 3 evaluates the energy gain and benefits from a regenerative braking system (RBS). Measurements on the vehicles are conducted in a controlled environment on a commercial chassis dynamometer using international drive cycle standards. The study coupled changes in energy recovered and driving range due to the RBS settings with investigations into the time of use of the friction brake.

Chapter 4 investigates an EV converted Ford Focus modified and configured to operate the AC compressor solely from kinetic energy recovered from the drive train when coasting or slowing down. The study investigates how the vehicle's energy efficiency improves by synchronising auxiliary loads with the vehicle drive train on a real road driving cycle pattern.

Chapter 5 continues in investigating inefficiencies and how energy consumption can further be improved. The study describes how an EV was exposed to a series of various supposedly more efficient, high-load accelerations and decelerations. The experiment addressed how energy consumption improves by operating an EV under an extraordinary driving style.

Chapter 6 investigates the relatively new charge technology, fast-DC charging. It outlines a study on two commercially available EVs exposed to a series of discharge and fast-DC charge cycles to measure cell balance and charge capacity. It was of interest to discover if the

vehicles' battery management systems were capable of successfully balancing individual cells and hence maintaining the batteries' charge capacity.

Chapter 7 continues on the fast-DC charging technology with its associated drawback. It reports on the impact on the drivable range from the combination of driving EVs at highway speeds, using auxiliary loads such as heating or air conditioning, and reduced charge capacity from fast-DC charging and discharge safety margins. In this study, these parameters were investigated and their impact on energy consumption and drivable range of EVs analysed. In addition scenarios were modelled in which the range was calculated based on the available energy from an 80% capacity fast-DC charged battery that discharges until the vehicle reduces its power in 'limp-home mode'.

Finally, a summary and outlook is made in Chapter 8, along with suggestions for future work.

Chapter 2

Background

2.1 Overview

In this Chapter an introduction is given to electric vehicles. A literature review is undertaken on the state-of-art with respect to several aspects of plug-in hybrid vehicles (PHEVs), electric vehicles (EVs) and associated issues.

2.2 Hybrid, Plug-In-Hybrid and Full Electric Vehicles

In 1997, for environmental and fuel economic reasons, Toyota released the Prius, the first mass-produced hybrid electric vehicle (HEV) [24]. A HEV incorporates two different motor technologies for the propulsion; it is usually powered by an electric motor and an internal combustion piston engine (ICE). A HEV's battery cannot be recharged or operated from an external electricity source. All the energy required for traction and auxiliary loads is extracted from combustion fuel (petrol, diesel, gas, bio- fuels etc.). The engine's generator provides electricity for the traction battery. The battery provides power to the electric motor for driving in relative short stop and go scenarios and this reduces vehicle emissions. The main benefit of the traction battery is that it can recharge by absorbing the vehicle's kinetic energy and operating the electric motor as a generator, hence reducing fuel consumption and emissions. Depending on the vehicle's power source configuration, a HEV might also benefit from higher acceleration rates. By implementing both, an electric motor and an ICE into the vehicle, the vehicle computers can drive both power units in series or parallel. However, in regards to

environmental issues, a HEV still produces exhaust gas emissions and cannot be operated from a renewable electricity source such as a roof top solar system.

To address this issue, plug-in hybrid vehicles (PHEVs) were introduced to the mainstream market. Their larger traction battery enables the user to drive the vehicle with the electric motor for much larger distances compared to a HEV. A further benefit of a PHEV is its on-board battery charge equipment. Drivers can recharge the PHEV traction battery from any electricity source assuming its voltage and current levels match the system.

Depending on the size of the electrical storage system and the required distance to be travelled, PHEVs have the potential to be operated with zero tailpipe emissions provided they are recharging from renewable energy sources, e.g. from a simple home roof-top photovoltaic (PV) system. The main disadvantages of PHEV's is that they need to carry a relative heavy combustion engine which requires maintenance, a fuel tank, fuel which need regular replacement (burned in the ICE), filters, pumps, coolant and exhaust gas systems etc.

In contrast to HEVs and PHEV, a full EV, otherwise known as battery electric vehicle (BEV) or all-electric vehicle, does not have a combustion engine with its associated drawbacks. All the energy required for the electric motor to operate the vehicle is from the on-board electricity storage system.

2.3 PHEV and EV Charging Methods

EVs can be recharged from an AC source by a vehicle's on-board charger or by an external DC charging station. Similar to a mobile phone, the properties of battery chargers, connectors, voltages and current levels have to match the device. Due to the vast amount of charger and connectors on the market, the International Electrotechnical Commission (IEC) developed standards for power levels and safety communication protocol between EVs and charging stations [25].

Currently EV recharging requires much more time than refuelling an ICE car. Although battery chargers and battery technology have improved over the last decades, they cannot keep up with the energy transfer rate compared to refuelling an ICE. In Australia, the slowest Level-1 or home charging can provide a maximum energy transfer rate of 2.4 kW. Level-2 AC fast charging can deliver 7 or 21 kW depending on the electrical phases used for the

charging system. Level-3 fast-DC charging charges EVs' batteries without the internal charger. The DC charger converts the mains AC to DC and connects directly to the vehicle's traction battery. For a test Nissan Leaf used for experiments, the maximum observed charge rate at the UWA charge station was 39 kW. Tesla, Inc. (formerly named Tesla Motors) developed a fast DC charger with a charge rate of up to 120 kW [26]. Major car manufacturers are planning a fast DC charging network across Europe with a charge rate up to 350 kW [27]. The charging time for an EV traction battery depends on the battery size, the battery discharge level, the level of charging power and the battery's acceptable charge rate.

2.4 PHEV and EV Power Trains

Regardless of the type of vehicle, the power train describes the components generating and transmitting the power to the road surface. The design of a power train is a challenging task since cost, and weight distributions are important factors for the vehicle dynamics and safety. Both the individual components in the power train and the control algorithms are part of a power train. Control algorithms in the on-board computers are critical for drivability, safety and efficient operation of the vehicle. Figure 2-1 shows block diagrams describing the layout of a typical power train for PHEV's and full EV's. A PHEV can be operated in full electric mode without the ICE. In this scenario both the PHEV and EV use the electric energy stored in the battery for traction power. The traction battery is connected to the motor controller (MC) and drives the electric motor (EM) according to the driver's demand. The electrical energy is converted into rotational energy driving gearbox, driveshaft's, bearings and wheels. If the vehicle needs to slow down the motor controller is capable of operating the electric motor as a generator, converting the vehicle's kinetic energy into electricity and storing it back in the battery. Depending on the PHEV power train configuration, the ICE can be operated together with the EM to generate extra traction power. In such a scenario, the energy from the fuel tank is converted to mechanical energy and drives the gearbox or driveshaft in parallel or in series with the electric motor. In the scenario where the battery is low and no recharge station is available, the battery can be recharged by the ICE. This is a very valuable option if the vehicle drives into an inner city with strict zero-emission policies. In such a scenario, the vehicle can charge its batteries by the ICE prior entering a zero-emission area. Another option of a PHEV

configuration is an EV with range extender (RE) as shown in Figure 2-1. The ICE is not connected mechanically to the drive train but to an electricity generator (GE) [28]. If the traction battery's capacity or charge level is insufficient, energy from the fuel tank can be used to operate the generator. Depending on the size of the generator and the energy demand from the vehicle the generated electricity will drive the EM directly or may also charge the traction battery in parallel.

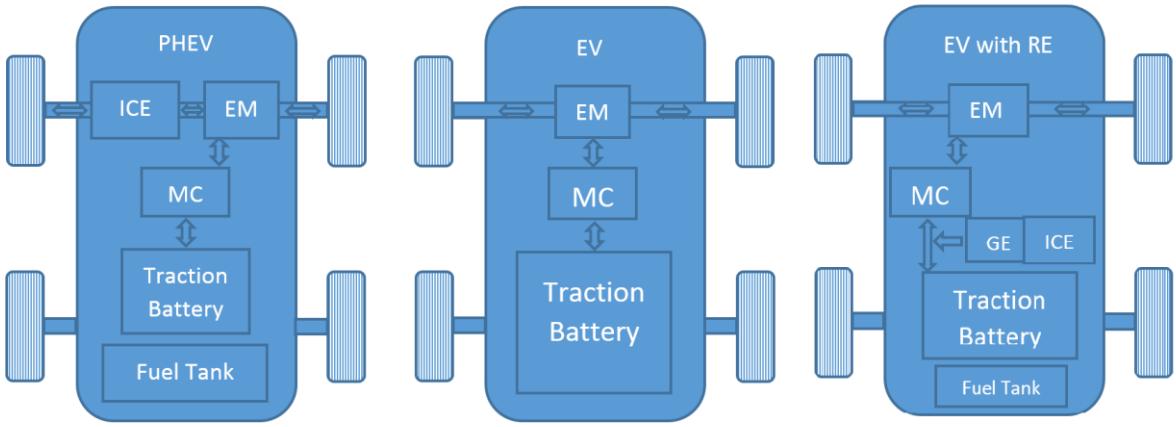

Figure 2-1: A block diagram describing the power trains of a plug-in hybrid vehicle (PHEV), full electric vehicle (EV) and EV with range extender (EV with RE)

2.5 PHEV and EV Energy Efficiency

Any type of energy conversion implies losses to heat. An ICE vehicle or PHEV driving in ICE mode converts energy from fuel to mechanical energy. Around 70% of the energy in an ICE is lost by exhaust heat, pumping and friction [29]. In spite of these relative large losses, ICE can drive much larger distances due to the nature of the dense energy content (per volume and per weight) of the fuel. In contrast, despite a EVs higher energy efficiency, its range is much shorter due to the low energy density of the traction battery compared to fuel. Furthermore, EVs requires long recharge times and are limited in recharge options. Hence, the efficient operation of an EV is critical. To drive a PHEV in pure electricity mode or operating an EV, a series of energy conversions along the power train are required with associated losses [30]. Figure 2-2 shows the energy flow from the traction battery to the wheels and

typical energy conversion efficiencies for an EV. Depending on the type of the battery and discharge rate the efficiency varies between 70% and 95% [31]. The MC in the power train converts the traction batteries DC electricity into AC which is required to drive the motor. Depending on its load and how fast the motor needs to be driven, its efficiency varies between 85% and 99% [32]. EV motor efficiencies are commonly between 82 % and 97 % depending on load and motor rotational speed [32]. Although the losses in motor and controller cabling are usually low, they must not be neglected and are part of the overall power train losses. Mechanical losses occur in reduction gearboxes, driveshaft, bearings and tyres. Mechanical friction in these components produces heat, which is lost, and not usable anymore for vehicle traction. A typical efficiency of the mechanical drive shaft is 95 % to 98 % [33]. The overall efficiency is the product of all efficiencies in the power train.

The energy required to drive an EV is not just for traction. As PHEVs and EVs also requires electricity for auxiliary loads such as lights, electronic entertainment systems, on-board computers, and heating and cooling systems. The energy required for auxiliary systems can be significant and influence the maximum drivable vehicle range.

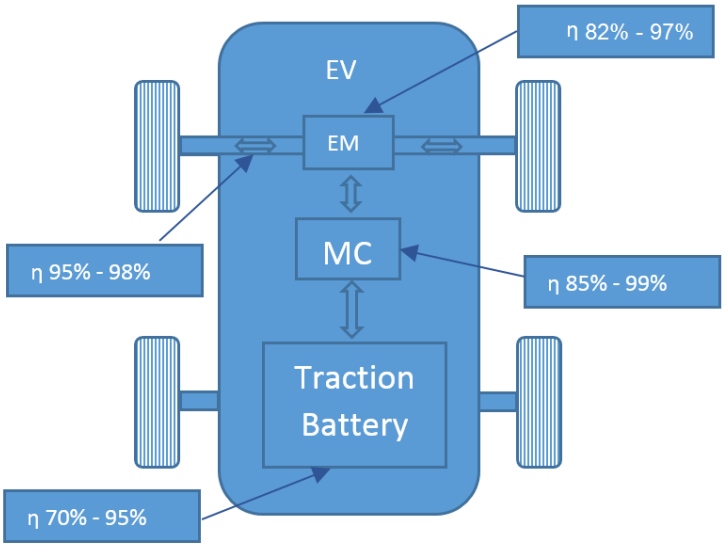

Figure 2-2: EV power train components with typical efficiencies

2.6 Issue 1, Electric Vehicle Short Range

Both EVs and conventional vehicles powered by an ICE require an energy storage device. During the vehicle's operation, energy is released and converted into mechanical energy to drive the car. Where an ICE has a fuel tank, an EV has a battery as a main energy storage device. The greater the rate of discharge over time, the shorter the vehicle's drivable range. The larger the energy storage, the further a vehicle can be driven. Furthermore, the efficiency and use of the available energy influences the vehicle's range.

Due to the high energy density of fuel, ICE cars can store much more energy than EVs. This means, that despite the relatively low energy conversion efficiency of an ICE, vehicles operated with fossil fuel can travel much further (without refuelling) than EVs.

The battery for current mainstream EVs, for example the Nissan Leaf, is sized for a range of approximately 172 km [34] . Although the majority of commuters travel less than 100 km a day [35] and a Leaf's range would be enough for daily commuting, it still may trigger some 'range anxiety' for some drivers. Range anxiety is a term describing the concerns of EV drivers not being able to find an opportunity to recharge the EVs traction battery before depletion [36].

Unlike ICE vehicles, EVs currently have very limited recharging opportunities. Although some fast-charge stations have been implemented [37, 38], charging is almost entirely limited to homes and businesses where recharging takes hours [39] compared to refuelling an ICE car which takes just a couple of minutes.

2.7 Improving EVs short range by Energy Recovery and Efficient Operation

To improve EV range, efficient operation of all vehicle systems and improved recharging technologies are important. To improve efficient operation, energy losses need to be identified. For example, a large amount of energy is lost during the slowing down or braking of a moving vehicle. Several studies have been conducted on the design of RBS and the storing of the recovered energy in super capacitors or batteries for later use [40-45]. An RBS is not just capable of recovering energy but also has other benefits such as reduced brake

operation time and is associated with reduced air pollution and reduced cost. At the time of the PhD project proposal the candidate was unable to find a published study that already investigated the performance and benefits of an RBS for a single vehicle in detail. As part of the work of this thesis, original data from the candidate's Master's in Renewable Energy at Murdoch University in Western Australia was re-analysed, the energy recovery of the vehicle modelled, the benefits from an RBS system evaluated and the results were collated in a publication. The chapter evaluated the energy gain and friction brake cost savings from an RBS in a commercial EV, the OEM Mitsubishi i-MiEV. Measurements were conducted in a controlled environment on a commercial chassis dynamometer using international drive cycle standards. The experiment coupled changes in energy recovered and driving range due to the RBS settings with investigations into the time of use of the friction brake. The performance study used multiple drive-cycle speed profiles and various RBS settings to compare energy recovery performance for a broad range of driving styles. This research forms Chapter 3 of this thesis.

It was found that regenerating, storing and retrieving energy caused inefficiencies due to inherent charge and recharge losses. At the time of this literature review, no studies have been found on innovative methods to overcome these issues and, in particular, of using a vehicles' kinetic energy directly for auxiliary loads instead of storing it. This lead to further work in this thesis, which describes a study on how kinetic energy from a driving EV can be used directly in order to improve efficiency. For the experiment, an EV-converted Ford Focus was configured to operate the AC compressor solely from kinetic energy recovered from the drive train when coasting or slowing down. The research addressed the question of how the energy efficiency improves by synchronising auxiliary loads, such as air conditioning, with the vehicle drive train on a real road driving cycle pattern. This research forms Chapter 4 of this thesis.

To maximize the range and usage of the relatively small energy storage in mainstream PHEV and EVs, efficient operation is critical. During experiments and investigations on EVs it was found that in mainstream EVs, waste heat from the motor controller is used as a heat source

for heating the EVs passenger compartment. The relatively large amount of heat available was an indication of energy losses from the motor controller, particularly if (heating is not required. It was found, regardless of traction power or energy regeneration capabilities (recuperation), each EV motor controller operates more efficiently under certain motor rotational speeds and loads [32]. Unlike internal combustion engine cars or hybrid cars, EVs do not have variable gearboxes that allow the rpm to be adapted to adjust the motor speed towards more efficient regions. However, the driver can actively influence the load by changing acceleration or deceleration rates. This can lead to a more efficient operation of the EVs' motor and controller and hence reduce the energy that is wasted into heat. Although EV efficiency tests, modelling and multi-gearbox efficiency tests have been conducted [46], many of these studies focused on following a speed profile with relative low changes in acceleration and deceleration rates. This observation led to the idea of an innovative experiment for this thesis. A Nissan Leaf EV was exposed to a series of high load variations in acceleration and deceleration to investigate how energy consumption and hence range can be improved by efficient driving techniques. This research forms Chapter 5 of this thesis.

2.8 Issue 2, Electric Vehicle Recharging Infrastructure

EVs' range, recharge opportunities and time to recharge are major barriers to mainstream acceptance. As discussed above, EVs have currently very limited recharging options. The implementation of recharging infrastructures for EVs faces a number of critical challenges such as electrical, strategic, electrical-grid regulation, energy engineering, economic and political [47-52].

Although fast-DC charging technologies reduce charging time significantly, an EV charging under fast-DC charge rates can only charge its traction batteries up to 80% of its full capacity. The charging of the remaining 20% is under reduced power and usually takes a long time due to the physical properties of an EV battery and the battery management system (BMS). To prevent battery cell damage during charge or discharge, the main BMS task is to monitor individual cell voltages and equalize them accordingly. Based on the engineering challenges for a BMS, a study was conducted on the unknown impact of fast-DC charging on battery cell

balance. A Mitsubishi MiEV and a Nissan LEAF were exposed to a series of discharge and fast-DC charge cycles to measure cell balance and charge capacity. The study found answers to the question of whether the vehicles' BMSs were capable of successfully balancing individual cells and hence maintaining the batteries' charge capacity and the vehicles' range. This research forms Chapter 6 of this thesis.

Fast-DC charging significantly reduces the recharging time and can be used to make longer EV trips possible, e.g. on highways between cities. Although some EV and hybrid car studies have been conducted that address separate issues, such as limited drivable ranges [53-55], charge stations issues [47-52], and impact from auxiliary loads on vehicle energy consumption and emissions [56], at the time of the literature review there was limited research on the impact on drivable range from the combination of these factors. The final study in this thesis aimed to resolve the question of how these parameters impact energy consumption and how they influence the drivable range of an EV and its efficient utilisation of the battery capacity. This research forms Chapter 7 of this thesis.

Chapter 3

Performance Evaluation of Regenerative Braking Systems

3.1 Introduction

The penetration and expansion of EVs in the marketplace has been hindered by issues such as high purchase costs, limited driving range, lack of charging infrastructure, lengthy charging times, and policy challenges [37, 57-68]. In 1997 Toyota brought out the Prius (model NHW10), the first factory-built mainstream hybrid EV [60, 69]. Since that time, car manufacturers, governments, academia, and EV enthusiasts have been increasingly investing in EV-related technologies [60, 70-78].

The use of energy recovery systems in vehicles gained wider popularity when it was introduced as an energy saving feature in Formula 1 racing, effectively making Formula 1 cars hybrid vehicles [76, 77, 79-81]. An electro-mechanical regenerative braking system (RBS) converts kinetic energy into electricity by using its driving motor in reverse and operating it as a generator during deceleration. An RBS is now a common feature used in all factory-built EVs to improve driving safety, range, and vehicle energy efficiency [75, 82-84]. Most present drive cycle standards for EVs measure vehicle energy consumption (defined as

net energy consumed from the battery per km travelled in Wh km^{-1}) enabling calculation of the performance improvements of the EV due to an RBS (defined as the energy in Wh recovered and delivered to the battery per km). Despite the advantages listed above, RBS disadvantages include the potential of driving load mismatch and dependency on battery state of charge (SOC) [73, 85, 86].

EVs with integrated RBS-ABS units transmit data between the anti-lock braking system (ABS) and the RBS control units to utilise the maximum possible energy transfer through the wheels without locking. This integration has introduced a higher level of complexity in RBS and brake system design optimisation in hybrid electric vehicles (HEVs). Complexities with safety considerations include a fully applied RBS causing the wheels to slip or lock and create dangerous driving situations. Several technical considerations (if inappropriately integrated and configured) can lead to trade-offs between vehicle safety and stability, high RBS conversion rates, and appropriate battery over-current protection.

Combining RBS control with friction brakes (blended brake control) in EVs can induce further challenges. Damping factors, power-train backlashes and the elastic properties of an electric drive train might excite driveline oscillations, challenging designers of blended brake control strategies. To overcome these issues and maintain appropriate vehicle dynamics, Lv et al. conducted intensive research in developing control algorithms to compensate for the power train flexibility [87] [88].

In addition to the technical aspects of an RBS, such as vehicle dynamics, safety and efficiency, the ergonomic design of the accelerator and brake pedal is also an important factor. Zhang et al. have carried out research on the optimisation of blended RBS and hydraulic brake systems taking all these factors into account in the design of an RBS control strategy. The research not only focused on the maximum RBS regeneration efficiency, vehicle dynamics and safety, but also incorporated optimal brake pedal comfort. It was found that a control strategy recovering the most energy would cause issues in terms of road safety and pedal comfort. The research revealed that by changing the control strategy and sacrificing some potentially available kinetic energy, the vehicle dynamics and pedal comfort improved [89]. Complexity for an RBS control strategy, however, increases by optimizing the RBS performance in conjunction with an ABS. Peng et al. [90] analysed limiting factors associated with slipping or locking wheels during braking of a vehicle, and developed a system to more

effectively control hydraulic friction brake pressures and the interaction with the RBS to improve efficiency of regeneration, even during emergency stopping. Other challenges for improving RBS performance include the EV electrical system design, as electric motors, controllers, batteries, and cable sizes must be optimised to enable effective energy transfer from the wheels to the electrical system. EV electrical systems with load mismatch increase stress on under-designed components, create excessive heat, and cause losses in performance. As the optimized control [89, 91] and fine-tuning of an RBS systems is a complex task, most factory EVs reduce the driver's choice of RBS settings to a small number of pre-set options.

The EV battery and its SOC also limit the RBS energy conversion efficiency, as many battery technologies are sensitive to high amperages and overcharging [92], and a fully charged battery is unable to store additional electrical energy [93, 94]. The driving pattern or drive cycle can also affect the utility of an RBS, as e.g. continuous driving without braking renders even an efficient RBS ineffective at improving system efficiency, performance, and range [75, 86, 93-95]. In another example, the design and performance of an electro-mechanical RBS integrated with an ABS on an electric bus, was investigated by Zhang et al. [96]. The testing was conducted according to the Chinese Urban Bus Drive Cycle and the efficiency of regeneration from real road braking was considerable – up to 66% depending on the RBS design.

The objective of this research is to quantify the energy recovery gain from an RBS under different vehicle settings, as well as different drive cycles and loads. Where other studies have investigated just the vehicle's drivable range [83, 97], energy consumption and regenerated energy from tests using standardized driving cycles [93, 95, 98, 99], in our study we have also quantified the time of use of the friction brakes. This parameter, often neglected, is important to investigate the efficient and cost effective operation of a vehicle.

A case study is undertaken using a Mitsubishi i-MiEV EV under different pre-set RBS options. The Mitsubishi is tested in a controlled environment on a chassis dynamometer, using both US and European drive cycle standards under different vehicle configurations and driving patterns. To better understand the RBS braking behaviour, the power flows in the drive train of the i-MiEV were mathematically modelled and the expected energy demand on the battery and energy recovery rates by the RBS were calculated.

3.2 Theory

3.2.1 *Vehicle Mathematical Modelling*

To simulate the expected energy recovery rates from the vehicle RBS and to analyse the braking behaviours, the various components of traction power demand on the cars' batteries were modelled mathematically [100] [101] and the energy consumption and energy recovery of the car was calculated to estimate the improvement in performance due to the RBS. In contrast to the very detailed modelling methodology from Lv et al. [87] [88] [102], and Zhang et al. [103], the output of our simplified model was compared with results from real-road driving on a specific vehicle, the i-MiEV, and the unknown parameters such as power train efficiency, motor and controller efficiencies, tyre rolling resistance and battery internal resistance were calibrated in the model accordingly. The energy consumption for required auxiliary vehicle electrical loads (base load) such as vehicle computers, displays and pumps, were measured and logged on a stationary vehicle and integrated into the model. The model thus used realistic values for input parameters to try and achieve an accurate estimation of the energy demands and recovery rates.

The traction power demand was calculated using Equation (3-1 [100].

$$P_{Tractive} = \sum_{i=1}^{i=N} \left[mgC_{RR} + \frac{1}{2}\rho\, C_D A_F \left(\frac{V_i + V_{i-1}}{2}\right)^2 + mr\left(\frac{V_i - V_{i-1}}{t_{inc}}\right) + mg(\sin\theta) \right] * \left[\frac{V_i + V_{i-1}}{2}\right] \quad (3\text{-}1)$$

Equation (3-1) contains four separate terms. The first term is the power required to keep the vehicle driving at a given speed i.e. the power required to overcome rolling resistance. This is given by the gravitational force (g = 9.81 ms-2), the vehicle's mass and the rolling resistance coefficient of the tires (C_{RR}). It depends on the specific vehicle used as well as its tyres and tyre pressure. The second term defines the power required to overcome air resistance. This depends on the vehicle's aerodynamic shape (C_D), frontal area (A_F), and the density of air (ρ

=1.2 kgm-3). Unlike the first term, which is constant, this term depends on the vehicle's speed (V) as friction between air and the vehicle's surface increases with increasing speed. The third and fourth term relate to the inertial resistance and account for the loss of power during acceleration (third term) and road gradient (fourth term). In addition, power loss due to rotary power is considered by increasing the third term by a compensation factor described as the rotational inertia compensation factor (r). Finally, the drive train losses resulting from battery discharge losses, cabling, motor and gears, and RBS efficiency were calibrated from real road experiments. $P_{tractive}$ was then multiplied by the drive train efficiency factor and the auxiliary vehicle electrical loads added (Equation (**3-2**).

$$P_{tractive} = \left(\eta_{dtrain} \times P_{tractive}\right) + P_{aux} \quad (3\text{-}2)$$

3.3 Materials and Methods

3.3.1 *Vehicle Configuration and Testing*

Table 1 is an overview of the EV parameters used for the experiments in this study. The Mitsubishi i-MiEV in Figure 3-1 is a fully electric car. The i-MiEV was designed with three driver selectable drive modes calibrated for vehicle drivability and battery efficiency reasons. The drive mode selector, a conventional, automatic-style selector lever with Park, Reverse, Neutral, Drive, C and Brake positions is an input parameter for the motor control unit (MCU) generating the AC voltage for forward or reverse driving. Through the mode selector the driver has the choice to drive between three different brake modes (characteristics), which each come with different pre-set levels of maximum braking torque, generated by the RBS.
The different levels of RBS torque include:

- Mode D (drive)
  the standard mode, selects a calibration in the MCU to generate a medium RBS torque.
- Mode C (comfort)
  for smooth driving characteristics, request the MCU to reduce the maximum RBS

torque. It is suggested by the manufacturer to use this mode for longer suburban drives.

- Mode B (Brake)
  instructs the MCU for strongest calibration of regenerative braking capability to maximize energy recovery. According the vehicle manual it is recommended to use this drive mode for downhill driving.

For later i-MiEV models, these RBS settings also influence the accelerator and brake pedal characteristics and the vehicle's energy consumption [104].

EV testing was conducted on a computer-controlled and calibrated test equipment and instrumentation system containing a chassis dynamometer with road load simulation capability at the Orbital facilities in Balcatta, Western Australia (Oakley et al. 2016). A chassis dynamometer is a device capable of measuring forces on a vehicle's wheels or engine with computer controlled data collection systems for characterising the performance of a range of vehicles, usually with the aid of pre-programmed drive cycles. Drive cycle testing was developed in the late 1960's for uniform emission testing on passenger cars with combustion engines [105, 106]. In this study, vehicle testing required the test driver to follow the profile assisted by computerised driving aids indicating the rate of acceleration and deceleration of the vehicle. The existing chassis dynamometer instrumentation logged the following parameters during the drive cycle analyses: ambient temperature; vehicle speed; and dynamometer force. In addition to the existing dynamometer instrumentation systems, a custom-made data acquisition system was designed, built, programmed and calibrated by the author to log the following data: date and time; vehicle main battery voltage (V); main battery charge current (A); main battery discharge current (A); motor controller temperature (°C); brake light status information (on/off); and brake pedal foot pressure (kg). Vehicle electrical energy consumption and production by the RBS was calculated from the logged data. The main parameters include battery voltage (V), current (A) and motor speed (RPM). The core of the data acquisition system (DAQ) was a National Instruments (NI) USB-6008 unit, capable of logging up to eight analogue input channels [107]. Figure 3-2 shows the hardware and user interface for the custom built instrumentation. The National Instrument USB-6008 requires a

PC with a user interface; an open source application programmed in LabVIEW © [108]. The graphical interface software was designed for the particular task of acquiring signals from the individual channels for measuring, calculating, displaying and logging vehicle data, and enabled modification such as inputting new sensor calibration factors. To ensure uniform testing according the ISO standards, two of the USB DAQ channel inputs were connected to commercial temperature sensors, which measured the ambient and vehicle controller temperature, respectively. To investigate the impact on the RBS from the brake pedal operation, an additional channel was used as an input from an industry standard brake pedal pressure sensor that converted the applied pedal force to a voltage. To acquire brake light information from the vehicle and to avoid intrusive vehicle modification, a photo resistor was placed in front of the brake light and the signal output of the sensor was connected to a channel of the USB DAQ. A further two channels were used to acquire calibrated vehicle speed and torque voltage from the chassis dynamometer

To measure the vehicle's power, a similar method was used to that in the RBS efficiency study conducted by LV et al [102]. To prevent intrusive vehicle modification for a torque sensor on the vehicle's drive shaft, the power (current * voltage) was measured as close as possible to the energy source, the battery. A further advantage of this method was that it accounted for most of the energy losses through the power train. The power was then calculated using Equation (3-3) and the energy consumption and energy recovered by the RBS were calculated using Equation (3-4).

The current was measured using a calibrated inductive current clamp ICA 32N with an accuracy of 2%. For the measurement of the relative high battery voltage of up to 400V DC, a calibrated voltage divider, based on two resistors, reduced the voltage to an acceptable level for the USB-6008 interface unit. The calibration of the instrumentation and chassis dynamometer system was conducted under the AS/NZS ISO 9001:2000 standard. After starting the application, raw sensor voltages and calculated physical quantity parameters where automatically stored to a spreadsheet file, as well as streamed and displayed on a PC screen.

$$P = IV \tag{3-3}$$

$$E_{cons} = \sum_{i=1}^{i=n} IV\, t_{inc} \tag{3-4}$$

The data was sampled at 500Hz[1], averaged and stored on a text file every second (t_{inc} = 1 s), and aggregated in a spreadsheet. The original experimental setup included a shielded current clamp connected to ground together with the NI battery voltage logger. During the test, the Mitsubishi i-MiEV's internal computerised circuit monitoring system detected a battery earth leak to ground and triggered a fault. This switched the car into 'limp mode', leading to a maximum controlled speed of 25 kmh^{-1} and a cessation of the test. Therefore, as it was not possible to record voltage and current simultaneously, an approximation of the EV energy consumption (Wh km^{-1}) was achieved by logging the battery voltage each second on a separate drive cycle, and averaged over the duration of the city and highway cycles. Lithium-ion batteries have a relatively flat discharge curve. Discharging a traction battery over the short driving cycles, under low battery loads (except the short 120km/h section of the drive cycle), showed that the battery voltage did not change significantly and hence, for this experiment, was assumed to be not sensitive to drive cycle repetitions in terms of calculating the energy consumption.

As the current values were also logged every second they were amenable to be multiplied by the averaged battery voltage, and the negative and positive currents individually integrated over the time of the whole drive cycle to calculate the EV energy consumption (Wh km^{-1}).

[1]Previous logging experiments showed that sampling at frequencies higher than 500 Hz caused inaccuracy in the data acquisition of the NI USB-6008 device, however, sampling at lower frequencies reduced the quality of the logged signals.

Table 3-1: i-MiEV Specifications [109]

Dimensions and weights	Overall length, width, and height	3475mm (L), 1475mm (W), 1610mm (H)
	Cross-frontal area, AF	2.37m^2
	Empty vehicle weight	1110 kg
	Empty vehicle weight measured prior to testing	Front: 521kg Rear: 604 Total: 1125kg
Power train		Rear mounted motor
		Rear wheel drive
		Reduction gear, final gear ratio of 6.066
		Tyre rolling resistance coefficient, C_{RR} = 0.35 [110]
Brake system	Front	Hydraulic operated disk brakes
	Rear	Hydraulic operated drum brakes
	Front / Rear	ABS, Electronic brake force distribution (EBD) and Active Stability Control (ASC)
	RBS	Category A* [111]
Motor	Type	AC, permanent magnet synchronous
	Maximum power	49kW @ 2500 – 8000 rpm
	Continuous power	N/A
	Maximum torque	180Nm @ 0 – 2000 rpm
Battery	Type	Lithium-Ion, Yuasa LIM 50E [112] [113]
	Nominal Voltage	330V
	Energy	16kWh
	Max. discharge current	300A (6C)
	Max. charge	125A (2.5C)

	current	
	continuous discharge current	N/A [113]

*According to International Standards, the RBS on the i-MiEV is classified as Category A (not interacting with the service brake). However, since the vehicle is equipped with an ABS, EBD and ASC, theses systems can interact with the service brake and RBS under certain conditions, so the i-MiEV RBS might be considered as a combination of Category A and B [111].

Figure 3-1 : Mitsubishi i-MiEV owned by UWA.

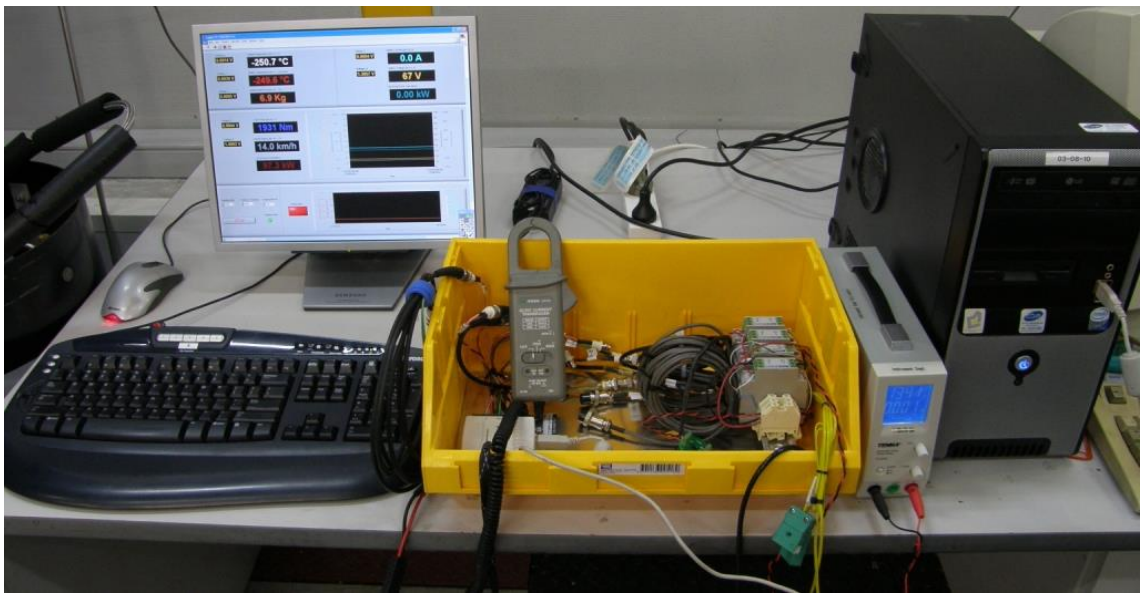

Figure 3-2: The custom-built instrumentation hardware and user interface used for testing at Orbital Engines' test facilities.

3.3.2 *Regenerative braking control strategy*

Figure 3-3 shows the drive train system overview of the i-MiEV. The DC current flow from the traction battery to the motor is controlled by the motor controller (MCU) converting the battery DC electricity into AC. At the motor, the electrical energy is converted into rotational energy and flows through the reduction gearbox to the wheels. One main advantage of a modern controller is its capability to operate the motor as generator (RBS). By slowing down a vehicle, the kinetic energy is dissipated in heat by the friction of the drive train, while the braking torque from the RBS is generating electricity. The generated AC electricity is converted by the motor controller back into DC and fed to the energy storage device, the battery. To maintain drivability and to protect the system, the currents (RBS and traction current) need to be controlled (Figure 3-4A).

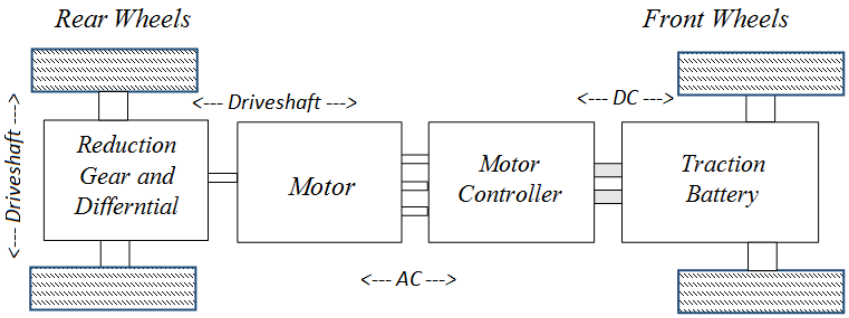

Figure 3-3: Schematic diagram of the drive train of the MiEV

The MiEV is manufactured with a hydraulic brake system with regenerative braking. Figure 3-4A is a diagram that illustrates how the RBS is activated and controlled by the acceleration pedal. From point X_2 towards full acceleration, the RBS is disabled. Provided the vehicle speed is above the RBS threshold speed of 16 kmh^{-1} (see Figure 3-5) and the releasing acceleration pedal reaches point X_1, the RBS starts to generate brake torque (Y_0) and decelerate the vehicle. The further the accelerator pedal travels to the point of complete release, X_0, the higher the RBS brake force. By fully releasing the pedal, X_0, the RBS maximum torque (Y1) is limited by the vehicle's speed and RBS setting as discussed in section 3.3.1. The RBS operation is further limited by the driving and road conditions. When entering a critical driving situation or when the wheels tend to lock on a low friction surface such as ice or oil, the ABS/ASC computer requests the RBS controller to reduce RBS torque. Depending on the stability of the vehicle, the hydraulic modulator might also interact to guarantee a safe driving condition. If the applied brake torque from the RBS is insufficient to slow down as required, or the vehicle speed is below 16 kmh-1 (Figure 3-5), the driver has to change over from the acceleration pedal to the brake pedal and apply additional brake force to the hydraulic friction brake system. When the brake pedal is pressed and the vehicle speed is above 16 kmh^{-1}, the RBS already generates full braking torque and by pressing the pedal further, only the friction brake force increases (Figure 3-4B).

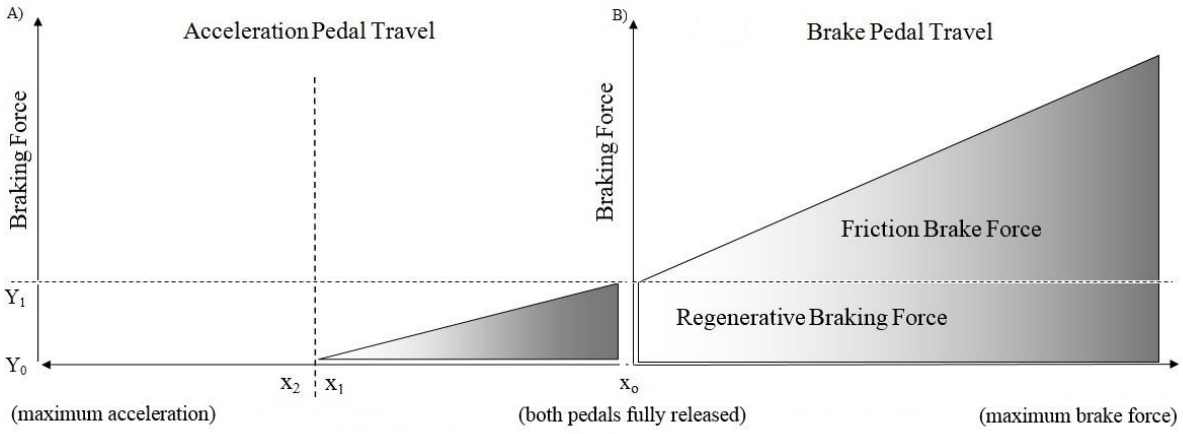

Figure 3-4: Diagram to illustrate RBS brake force in respect to acceleration pedal travel (A) and brake force in respect to brake pedal travel (B) assuming a vehicle speed larger than 16 kmh^{-1}

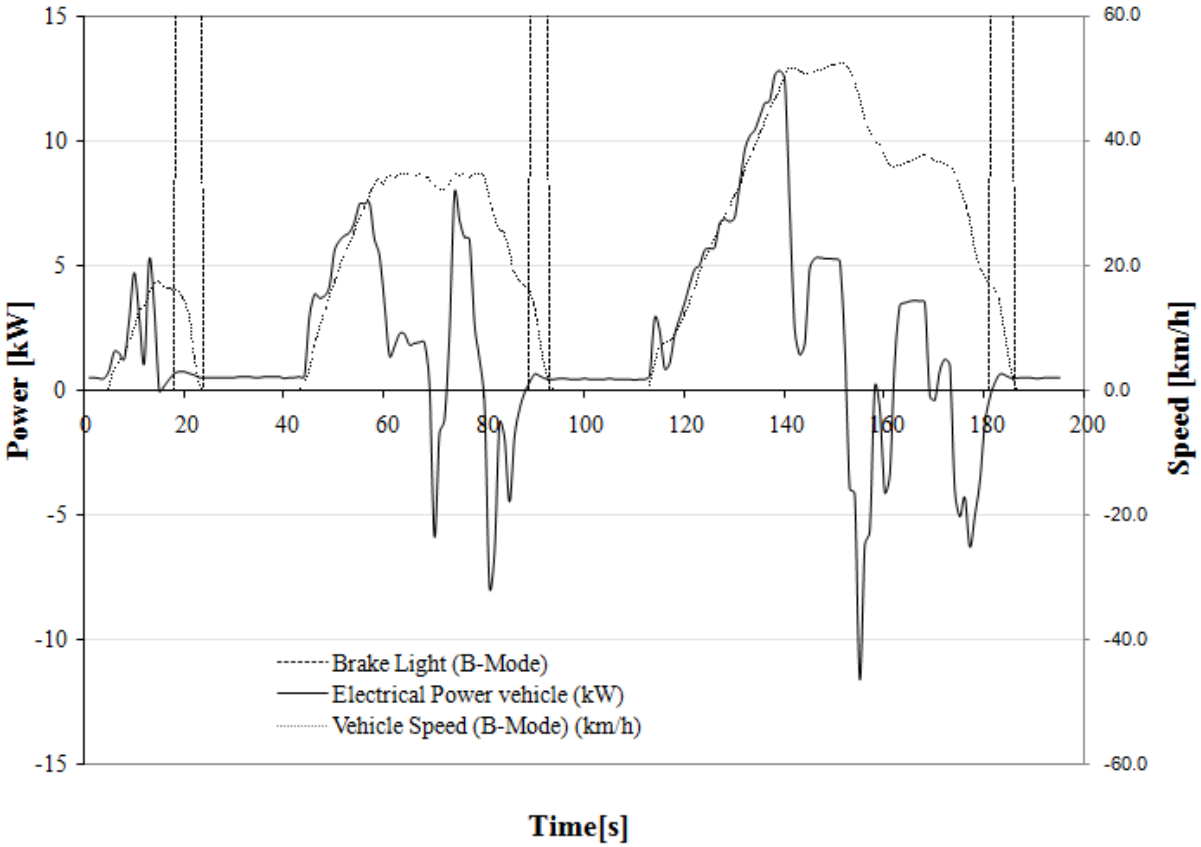

Figure 3-5: NEDC city driving cycle indicating the end of regenerating electrical power at the point when the RBS is disabled below its threshold of 16 km h^{-1} and the friction brake becomes active (brake light)

3.3.3 *Vehicle Testing Procedure: Choice of Drive Cycle Standards*

In this case study, the test method for the energy consumption was conducted in accordance to the United Nations R101 New European Driving Cycle (NEDC) standard [114], and the United States federal city driving pattern for vehicle testing (known as the FTP 75, or Federal Test Procedure) developed by the U.S. Environmental Protection Agency [115]. The tests were also conducted according to the Australian Design Rule (ADR 81/02), the NEDC urban and Extra-Urban cycle (Figure 3-6) [116]. For comparison, the U.S. FTP 75 exhibits a more 'aggressive' urban/city drive cycle than the ECE-15 urban drive cycles of the NEDC. The dynamic variation in the FTP 75 urban cycle is likely to represent a more 'real world' driving scenario than the ECE urban cycle with relatively consistent and slower driving conditions

[67]. The NEDC standard requires the vehicles and the battery to be conditioned prior to testing to provide uniform testing conditions for all types of vehicles and batteries. The key requirement includes the vehicle to have previously been driven for a minimum of 300 km and the vehicle's main battery to have been in operation for at least seven days. Furthermore, the main battery was required to be discharged and fully charged prior to a performance test. The EV tests were required to be temperature controlled between 20°C and 30 °C, with the vehicles tyres inflated to the pressure specified by the vehicle manufacturer. During the tests, all auxiliary devices such as the heater and air-conditioner were switched off. The test drive required two consecutive NEDC drive cycles with a maximum deviation of +/- 2kmh^{-1} in the speed profile. Table 3-2 shows the EV experiments.

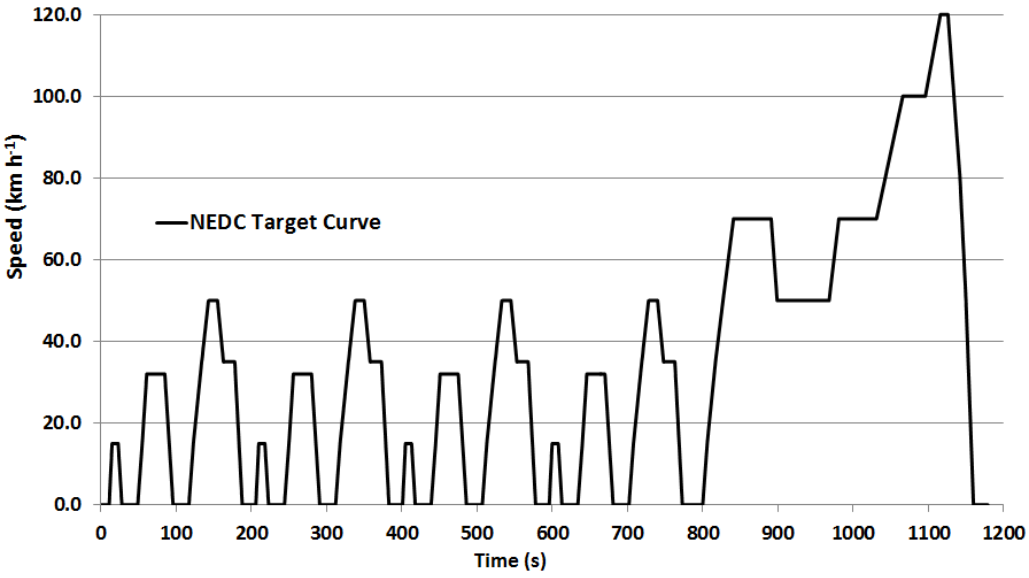

Figure 3-6: The New European Drive Cycle (NEDC) as a drive cycle example.

Table 3-2: The experiments conducted on the Mitsubishi i-MiEV.

Vehicle	Drive Cycle	RBS Settings	Initial Battery SOC
Mitsubishi i-MiEV	NEDC	D Mode	As per standard
	NEDC	C Mode	As per standard
	NEDC	B Mode	As per standard
	FTP75	D Mode	As per standard
	FTP 75	B Mode	As per standard
	FTP 75	C Mode	As per standard

3.4 Results

This case study investigated the EV energy consumption and improvement due to the RBS while driving under various drive cycles using the three i-MiEV RBS settings. To understand the MiEV's RBS braking behaviour, the vehicle's energy demands and energy recovery rates were modelled.

3.4.1 *Output of the Vehicle Mathematical Modelling*

The analysis of the model and of the braking behaviour was limited to the NEDC driving cycle and the maximum available torque in B-Mode. Figure 3-7 shows the model output for an NEDC driving test. The output was very sensitive to individual model parameters. For example, a slight change in the assumed drive train efficiencies can change the output significantly. Table 3-3 shows the calculated theoretical energy recovered during the deceleration sections. The results in the second column are calculated for deceleration to full stopping position of the vehicle. Note that these are theoretical recovery rates from the model and they ignore any RBS threshold. To realistically compare the model to the MiEV data from the chassis dynamometer (section 3.4.3), the table also shows data (third column) for

decelerating from the given driving speeds only down to the MiEV RBS threshold of 16 kmh^{-1}.

Table 3-3: The calculated theoretical energy recovered for the different deceleration speeds over the NEDC driving cycle to 16 kmh^{-1} and 0 kmh^{-1}.

Energy Recovery Speeds [kmh^{-1}]	**Recovered Energy [kWs] for deceleration to 0 kmh^{-1}**	**Recovered Energy [kWs] for deceleration to 16kmh^{-1}**
15 - 0	10	0
32 - 0	43	34
50 - 35	42	42
35 - 0	54	45
70 - 50	58	58
120 - 0	359	352
Total	**564**	**530**

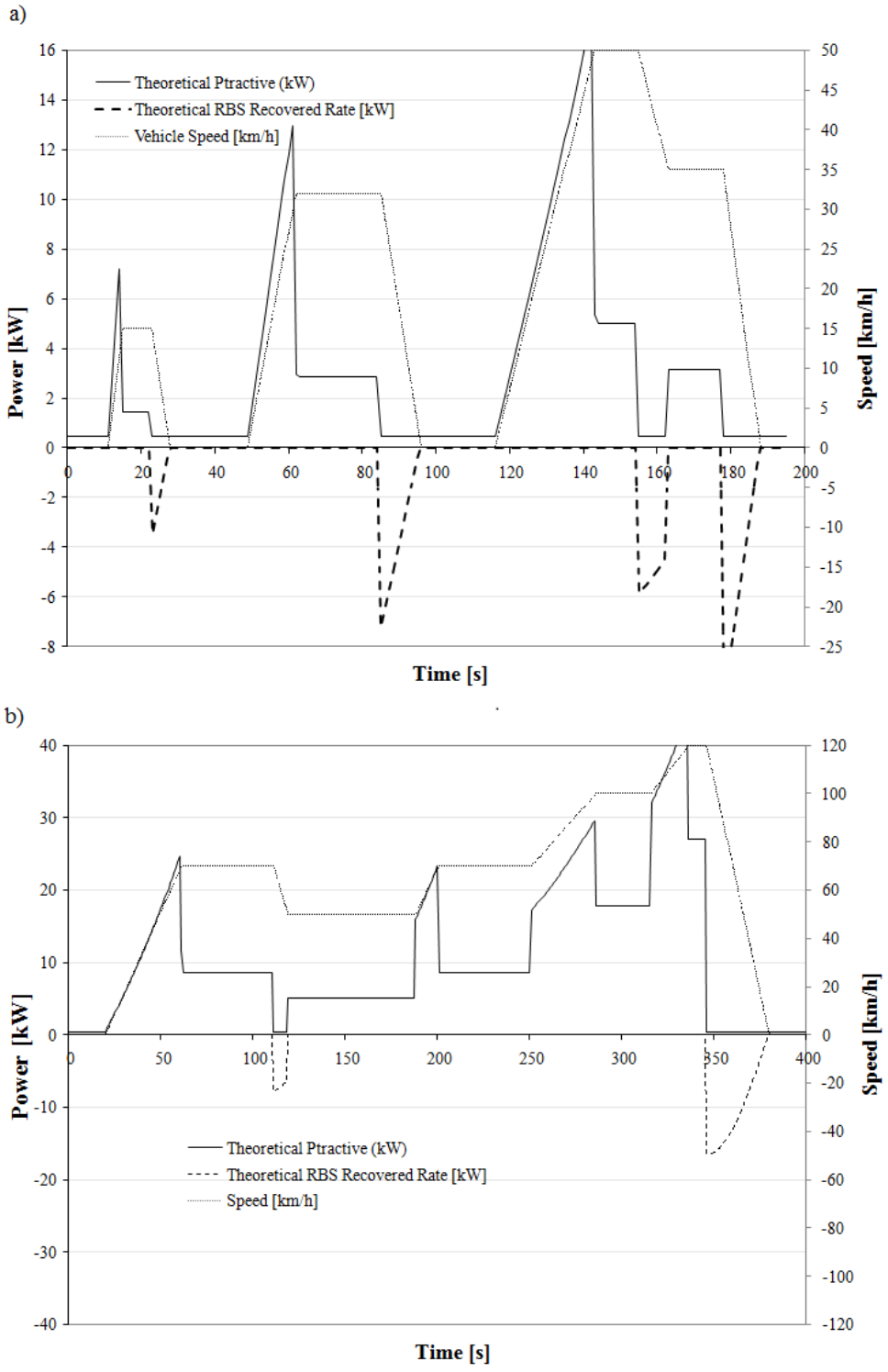

Figure 3-7: The city a) and highway b) drive cycle model output with speed profile, estimated energy demand and RBS energy recovery profile

3.4.2 *Performance Testing under NEDC Drive Cycle*

The NEDC drive cycle investigation of the RBS performance is shown in Figure 3-8. The figure shows the recorded speed and current profiles of driving in RBS modes C, D, and B. During acceleration the current increases and during the vehicle's deceleration the RBS recovers energy and recharges the battery (indicated by the negative current on the scale). RBS mode C generated lower currents during deceleration, while mode B generated the highest currents for the battery and the medium RBS mode (D) generated current levels between modes C and B. These RBS regeneration measured results were found to be consistent with the EV user manual. Table 3-4 shows the energy consumption calculated (without charge losses) and the energy consumption improvements due to the RBS. Mitsubishi states the i-MiEV energy consumption is 135 $Whkm^{-1}$ [117], and for comparison, the experimental test results on a i-MiEV conducted in 2009 by Walsh at the University of Sheffield [82] determined a consumption of 140 $Whkm^{-1}$ driving two consecutive NEDC cycles under the R101 standard. The energy consumption of the i-MiEV measured in this research for the NEDC drive cycle was 120 $Whkm^{-1}$ (excluding charge losses). Allowing for a charge efficiency of 0.86, this agrees well with the energy consumption stated by Mitsubishi [117] and Walsh [82]. REV/UWA has also completed on-road testing of the i-MiEV in a UDC/EUDC cycle akin to the NEDC, which resulted in a 110 km range for a full charge, which equates to an average energy consumption of 145 Wh km^{-1}[118]. This analysis found the i-MiEV RBS in C mode recovered the least amount of energy (16 Wh km^{-1}), B mode recovered the most energy (21 Wh km^{-1}), and D mode recovered an intermediate amount (19 Wh km^{-1}). However, due to the higher energy consumption during D and B modes, the EV energy consumption showed no significant improvement compared to mode C. As discussed in the introduction, drive mode selections will influence the vehicle's energy consumption. For the later models with ECO mode, the manufacturer provides clear information of the reduced torque and impact on energy consumption of the RBS, depending on the selected drive modes. For earlier models with a C-mode RBS, there was no information available if and how the C-mode setting influences the pedal and motor torque characteristics and hence the energy consumption. However, one reason for improved energy consumption in C-Mode may be the different MCU pedal and torque calibration, which might better load-match the NEDC driving. This assumption is supported by the energy consumption result below in

Table 3-6. By driving with a different speed (load) profile, FTP75, the energy consumption in C-mode was actually higher than in D-Mode.

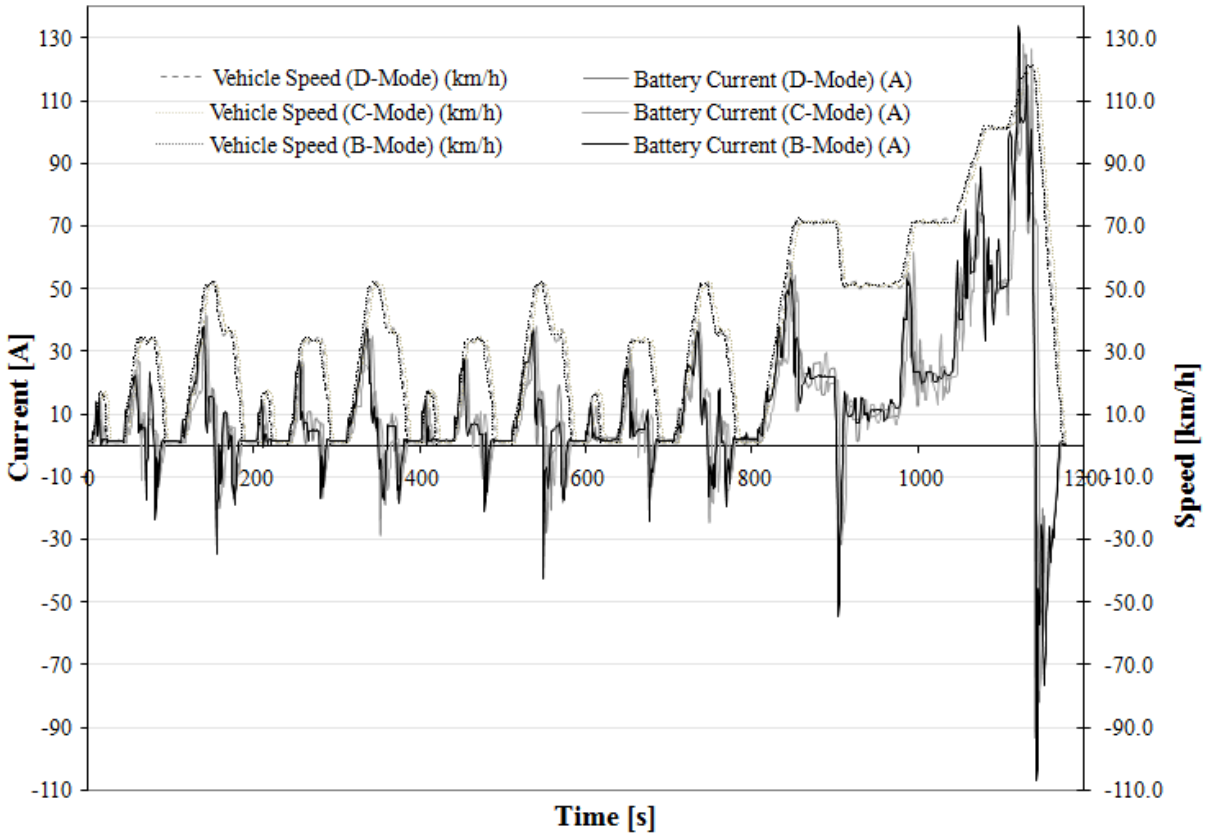

Figure 3-8: i-MiEV speed and current profile during three NEDC drive cycles for modes C, B, and D.

Table 3-4: NEDC RBS performance and energy consumption for mode C, D, and B.

	NEDC i-MiEV C Mode	**NEDC i-MiEV D Mode**	**NEDC i-MiEV B Mode**
Wh km^{-1} without RBS	136	138	142
Wh km^{-1} with RBS	120	119	121
Improvement (Wh km^{-1})	16	19	21
Improvement (%)	12	14	15

On the last NEDC drive cycle, the vehicle is required to accelerate to 120 kmh^{-1} and then slowly come to a full stop. This enables the calculation of the theoretical kinetic energy available to the RBS (Equation (3-5). By integrating the interval between the last point of maintaining a 120 km h^{-1} speed and the point at which the vehicle comes to a complete stop, the theoretical kinetic energy available to the i-MiEV RBS is 625 x 10^3J (0.174 kWh). The measured electricity generated by the i-MiEV RBS over the interval was 378 x 10^3 J (0.105 kWh), achieving a RBS regenerating efficiency of 60.5% for this selected section of the drive cycle (by (3-6).

$$E_k = \frac{1}{2} m v^2 \tag{3-5}$$

$$\eta_{regen} = \frac{E_{regen}}{E_k} \, x \, 100\% \tag{3-6}$$

This approximation of the RBS efficiency is only true assuming the friction brake pedal was not pressed during the deceleration from 120 km h^{-1} to a full stop and the RBS would have generated electricity close to 0 km h^{-1}. Analysing the data from the last NEDC drive cycle shown, the brake pedal was pressed at a speed from 16 km h^{-1} to 0 km h-1 (Figure 3-9) influencing the efficiency of the RBS. At the same time and speed, the RBS threshold disabled generating brake torque, so from that point on electricity was used rather than generated. Therefore, the efficiency was recalculated based on a kinetic energy and the energy recovery from a speed from 120 km h^{-1} to 16 km h^{-1}. Correcting the efficiency by considering the RBS threshold and not using the friction brake improved the RBS efficiency to 61.7%.

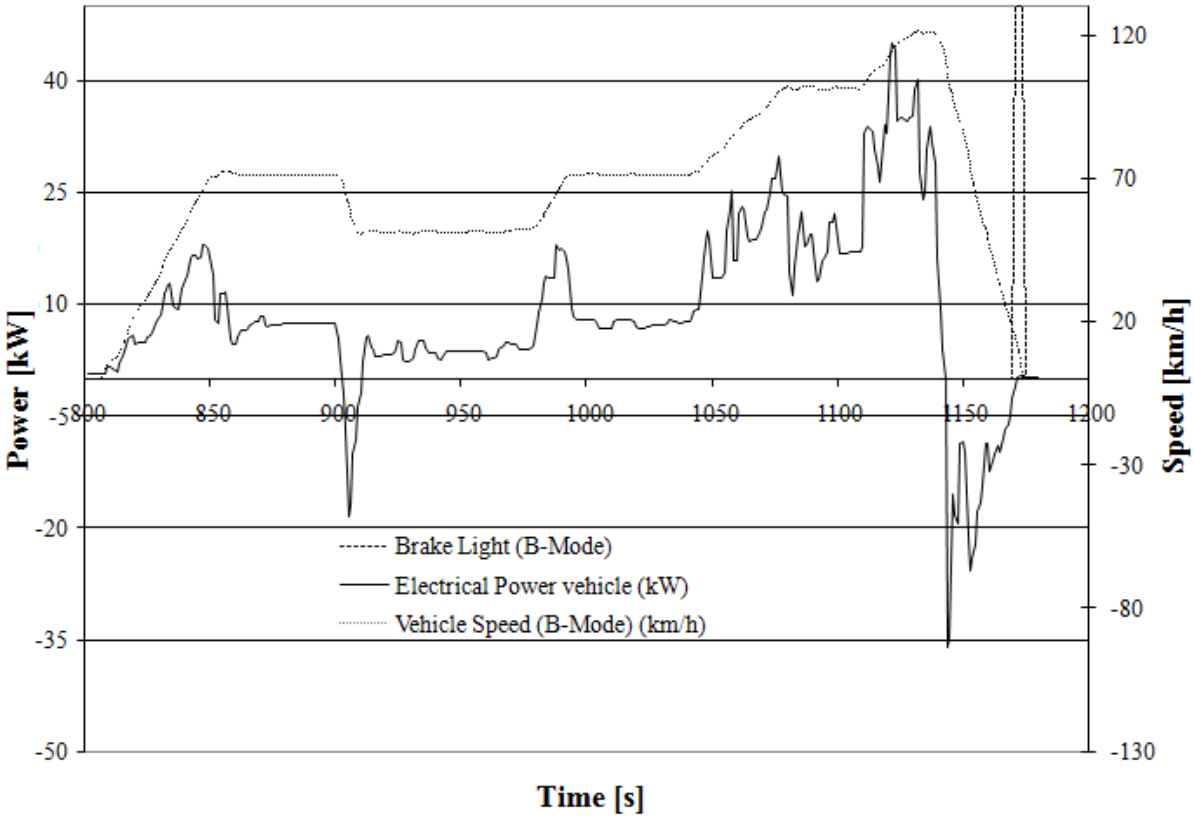

Figure 3-9: The NEDC Highway section speed profile, traction, regeneration power and the short period of the friction brake (brake light) in use below 16 km h^{-1} near the end of the highway section.

3.4.3 *Comparison between NEDC chassis driving and model output*

To better understand the MiEV RBS brake behaviour the energy recovery of the vehicle was modelled and its output compared to the results from chassis dynamometer driving.

Table 6 shows the calculated energy consumptions to a full stop, to the RBS threshold of 16 kmh^{-1} (brackets) and the measured recovered energy. The data indicate the importance of considering the RBS threshold. Although, at 16 kmh^{-1} there is still kinetic energy available, the RBS is disabled and hence does not feed electricity back to the battery. Comparing calculated and measured data considering the RBS threshold shows better agreement with the

measured data from chassis dynamometer driving. Although some individual drive cycle recovery rates deviate from the model significantly, the overall recovered energy lies within 2.5%. It is assumed that the deviation on some of the individual cycles were caused by deviation of +/- 2kmh^{-1} in the speed profile drive cycle speed (change in available kinetic energy), tolerances of the RBS threshold, the relatively short deceleration measurement time, and the relatively long logging intervals (one second).

Table 3-5: Comparison between RBS regeneration from model and from chassis dynamometer driving

Recovery Speeds	**Recovered Energy (model) [kWs]**	**Recovered Energy chassis dyno [kWs]**
15 – 0	10 (0)	0
32- 0 (16) kmh^{-1}	43 (34)	26
50-35 kmh^{-1}	42 (42)	40
35-0 (16) kmh^{-1}	54 (45)	31
70-50 kmh^{-1}	58 (58)	68
120- 0 (16) kmh^{-1}	359 (352)	379
Total	**564 (530)**	**544**

3.4.4 *Performance Testing under FTP 75*

The FTP 75 drive cycles, under identical conditions to the NEDC drive cycles, generated similar results to the NEDC drive cycles for each RBS mode. However, the overall energy consumption was less per km for the FTP 75 drive cycles, and the more frequent braking profile resulted in a greater utility of the RBS, and associated EV performance

improvement (Figure 3-10 and Table 3-6). Table 3-6 shows that the best performance (Wh km^{-1}) for the i-MiEV FTP 75 test occurred in D mode.

For all i-MiEV drive cycle tests the brake pedal pressure was found to make no difference on the RBS performance. This was because the level of applied RBS braking force is controlled by the acceleration pedal and is independent of the brake pedal. The brake pedal pressure and the operation of the brake light were logged over the drive cycles. Table 8 shows the friction brake operation time (in seconds) for each drive cycle. Between modes C and B, there was a significant difference in the duration where the friction brake was in use.

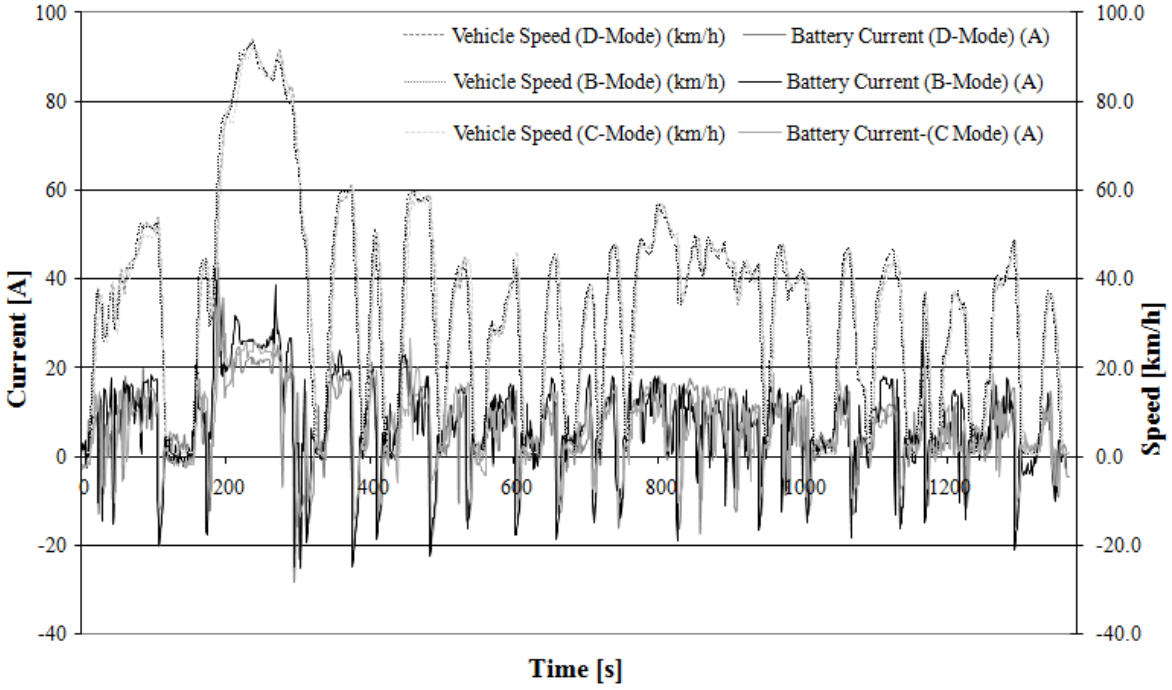

Figure 3-10: i-MiEV speed and current profile during three FTP 75 drive cycles for modes C, B, and D.

Table 3-6: FTP 75 RBS performance and energy consumption for mode C, D, and B.

	FTP 75 i-MiEV C Mode	**FTP 75 i-MiEV D Mode**	**FTP 75 i-MiEV B Mode**
Wh km^{-1} without RBS	81	79	93
Wh km^{-1} with RBS	70	62	77
Improvement (Wh km^{-1})	11	17	16

Improvement (%)	13	22	18

Table 8: i-MiEV friction brake operation time (s) for each drive cycle and mode.

Cycle and Mode	**Operation Time of Friction Brake (s)**
NEDC C Mode	109
NEDC D Mode	77
NEDC B Mode	46
FTP 75 C Mode	157
FTP 75 D Mode	122
FTP 75 B Mode	85

3.5 Discussion

3.5.1 *Mitsubishi i-MiEV RBS Performance*

The theoretical kinetic energy available from the Mitsubishi i-MiEV travelling at a speed of 120 km h^{-1} was 625 x 10^3J, with the RBS being able to generate 392 x 10^3 J of electricity over the selected drive cycle interval. This corresponds to a maximum of around 62% of the available kinetic energy converted over the small interval. However, driving the i-MiEV under different drive cycles and RBS settings over longer intervals demonstrated a wide range of RBS efficiency values. The RBS improved the energy consumption of the i-MiEV between a high of 22% on the FTP 75 drive cycle in mode D, and a lower 11% on the NEDC drive cycle in mode C. Such a large range shows how significant the RBS performance depends on the driving patterns and the RBS configuration. It is also important that the RBS settings are set to match the vehicle load, as a fully applied RBS does not necessary provide the best

performance for a driving pattern. For example, the FTP75 drive cycle on the higher RBS setting did not recover the most energy per km. Although the higher RBS electricity generation in mode D relative to mode B was not significant, the authors assume that the FTP75 load profile matched the i-MiEV's mode D to a higher degree than B, resulting in slightly more energy recovery.

The calculated results from the simplified vehicle model showed good overall agreement with the energy recovery rates measured on the chassis dynamometer driving. To improve the results on the individual drive cycles shorter logging intervals and very accurate speed profile driving should be used.

In addition to energy consumption improvements by an RBS, there are several other benefits to using an RBS. An RBS extends the vehicle's range, therefore reducing driver 'range anxiety', while also reducing wear on the vehicle's brake components.

When driving the i-MiEV on the FTP75 in mode B compared to the mode C, the operation of the friction brake reduced to almost half (from 157 seconds to 85 seconds). This not only reduces vehicle operation cost but also reduces noise and particulate emissions, which have a negative impact on air quality and consequently population health [119-121].

Many factors such as vehicle brand and model as well as driving style influence the servicing cost of vehicle braking systems. A brake component service life depends on several factors and is difficult to model and predict [122-124]. An accurate and detailed cost analysis based on established metrics, as for example Australian vehicle operating costs (VOCE) studies [125], is beyond the scope of the current investigation. However, a simple back of the envelope calculation for cost savings from an RBS is performed based on the following assumptions:

1) The RBS is installed in a frequently driven EV such as a courier service car
2) The EV drives 40,000 km per year
3) An assumed annual servicing cost for brake components is $AUD 500.- ** [126]

**The assumed annual brake servicing cost might vary significantly between car manufacturers and dealerships and local maintenance service stations.

A reduction of the operation time of the friction brake by around 50%, as discussed above, means that the lifetime of the friction brake is almost doubled. Hence, for the above assumptions, an annual saving of $AUD 250 can be assumed. These cost savings would accumulate over the years and could contribute to e.g. a new EV traction battery. Such hidden cost benefits in the use of EVs (and there are many other cost savings related to oil, filters, timing belts, air, fuel and oil filters, spark plugs, coolant etc., that are not discussed further in this study) allow EVs to better compete with conventional combustion engine cars in terms of operating and life cycle costs.

3.6 Conclusion

Our results demonstrated the introduction of RBS reduced energy consumption, and thereby increased the driving range between 11-22% (OEM Mitsubishi i-MiEV), depending on the drive cycle settings on the chassis dynamometer and RBS parameter. This represented a significant improvement in performance and energy consumption. The vehicle energy recovery model showed good agreement with the results from chassis dynamometer driving. Though additional analysis of the model is required under different drive cycles and RBS settings, this is a promising model that can be further developed to gain greater insight into vehicle RBS braking behaviour for EVs in general.

Actual driving or ‘real world’ testing results may differ from the chassis dynamometer testing. For the RBS to operate at its maximum efficiency, it must be fine-tuned to match EV load and driving style, as well as interfaced with an ABS. The results further showed that driving an EV with a RBS increases the efficient use of friction brakes, reduces the negative impact on air quality, while also reducing the maintenance costs significantly.

Chapter 4

Enhanced EV and ICE vehicle energy efficiency through drive cycle synchronisation of deferred auxiliary loads

4.1 Introduction

Limited vehicle driving range, recharge infrastructure, and energy policy hinder electric vehicles (EVs) as a mainstream road transportation technology [57-64, 67, 68, 71, 72]. Energy from the EV main battery is required not just to drive the vehicle, but also to provide energy to the vehicle auxiliary loads [76, 127-129]. Auxiliary loads can be significant for heating and cooling the vehicle passenger compartment [130, 131]. Driving with air-conditioning (AC) systems in operation can use up to 20% more energy and reduce drivable vehicle range [132]. In addition, operating brake booster vacuum pumps, power steering pumps, electronic devices such as navigation systems, car computers and car stereos can add up to significant energy consumption, depending on driver preferences [74, 76, 128, 133, 134]. A considerable amount of energy is lost by operating friction brakes, and the majority of internal combustion engine (ICE) vehicles and EVs that do not have regenerative braking waste the kinetic energy available [40, 75, 85, 96]. Previous driving cycle experiments have shown that the amount of

kinetic energy available for potential reuse is significant and depending on the vehicle mass and the drive cycle, can increase vehicle energy efficiency by up to ~20%. Conventional vehicles use mechanical friction brakes that convert the vehicle's kinetic energy directly into waste heat and recently developed kinetic energy recovery using electric generators, flywheels, mechanical springs, compressed air absorbers (etc.) have been utilised to increase vehicle energy efficiency [40-43]. This research investigates the benefits of synchronising auxiliary loads with the vehicle's driving cycle to immediately use available kinetic energy rather than convert and store it in a battery with the associated conversion losses and micro charging issues. The aim of the experiment was to assess improvements in EV energy efficiency and to ascertain whether it is possible to maintain a comfortable temperature in the car by driving an AC compressor solely by the vehicle's kinetic energy during coasting or slow down. As compressors on cooling devices (fridges, AC, etc.) generally run on specified duty cycles, the experimental design enabled the option of synchronising the duty cycle to the drive cycle by operating the vehicles compressor every time the vehicle was slowing down or coasting.

4.2 Method

The test car (Figure 4-1) is a standard factory Ford Focus ICE vehicle that was converted by EV-Works in Landsdale, Western Australia (WA) into an all-electric EV and used in the WA Electric Vehicle Trial [118]. The EV is equipped with an electric main drive motor (80kW), controllers, a main battery (144V, 23kWh), and a manual factory gearbox. The Ford Focus' AC compressor is driven mechanically by a belt from the main motor drive shaft as commonly implemented in standard IC vehicles. The direct drive provided the option to drive the compressor mechanically, solely by recuperation through the vehicle's drive train whenever the vehicle was slowing down or coasting (Figure 4-2). Although the compressor is the largest energy consumer in an AC system, a considerable amount of energy is used for the AC condenser fan, vehicle compartment fan, and electrical compressor clutch - all powered from the main battery. While test driving on a chassis dynamometer provides a more uniform test environment [106, 114, 135], the absence of direct sunlight and heat makes AC testing on

an indoor chassis dynamometer unfeasible. Therefore, road testing was used to ensure realistic driving conditions where solar radiation and high temperatures are naturally present.

Figure 4-1 The research test vehicle: a Ford Focus converted to an EV

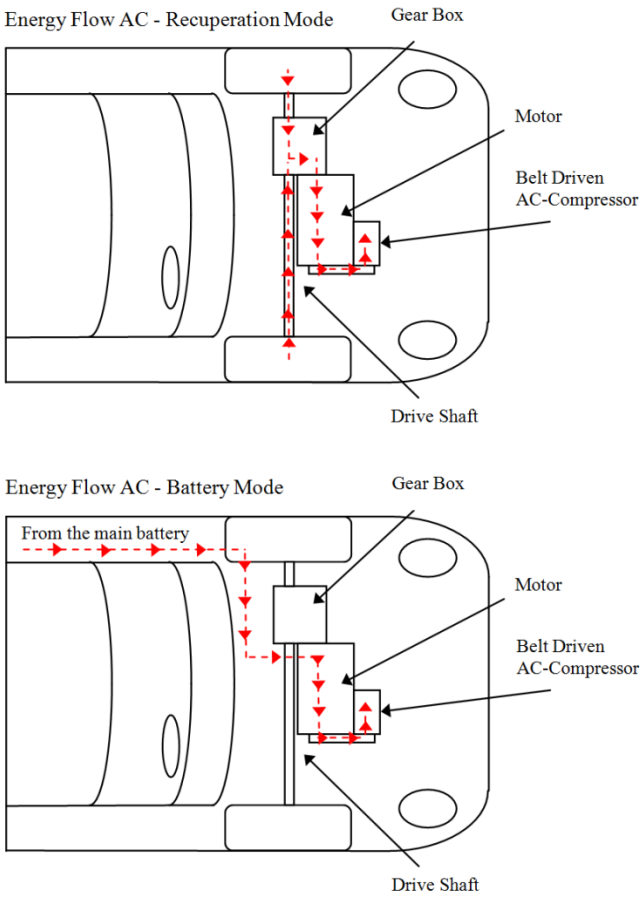

Figure 4-2 Power flows: schematic of the EV AC compressor driven by the main motor drive shaft in recuperation mode (top) and driven by the main battery in standard mode (bottom)

A 27 km test route was selected to represent city driving (Figure 4-3). The intention of the selected route was to create a relatively uniform driving pattern similar to the US Federal FTP75 standardised vehicle drive cycles commonly used in the automotive industry. The route starts at the University of WA in Crawley and follows Stirling Highway to Fremantle, with the midpoint of the journey between the west and east bridges across the Swan River; the return journey completes the route, terminating back at the university campus. To standardise the influence of incident solar irradiance on the vehicle temperature in the passenger compartment, the experiment commenced in November when the sun at solar noon is relatively normal to the Earth's surface. To achieve uniform testing conditions, the test drives were conducted over six consecutive days, starting each day at 11.45 AM and finishing at

2.15 PM. To reduce the influence from clouds on outdoor AC testing conditions, the test drives were conducted on a series of days with a relatively stable weather pattern with clear skies (Figure **4-4**).

Figure 4-3 The test drive route from the University of WA in Crawley to Fremantle, and back again

The level of thermal comfort of a person is a subjective concept specific to individuals and is dependent on external and environmental conditions on the whole body and individual body parts, and is also related to metabolic heat production and resultant body temperature adjustments [136]. For a passenger in a vehicle, the interaction of convective, radiative and conductive air exchange is very complex and a number of comfort indices are used, which rely on a variety of parameters to determine the degree of general comfort such as hypothalamus temperature, mean skin temperature, thermal insulation of clothing, air temperature, mean radiant temperature, air velocity, and humidity ratio [137, 138]. A standard

procedure is to use thermal manikins, surface sensors that simulate human bodies positioned in the vehicle seats, together with physiological and psychological comfort models, to assess passenger comfort in vehicles [139, 140]. In this preliminary study, for the purpose of simplicity only the ambient temperature and the EV passenger compartment temperature and RH in the different test drive configurations were measured and compared. The preselected temperature for the EV AC system while in standard operation was selected at a comfortable level for the driver, and was used as a benchmark to compare temperature and humidity levels achieved during the driving in recuperation mode. Prior to testing, the EV battery was fully charged and the vehicle was parked in the shade to prevent preheating by direct sunlight. Table 4-1 shows the testing strategies with its three different driving modes. During each test day the first test drive was driving with the AC in recuperation mode where the AC compressor was driven solely by kinetic energy. The second test drive on each day had the AC system switched on (standard operated without modification) and the third test drive had the AC switched off. The sequence of the experiments was chosen so that driving the first two experiments with AC kept the car's interior at a steady temperature. It was assumed that the driving without AC first (with open windows), would have heated up the car's interior excessively and would have influenced the subsequent experiments.

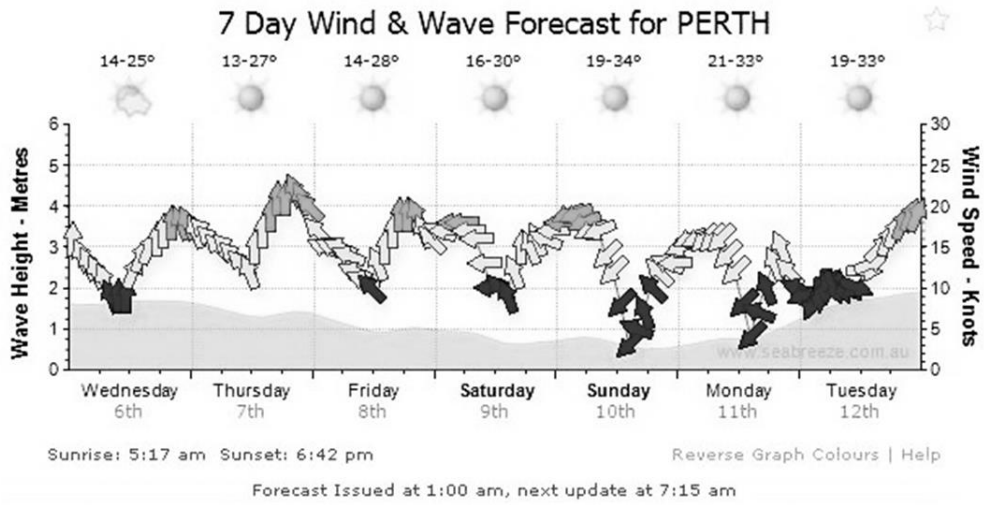

Figure 4-4 Weather patterns during the period of the outdoor EV testing [http://www.seabreeze.com.au/graphs/wa.asp]

Synchronising the AC duty cycle to the drive cycle by operating the compressor when the vehicle was slowing down or coasting required a modification of the electrical components of the AC system. The manufacturer's control strategy was bypassed by installing an AC clutch relay controlling the compressor so that the compressor only operated during the times when kinetic energy was available (Figure 4-5 and Figure 4-6). The system was designed such that when the inside temperature rises above a given temperature set point, the modified control system would be overridden and the compressor would operate as per the manufacturer's control system. The software was written by the primary author to log accelerator pedal position, vehicle speed, and passenger compartment temperatures. According to the vehicle status, the National Instrument (NI) interface switched the relay and the AC compressor on or off regardless of the manufacturer's control strategy. As modern cars with full electronically-controlled AC systems and engine management are interconnected by data-bus system (such as controller area networks or FlexRay), the modifications developed here can be easily implemented on modern EV and ICE vehicles, including other non-road modal transport.

Table 4-1 Testing schedule and AC operation modes during driving

Day	*Experiment*	*Day*	*Experiment*
1	1: AC ON; Recuperation ON	4	10: AC ON; Recuperation ON
	2: AC ON; Recuperation OFF		11: AC ON; Recuperation OFF
	3: AC OFF		12: AC OFF
2	4: AC ON; Recuperation ON	5	13: AC ON; Recuperation ON
	5: AC ON; Recuperation OFF		14: AC ON; Recuperation OFF
	6: AC OFF		15: AC OFF
3	7: AC ON; Recuperation ON	6	16: AC ON; Recuperation ON
	8: AC ON; Recuperation OFF		17: AC ON; Recuperation OFF

9: AC OFF 18: AC OFF

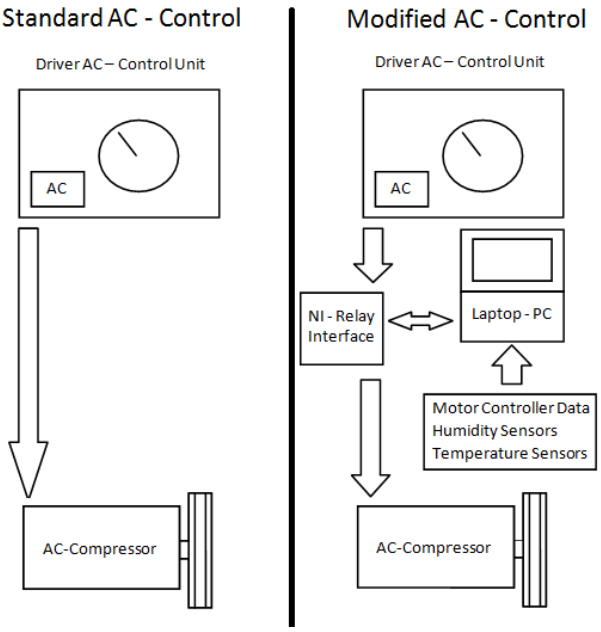

Figure 4-5 Schematic of a standard AC control system (left), and the modified AC control system (right) developed for the experiment

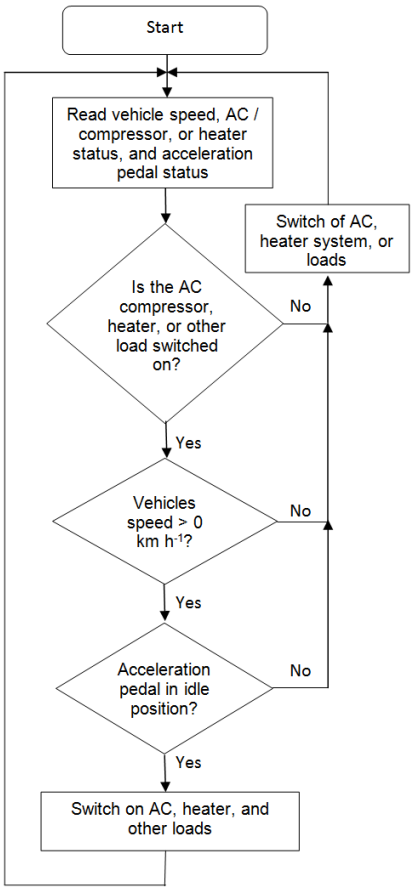

Figure 4-6 A flow chart of the control strategy for the modified AC control system

Figure 4-7 shows the custom-made data acquisition system designed, built, programmed, and calibrated under the AS/NZS ISO 9001:2000 standard to log: date and time; passenger compartment temperature; outside temperature; outside relative humidity (RH); passenger compartment RH, and vehicle speed. The passenger compartment temperature and humidity sensors were mounted at chest height in the centre of the EV. The outside temperature and humidity sensors were mounted in a shaded area underneath the EV to prevent direct solar irradiance influencing the readings. The EV chassis temperature was manually recorded by a hand held laser thermometer before and after each test drive. Quantification of the energy consumption (Wh km^{-1}) from the EV main battery during test drives was achieved by multiplying the logged average battery voltage, using the EV motor controller, by the battery Ah readings from a TBS energy meter, and dividing by the distance driven. The energy consumption was calculated without considering EV recharging losses.

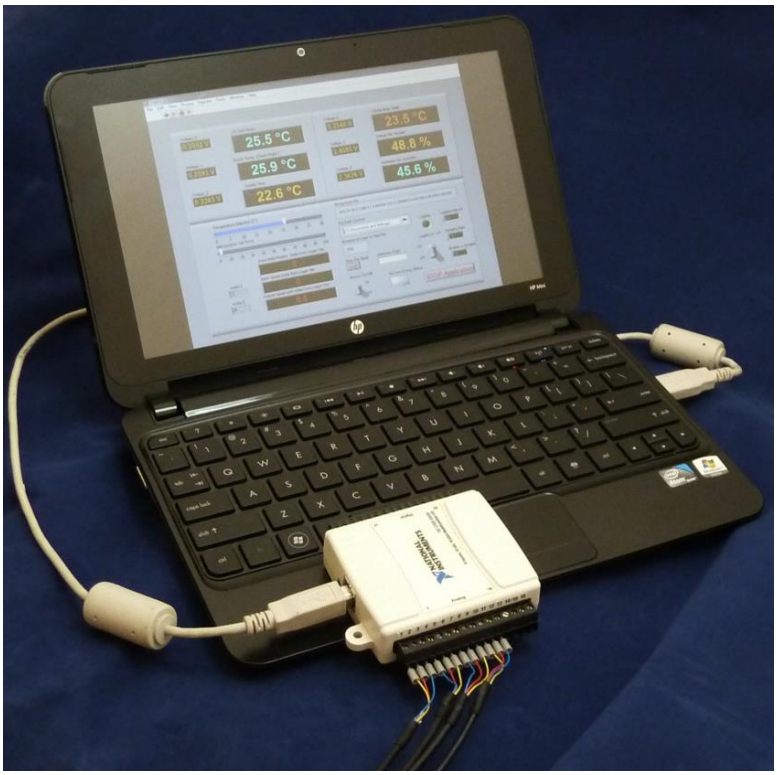

Figure 4-7 The custom designed logging system

4.3 Results

4.3.1 *Comparison of energy consumption*

Figure 4-8 shows the average energy consumption for each of the six days, as well as the overall average energy consumption when driving under the three different AC operating conditions. Despite the changing traffic conditions on the roads over the six days, the energy consumption for each day was relatively uniform. As expected, on all test days driving in AC recuperation mode required less energy than driving with the AC switched on, and driving without the AC achieved the lowest energy consumption. Figure 4-8 shows that in terms of overall average energy consumption, the highest value was 156.1 Wh km^{-1} with the AC

switched on, followed by driving with AC and in recuperation mode (148 Wh km^{-1}), and the lowest value was when the AC was off (139.9 Wh km^{-1}). Figure 4-9 shows a time series selection of one test drive cycle EV speed and compressor status when driving in recuperation mode. The data overlay shows how the compressor was switched on and off by the modified controller, triggered by the falling edge of the EV speed profile. The majority of the time in recuperation mode the compressor was driven by the vehicles kinetic energy. The modified control system was overridden for a couple of seconds only on the hottest days. The authors note that the speed profile is similar to standardised drive cycle profiles such as the FTP75 US Federal Drive Cycle.

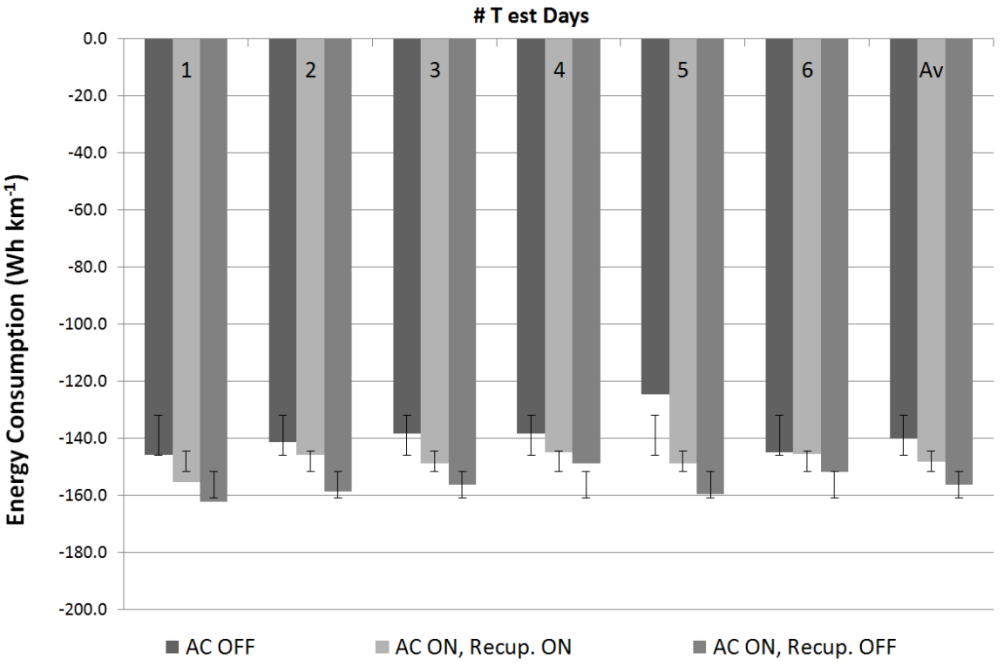

Figure 4-8 The Ford Focus EV average energy consumption over the six testing days and the overall average (in Wh km^{-1}) with standard deviation error bars

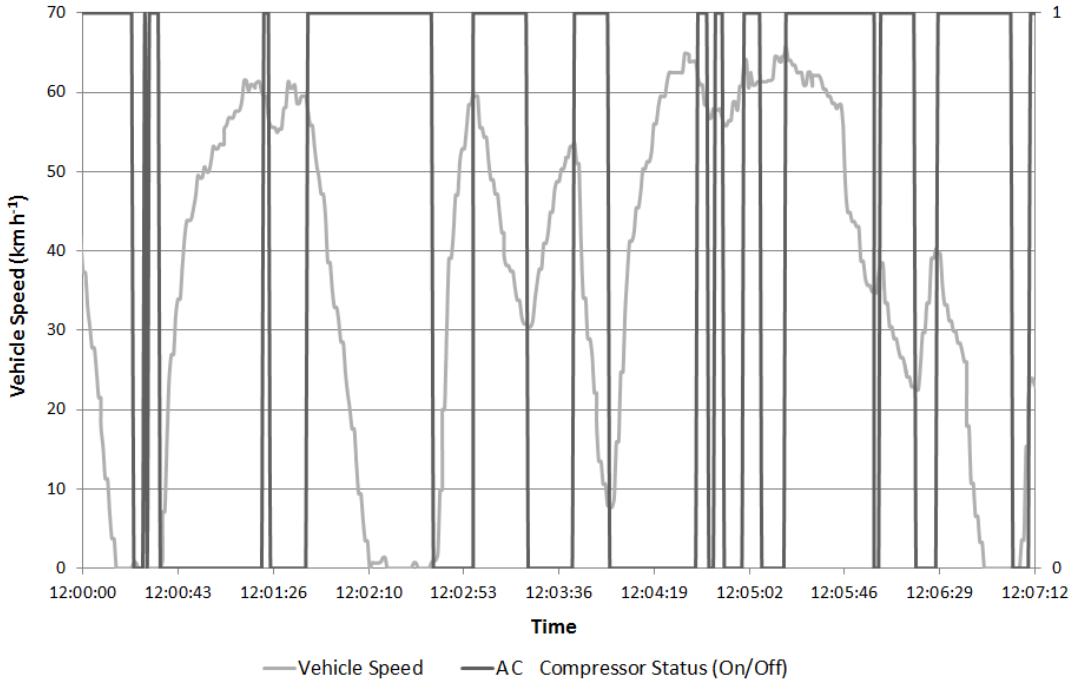

Figure 4-9 EV speed profile and compressor status operated primarily by recuperation

EV and passenger compartment temperature and humidity

Figure 4-10 presents the EV chassis temperature before and after each individual experiment, as measured by the hand held laser thermometer. The vehicle temperature variation (increase or decrease) during the test drives were between 2^0C to 8^0C. Over the course of the six test days the vehicle experienced an approximate increasing temperature gradient of between 1^0C to 3^0C due to the increasing daily weather maximums (between 25^0Cto 33^0C). The moderate chassis temperature fluctuations demonstrate a relatively uniform testing period for the daily consecutive test-drives. Figure 4-11 shows 16 min of the recorded temperature over the course of a test drive. For both AC modes, the falling passenger compartment temperatures indicate that the AC compressor is in operation whilst rising temperatures indicate that the AC compressor is switched off. In AC recuperation-mode the compressor was switched on by the modified control system whenever recuperation was possible. Therefore, as long as the inside temperature does not exceed the set point, the AC duty cycle and hence the temperature fluctuation was governed by the driving pattern. In contrast, the compressor duty cycle in the AC mode was controlled by the standard AC control mechanism. Both modes (AC ON;

Recup. ON) and (AC ON; Recup. OFF) show a similar temperature fluctuation of +/-2^{0}C due to their respective AC compressor duty cycles. Figure 4-12 is a scatter plot of the passenger compartment and outside air mean temperature versus the RH over the 18 test drives and three different driving configurations. The measured mean outside road air temperatures and RH ranged 25^{0}C to 41^{0}C and 6% to 50%, respectively. The average difference in passenger compartment temperature and RH in recuperation and standard modes over the six days was 0.6^{0}C and 5%, respectively. Thus driving in AC recuperation mode results in slightly higher temperatures and humidity but in general, the temperature range for both modes were similar, with 24^{0}C to 26^{0}C in recuperation mode and 24^{0}C to 26^{0}C in standard mode. There was greater variation in the RH range for both modes with 37% to 55%, in recuperation mode and 28% to 55%, in standard mode. Since the car windows were open during driving tests without AC, the passenger compartment temperatures and RH followed the outside temperatures and RH.

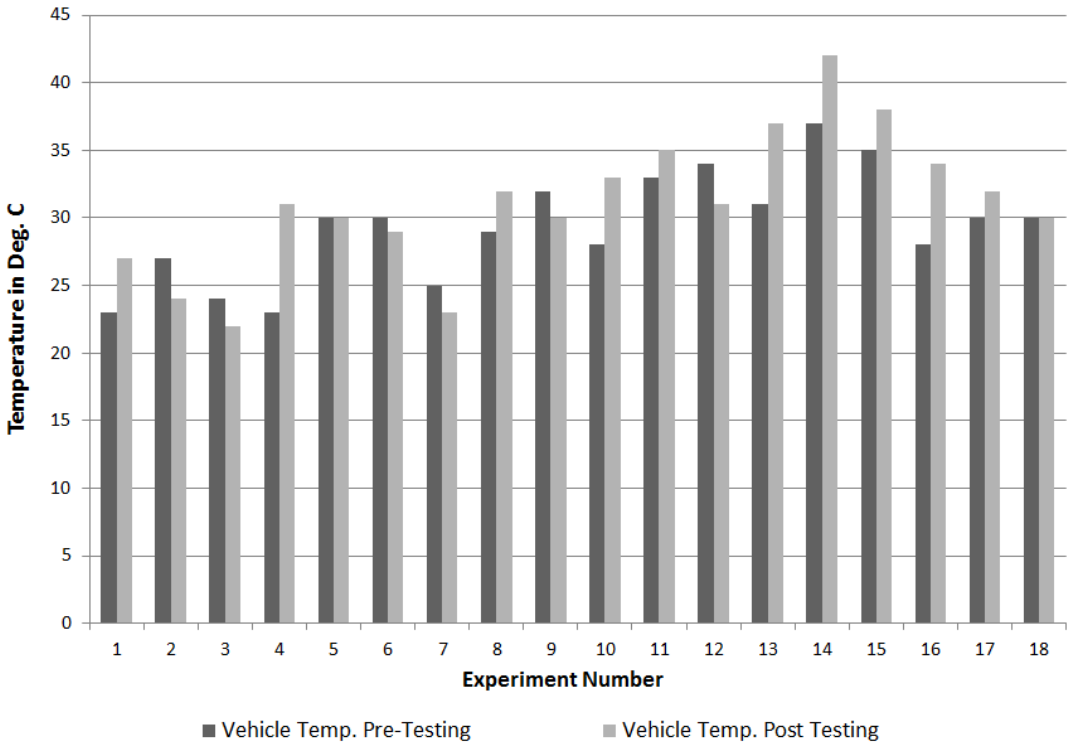

Figure 4-10 Vehicle chassis temperatures during the course of the experiments

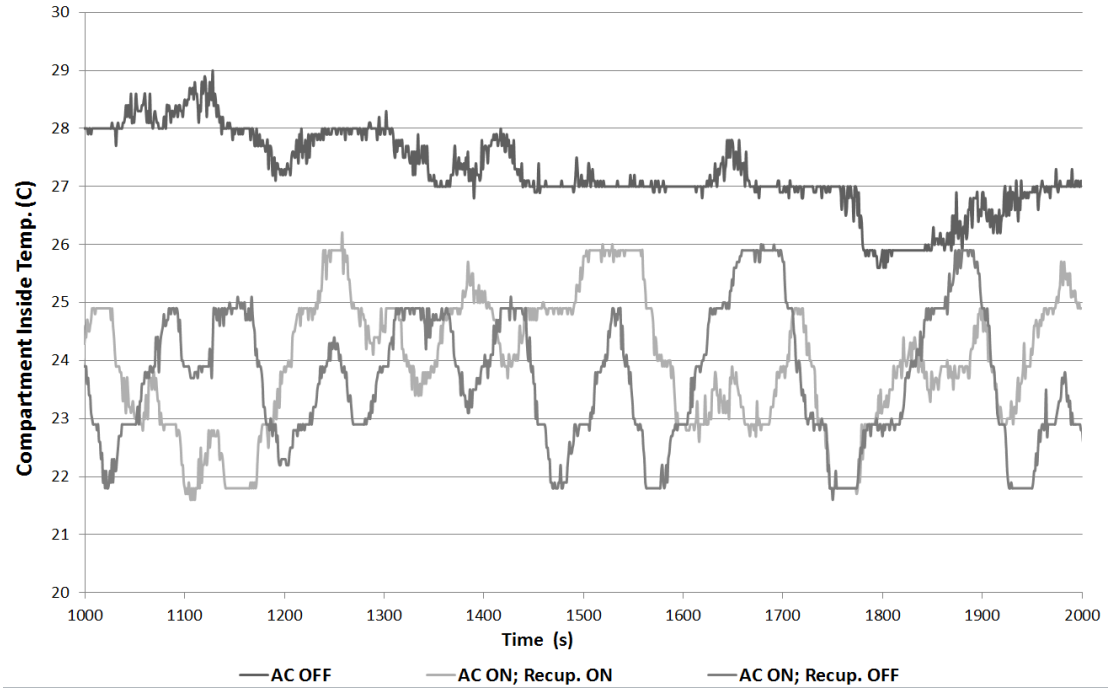

Figure 4-11 EV passenger compartment temperature fluctuations over 16 minutes of a test drive

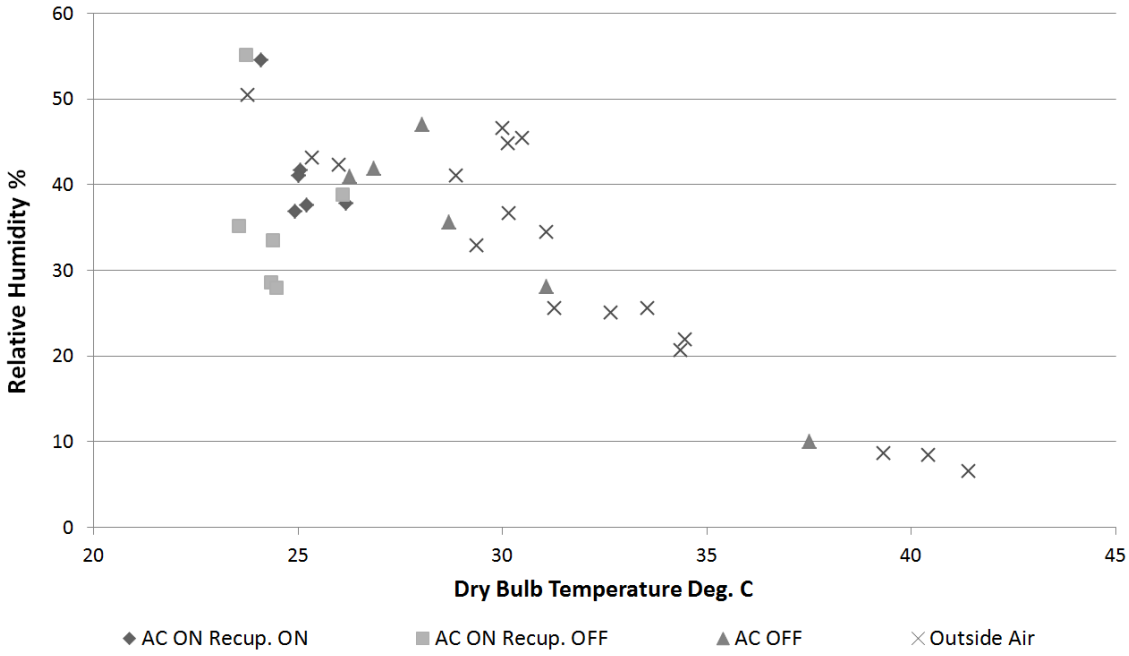

Figure 4-12 Outside air and passenger compartment mean temperatures and humidity over the six test days under different driving configurations

4.4 Discussion

4.4.1 *Energy consumption*

The overall energy consumption of each driving mode over all test drives was relatively stable. The lowest energy consumption was measured on day five (a Sunday) without AC, and was assumed to be due to less traffic congestion on that day. The results demonstrate that driving the vehicle with AC increased the energy consumption by 11.6% compared to driving without AC. By driving the EV in recuperation mode the energy consumption increased by only 5.8% compared to driving without AC. This represented a saving of 8.1Wh km^{-1}, or about half the energy recovered by previous research by the authors on a Lotus Elise EV conversion with a regenerative braking system (RBS) on a comparable drive cycle. In a vehicle with an RBS and without the synchronised auxiliary system the 8.1Wh km^{-1} would be reduced by the losses associated with the EV battery charging and discharging. Similarly, in a conventional ICE vehicle with a synchronised auxiliary system, this would enhance energy efficiency even without a RBS or battery storage system.

Energy efficiency values are in terms of the power consumption from the battery compared to the distance driven. If the recuperated kinetic energy could run all components of the AC system then one would expect the energy efficiency to be similar to the situation with the AC off. As mentioned in Section 4.2, not all the energy required for the AC system, however, can be recovered from the available kinetic energy. The main battery is required to power the AC condenser fan, vehicle compartment fan, and electrical compressor clutch, with the AC condenser fan alone drawing approximately 300W of power. Figure 4-11 shows that there are differences in the duty cycling of the AC compressor in the two different modes. In standard operation the duty cycling is temperature dependent. When the desired temperature is achieved, the control system switches off the compressor, and when the temperature increases above a preset level, the compressor is switched on again. Such an on/off scenario was observed during the test drive with AC switched on. In recuperation mode, the compressor

was switched on by the modified control system whenever recuperation was possible and the AC duty cycle was vehicle speed dependent, as illustrated in Figure 4-9. The difference in these duty cycle operations is another reason that explains the relative energy efficiency values for the two modes in relation to the situation with the AC off. However, if the inside temperature exceeded the set point while driving with the AC in recuperation mode, the AC operation would revert to standard mode. This was a limiting factor in the energy efficiency gains of operating the AC in recuperation mode.

4.4.2 *Temperature and RH*

Figure 4-11 and Figure 4-12 show that the available kinetic energy from the EV thermal mass enabled the maintenance of temperatures and RHs within a similar comfort region as driving with the AC switched on. Driving without AC required opening the windows of the EV. Although some airflow from the outside provided some relief during the milder days, the driver experienced significant discomfort during the warmer days. Figure 4-12 shows how the test drive inside temperatures without AC followed the ambient temperatures through to the hottest day when 41^0C was recorded. Furthermore, solar radiation, noise, and air pollution levels inside the passenger compartment by driving the vehicles without AC and with windows open reduced the driver's subjective comfort level. The results demonstrate it is possible to maintain the test driver's subjective comfortable temperature (< 25°C) and humidity (<55%) levels inside the EV by operating the AC compressor solely from recovered kinetic energy. The driving style is an important factor to consider for the recuperation system as significant amounts of kinetic energy would be lost as heat by abrupt braking. The authors emphasise that efficiently driving a car with recuperation systems requires drivers to be cognisant of immediate traffic conditions ahead, and the use of moderate braking. Additional limitations of this research include the recovery of kinetic energy to drive large loads such as an AC system, the success of which depends on how much energy can be saved, and if a comfortable level of car inside temperature can be maintained. The research did not include the efficiency investigation of the whole AC system. It was limited to investigate options to drive the compressor by kinetic energy. Further research may include investigating the efficiency of the AC system with its fans and insulation properties and the cooling

performance in conjunction with a latent cold storage system, and a detailed study about thermal comfort in a vehicle using surface sensors that simulate human bodies in seats and additional physiological and psychological comfort models.

4.5 Conclusion

The findings show the potential for increasing the energy efficiency of EV, ICE, and hybrid vehicles by recuperating energy through synchronising a large auxiliary AC load. The results show that a considerable amount of kinetic energy is available to operate an AC system or other large auxiliary loads during urban driving. The drive cycle and auxiliary AC load synchronisation was effective at maintaining a comfortable range of passenger compartment temperature and humidity when in recuperation mode, while a very uncomfortable cabin environment was experienced on days without AC operation during the warmer (>40^0C) ambient temperatures. Modern vehicles with electronically-controlled AC and engine management systems interconnected by a data-bus system may be modified to synchronise with the AC system using a simple software update only. Implementing similar recuperation strategies into mainstream EVs, hybrids, and ICE vehicles will require further research, including: impacts on the AC compressor clutch or other AC components of an assumed increase in short-run duty cycles, and: the option of using a latent cold storage system with the AC to store the additional kinetic energy available and enable improved synchronisation. The authors also recommend researching the influence of ‘everyday’ driving behaviour on EV and ICE vehicle energy efficiency modifications.

Chapter 5

Smart Accelerating and Braking Achieving Higher Energy Efficiencies in Electric Vehicles

5.1 Introduction

The overall efficiency, energy storage capacity, recharge technology and driving range for EVs have increased significantly over the last decade. If the energy to charge the EV is generated from fossil fuels, however, efficient operation is critical to utilize the potential range and to reduce CO_2 and other emissions.

In contrast to a plug-in hybrid electric vehicle (PHEV) an EV does not accommodate a combustion engine (ICE) (Figure 5-1). The main components of an EV power train are the traction battery, cabling, motor controller (MC), an electric motor (EM), reduction gear, drive shafts, bearings and wheels.

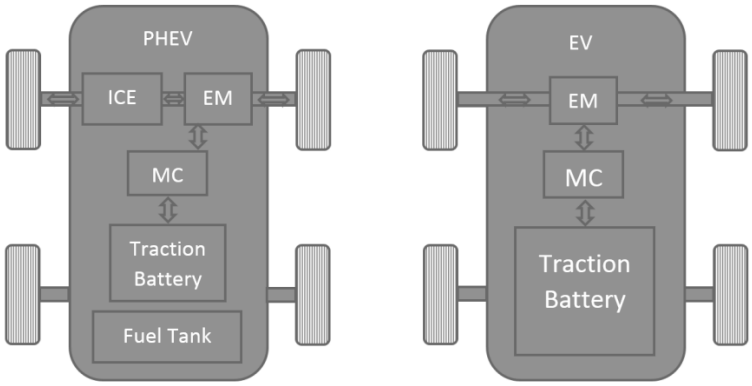

Figure 5-1: A basic block diagram of a power train of a PHEV and EV

Every component in the power train has inherent losses. Power train efficiencies vary depending on environmental, vehicle and driving conditions. For example, the traction battery's internal resistance increases under very cold environmental conditions reducing its efficiency.

The electrical flow rate of the current from the battery to the motor is controlled by a motor controller, which determines the drive direction, vehicle speed and acceleration. In modern EVs the controller is also responsible for deceleration. By using its traction motor as a generator, it converts the moving vehicle's kinetic energy into electricity and feeds it back to the battery. Different types of electric motors and controllers have different efficiency regions, which depend on load and rotational motor speeds, or revolutions per minute (rpm). Figure 5-2 shows an example of a motor and inverter efficiency map with overlaid test results from an experiment on a Nissan LEAF conducted by Oak Ridge National Laboratory (test results not further discussed) [32]. In Figure 5-2, the vertical axis shows the torque (load) applied to the motor and controller and the horizontal axis shows the motor's rotational speed, which increases proportional to the vehicle speed. Accelerating a vehicle under low loads, the controller and motor would operate briefly under high torque and then at low torque, mainly on the bottom of the chart under relatively low efficiency. Increasing the load at already low speeds and maintaining it would drive the motor and controller into the more efficient (dark) regions. The research question for this study is how EVs need to be operated such that rpm and motor load match the more efficient (darker) regions.

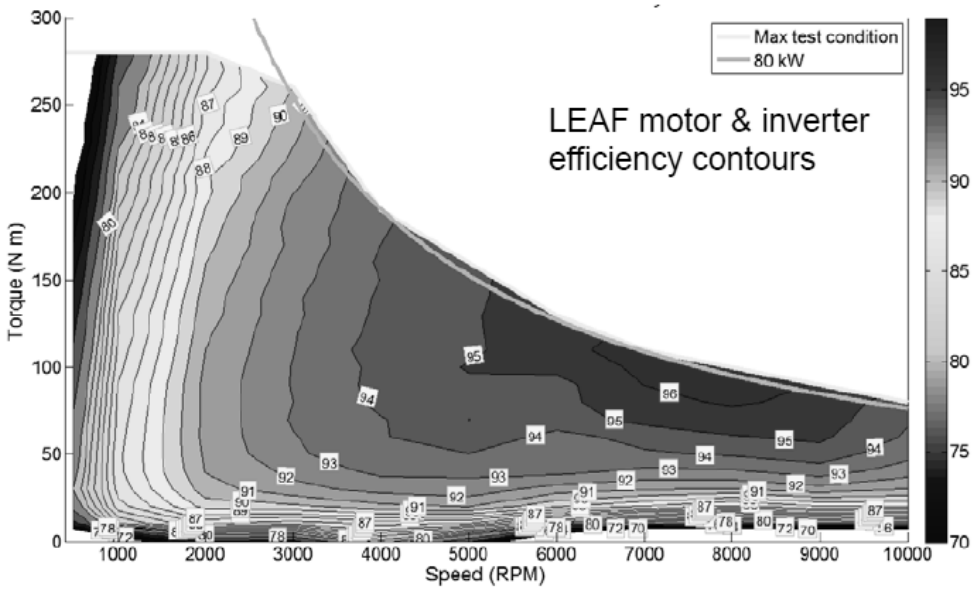

Figure 5-2: A Nissan Leaf efficiency map and overlayed test results at 80kW up to 10,000 rpm Reproduced with permission from Oak Ridge National Laboratory [32]

In a stop-and-go scenario typically for inner city driving, cars have to accelerate and decelerate frequently. Depending on driving style and traffic conditions, EV motor loads and rpm change continuously. Unlike combustion engine and hybrid vehicles, EVs do not shift gears, which means that the ratio of motor rpm to vehicle speed is fixed i.e. the driver cannot influence motor rpm versus vehicle speed. In contrast the load (Nm) can be adjusted by the vehicle's acceleration or deceleration rate. If an EV's motor and controller are loaded low, their efficient region (Figure 5-2, dark region) might be missed. Currently there is no driver feedback on a EVs instantaneous acceleration or deceleration rate on commercially available EVs. As a consequence, accelerating or decelerating throughout efficient regions is difficult to achieve, even if the driver is aware of these effects. A potential solution to overcome this issue is to implement multi-speed EV transmissions [141] [46] [142] but this would result in higher costs and the increased vehicle weight might cause additional efficiency losses.

So far, a number of studies have investigated real road energy consumption[143] [144] [145] and energy consumption modeling [146] [147] [148] [149], efficient operation and

performance of energy recovery systems (RBSs) in PEVS and EVs [150] [151] [152] [153] [154] [99], modeling on PHEVS and EVs drive trains [155-157] [158, 159] and studies motors and controllers have been conducted under various driving scenarios and driving conditions[160] [161]. Most of these studies are focused on efficiency, energy consumption and RBS gain by driving along speed profiles on a predefined standardized driving cycle [162]. For example on the New and Extra European Driving Cycle (NEDC, EUDC) the speed changes significantly from 0 km/h to 120 km/h. In these driving cycles, however, acceleration and deceleration rates remain low and do not change significantly [163] [32]. Such a driving pattern might not require a high load for the motor at low speeds and might operate inefficiently. In contrast, this study focuses on the impact of significantly changing the load by changing the rate at which the EV accelerates to a particular, fixed speed. Under real road conditions, the authors investigate whether it is possible to load the power train early at low driving speeds (*smart acceleration*) in order to operate the EV in its most efficient region as early and for as long as possible. This research aims to test whether such a driving technique can reduce energy consumption or whether other factors in the power train might reduce efficiency under high loads and therefore outweigh the expected efficiency gain. Furthermore, the authors investigate how efficiency changes under deceleration via RBS (*smart braking*) by changing the loading (*deceleration rate*) of the motor operating as a generator (*recuperation*). Although Vaz et al. [164] investigated the effect of high loading of controllers and motors using numerical modeling, there are currently no studies that investigate this issue on a EV under real road conditions. This research aims to address this gap in the literature.

5.2 Methods and Materials

5.2.1 *Road and test-drive conditions*

To observe the change in efficiency for specific acceleration and deceleration rates, a battery EV was exposed to a series of acceleration and deceleration scenarios for a predefined speed and distance to be driven. The test-driving was conducted on a used Nissan Leaf (32,000 km). The Leaf is manufactured with an 80 kW (110 hp), 280 Nm electric motor and a 24 kWh traction battery. The test runs were carried out on an 800m long and flat public road, running north-south. The experiment was conducted over several days but under almost identical

environmental and vehicle conditions, such as temperature, wind and dry road surface. For all tests, auxiliary loads such as heater, air conditioner and headlights were switched off. Although the tests were on a flat surface and scheduled for calm days, each test involved driving the Leaf in both north and south directions along the test run and the results were averaged to compensate for small changes in surface or wind directions. The test driving for the acceleration experiment involved a total of 50 test drives with ten drives (five times north and five times south) for each of five different acceleration rates. The deceleration experiment involved 30 test drives with ten drives (five times north and five times south) for each of three different regenerative braking system (RBS) settings.

To maintain an identical state of charge (SoC) of the traction battery, the vehicle was fully charged on each new test day. In order to achieve uniform test conditions, the tyre pressure was checked before each test drive and the vehicle was always driven the same distance to the same test area. Before conducting a new full set of tests, some previous tests were repeated and the results compared to ensure identical test conditions and reproducibility of the results.

5.2.2 *Acceleration and deceleration tests*

To characterize the required loads for the motor and controller, preliminary acceleration tests were conducted and analyzed. These test provided an indication of the required accelerating and decelerating rates to load the motor and controller across its inefficient and efficient regions.

It was assumed that the relatively low EUDC acceleration rate would operate the vehicles motor and controller below and outside its efficient region. Therefore as a starting reference the aim was to accelerate the vehicle as close as possible to a rate of 0.47 m s^{-2} so as to follow a EUDC [163] [32] while limiting the speed range from 0 to 70km/h. The acceleration rate (load) was then further increased in five steps until full load and acceleration was achieved.

The slowest acceleration rate resulted in the longest distance covered and this distance was used as the base case. Obviously, the faster acceleration rates reached 70km/h in a shorter distance. To correct for the energy used over the remaining distance, the vehicle's energy consumption at a cruise speed of 70km/h was measured separately and added for the remaining distance. This method was applied because preliminary tests showed that logging

energy consumption over the acceleration section as well as the remaining distance resulted in inaccurate measurements. This was due to the time required for the vehicle to stabilize the speed and energy consumption at 70km/h, limited sampling rates and the relatively short distance driven for the compensation. The same technique was applied for the deceleration experiment. To cover the same distance, test-drives with high deceleration rates required the EV to slow down at a later stage of the test run. The energy required for the compensation distance driven at a stable speed of 70km/h was added to the overall energy recovered. 70km/h was chosen because it is a common speed limit in the urban areas of Perth, Western Australia, where the experiment was conducted.

To achieve a uniform and consistent acceleration demand signal, an adjustable mechanical pedal stop (Figure 5-3a) was installed. During the experiment each acceleration rate was predefined and the mechanical pedal stop adjusted accordingly. During each acceleration test the pedal was pressed until the mechanical stop limited the movement of the acceleration pedal. For the full acceleration, the mechanical pedal stop was removed and the pedal operated at the full power position.

Table 5-1 shows how the acceleration rates from 0 to 70km/h and how it relates to the more commonly used acceleration time in seconds.

Table 5-1: Acceleration rates and times taken in accelerating from 0 to 70km/h

Acceleration	***[m·s^{-2}]***	***Time for 0 to 70 km/h [s]***
	0.49	40
	0.66	30
	0.92	20
	1.26	15
	2.77	7

For the deceleration scenarios the experiments aimed to slow down the vehicle by recuperation only i.e. not using the friction brakes. To obtain the three uniform deceleration rates the vehicle was decelerated by manufacturers preset settings in two cases and by a driver-controlled RBS setting in the third case. The first setting, D-Mode, provided the lowest RBS setting (low load) and hence low deceleration rate. The second setting, Eco-Mode, provided a stronger RBS setting (medium) and a higher deceleration rate. The highest and full deceleration rate was achieved by manually controlling the RBS settings by the brake pedal. For the full RBS load the pedal was pushed until the vehicle's internal power meter showed full recuperation power (Figure 5-3b) but without activating the friction brakes. At the lower RBS threshold the RBS management system disables the regeneration and causes a gap in brake torque. This was noticeable by the driver and an indication the friction brake was not activated during the particular deceleration.

As this test was carried out under real road conditions on public roads, a computer-controlled servomotor generating a uniform motor controller demand signal could not be used due to safety reasons.

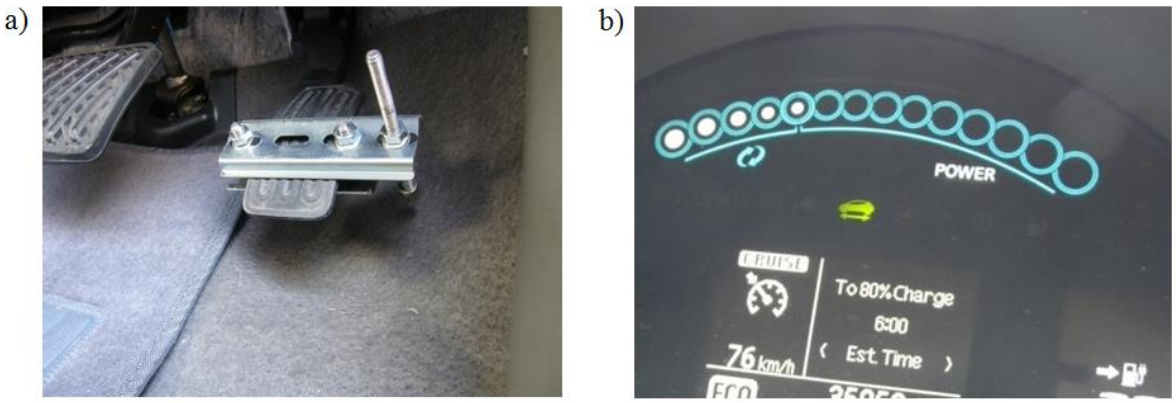

Figure 5-3: (a) An adjustable mechanical pedal stop provided a uniform acceleration demand signal and (b)the vehicle's internal power meter under full recuperation provided driver feedback for the highest deceleration scenario

5.2.3 *Data collection during test drives*

The following parameters were logged during the test drives: energy consumption [Wh], voltage [V], current [A], battery temperature [°C], time [s], distances [m], speed [$m \cdot s^{-1}$], torque [Nm] and motor rotational speed [rpm].

To monitor the change in energy consumption and hence the energy efficiency of the vehicle during the acceleration and deceleration experiments, the battery power [W] was obtained from the vehicle's internal instrumentation system via the controller area network (CAN). To include cabling and other losses in the electrical and mechanical drive train system, the experiment focused on the battery power rather than the motor power.

It was of concern that the battery temperature would increase during the experiments, in particular by accelerating several times under full load. An increased battery temperature potentially changes the internal resistance and it was thus important to record the battery temperature to check the extent to which the measured energy data might be distorted. The Nissan Leaf battery pack accommodates internal temperature sensors and the temperature data were available from the vehicle's CAN bus.

The CAN bus was accessed via an onboard diagnostic connector (OBD2) [165]. For the hardware interface a commercially available CAN tool was used [166] [167]. During preliminary tests the data from the CAN tool was transmitted via a Bluetooth terminal to an Android computer system. Preliminary results showed that commercially available CAN software update rates were too slow. For example, the Leaf Spy Pro CAN bus application update rate was limited to 0.5 Hz [166]. Our tests showed that Leaf Spy Pro requests a significant amount of data (up to 153 variables) from the CAN bus, resulting in slow update rates. Many of these variables were not required for our experiment, however the application did not allow for only selected variables to be accessed. To increase the update rates, a custom built LabView [163] application was programmed and only the data required for our experiment were transmitted. Specific hex commands for the selected data were transmitted via the CAN bus interface [165]. Data was averaged and logged every second to a text file for subsequent analysis.

To further reduce the data requests on the bus, the vehicle speed was acquired from an external GPS device (5Hz update rate) rather than through the GPS data from the CAN bus [167]. The data from the GPS device was streamed via USB in parallel to the LabView

application (Figure 5-4). In addition to these parameters, there was a need to obtain information on the motor torque. While this could be achieved using an onboard rotary torque transducer kit, it would require intrusive vehicle modification. Instead motor rotational speed [rpm] and battery power [kW] data were used to approximate the motor torque [Nm]. The disadvantage of this technique is that it introduces uncertainty due to the unknown power losses between the battery and the motor. The battery power will be higher than the motor power so the calculated torque will be somewhat overestimated. Since these experiments focus on the change in torque (relative torque) rather than absolute torque, this error was assumed to be negligible.

5.2.4 *Data analysis*

The measured energy [Ws] consumption was derived by integrating the battery power over the acceleration time and averaging over the driving period. The calibration and accuracy of all instrumentation used in the experiments was limited to the short CAN bus update rates, the vehicle's unknown internal sampling frequencies, as well as the EVs manufacturer's instrumentation calibrations and quality standards.

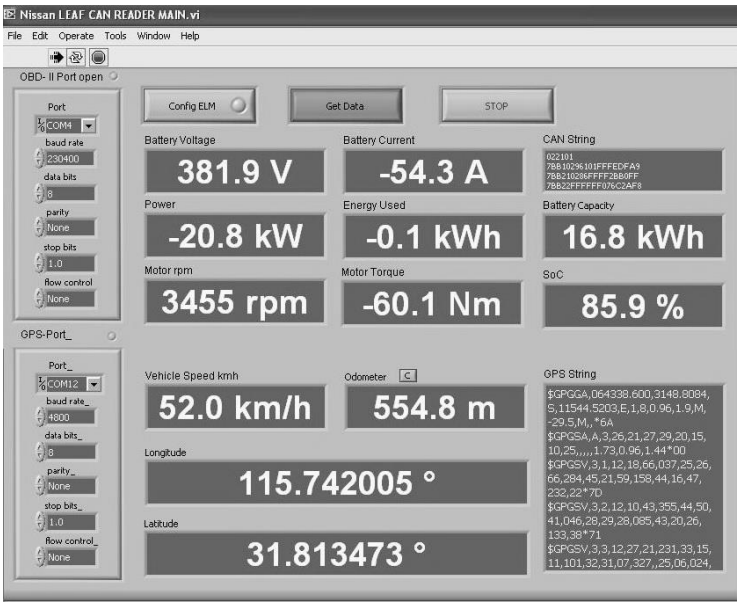

Figure 5-4 Screenshot of the custom built LabView windows application acquiring data from the CAN bus and the GPS module

5.3 Measurements and Results

Eighty test-drives under real road conditions with predefined and controlled acceleration/deceleration rates were carried out using a Nissan Leaf. For each test-drive, the energy consumption [Wh], voltage [V], current [A], battery temperature [°C], time [s], distances [m], speed [km/h], torque [Nm] and motor rotational speed [rpm] were recorded using a custom-built Labview CAN bus application data-logging tool. The custom-built CAN bus application sampling rate logged data reliably up to 2Hz. Faster sampling rates, up to 4Hz, were possible, but sampling at these rates over longer times, such as over the time of an experiment, resulted in unreliable data acquisition. Thus a reliable sampling rate of 2Hz was used for all test drives.

During the eighty accelerations/decelerations the custom-built Labview CAN bus application provided a reliable data-logging tool. Adapting the source code can make this tool suitable for experiments with other EVs as well. For logging acceleration and deceleration rates, both the simple mechanical stop mounted on the acceleration pedal, as well as the Eco-, D- and Manual-mode of the RBS were accurate and reliable.

5.3.1 *Energy requirements for different acceleration rates*

Figure 5-5 shows the energy required to accelerate from 0 -70 km/h, split into the energy for acceleration, cruise, and total energy during the series of five acceleration rates. As each test drive was over the same distance of 505 ± 17m, the energy required to drive at cruise speed was added to the four faster accelerate rates. For the cruise energy at 70km/h an average energy consumption of -125 ± 11Wh/km was measured, where the convention is to use a negative sign for energy consumption. During the acceleration experiment the slowest acceleration rate 0.49 $m \cdot s^{-2}$, almost identical to the target 0-70km/h EUDC acceleration rate of 0.47 $m \cdot s^{-2}$, required 178 ± 4Wh of energy. The increased acceleration rates to 0.67 $m \cdot s^{-2}$, 0.93 $m \cdot s^{-2}$ and 1.26 $m \cdot s^{-2}$ required -153 ± 3Wh, -159 ± 3Wh and -172 ±4Wh, respectively. Under the vehicle's full acceleration rate of 2.78 $m \cdot s^{-2}$ the energy required was -184 ± 13Wh. To complete the remaining distance of 505m the vehicle required between -12Wh to -50Wh ± 0.5Wh.

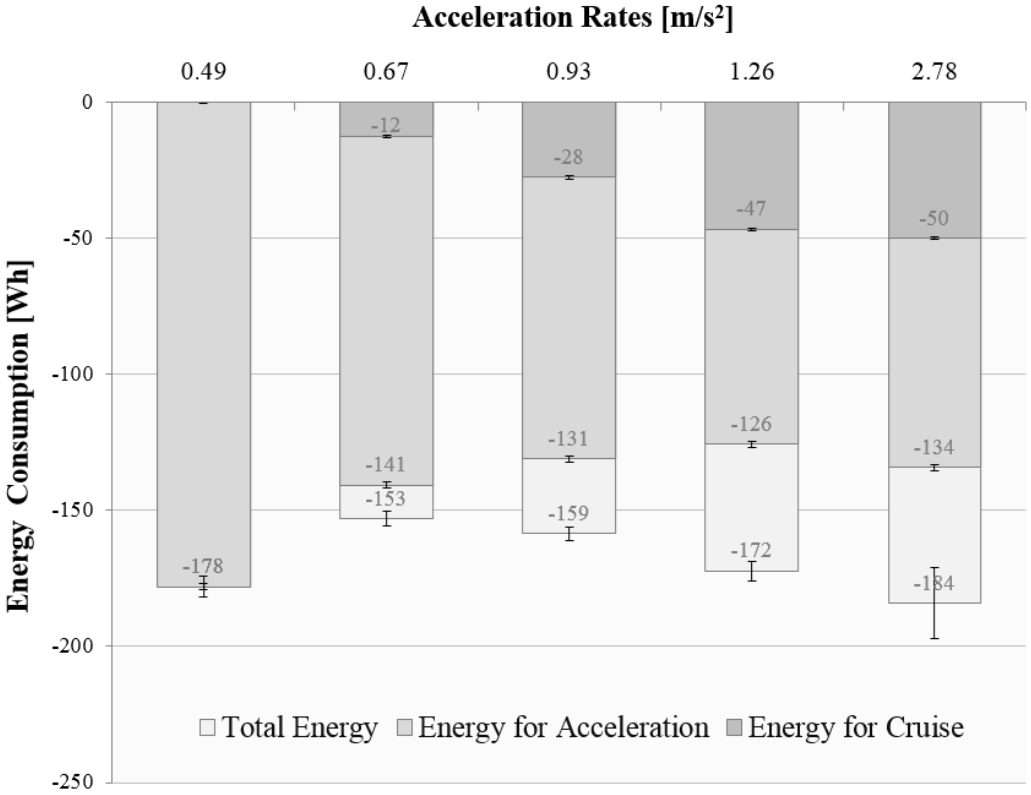

Figure 5-5: Energy requirement for accelerations, cruise, and total energy during for different acceleration rates

The main focus of this study was to investigate whether changing the acceleration rates would allow the motor and controller to operate in the optimal region of the efficiency map. Figure 5-6 shows measured and calculated variables overlaid onto a scaled section of the Nissan Leaf's efficiency' map. It shows how the increased acceleration rate requires a higher torque with an increased load at relatively low rpm or vehicle speed. According to the efficiency map, the maximum indicated controller/motor efficiency was 94%, occurring over a short period of motor speeds (between around 3,700rpm and 4,500rpm) at an acceleration rate of 1.26 $m \cdot s^{-2}$ and a torque of around 80Nm. While the traces for the four lower acceleration rates are following the efficiency map, the trace for the highest acceleration rate of 2.78$m \cdot s^{-2}$ overshoots the theoretical maximum torque. Potential reasons for this are further discussed below.

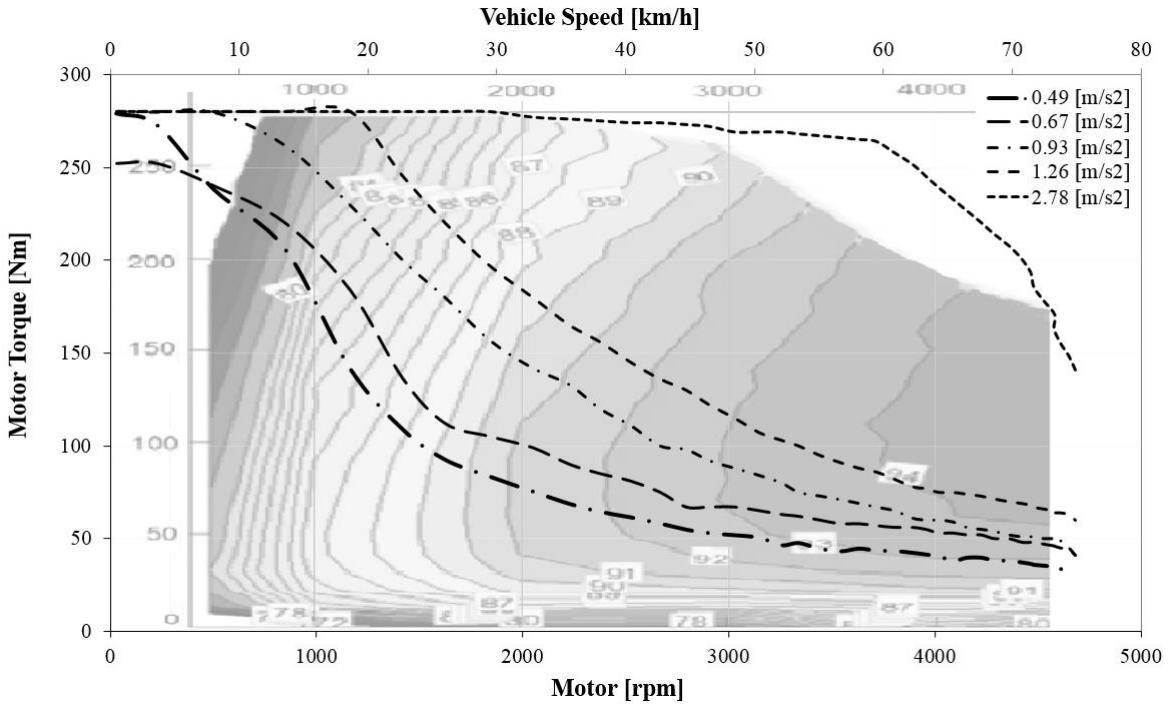

Figure 5-6: Measured data from test drives with five different acceleration rates overlaid onto a section of the Nissan Leafs motor and controller efficiency map (Background reproduced with permission from Oak Ridge National Laboratory [32]

Energy recovered from different deceleration rates

Figure 5-7 shows the energy recovered during deceleration from 70 km/h – 0 km/h, the cruise and total energy (gained net energy). During the slowest deceleration rate of -0.34 $m \cdot s^{-2}$, driving in D-Mode, the RBS recovered an average energy of 36Wh ±1Wh. Over the whole decelerating distance of 554m ± 7m the vehicle continuously decelerated from 70km/h to 0km and no cruising energy was added to the recovered energy. Thus, the recovered energy and net energy are identical with the gained net energy. The same holds for the acceleration of all test-drives covered the same distance. As discussed under *Acceleration and deceleration tests*, the energy required to drive at cruise speed was added to the two lower deceleration rates (Eco-mode and Manual). In Eco-Mode the extra cruise energy was -29Wh ±0.5Wh. Increasing the RBS setting to Eco-mode the deceleration rate increased to -0.57$m \cdot s^{-2}$, resulting in the average recuperated energy to increase to 58Wh ± 1Wh. In Manual mode (the strongest RBS setting) the vehicle was decelerated at a rate of -0.88$m \cdot s^{-2}$ and recuperated 63Wh ± 1Wh. Due to the

even shorter deceleration distance, the compensated energy for cruising at 70km/h increased to -46Wh ± 1Wh. Adding the cruise energy to the recuperated energy resulted in a net energy gain of 36Wh for the D-Mode, 29Wh for the Eco-Mode and just 17Wh for the Manual mode respectively. Although Manual-mode recovered most energy than D-Mode and Eco-Mode, its net energy recovered was lower due to the longer cruise period.

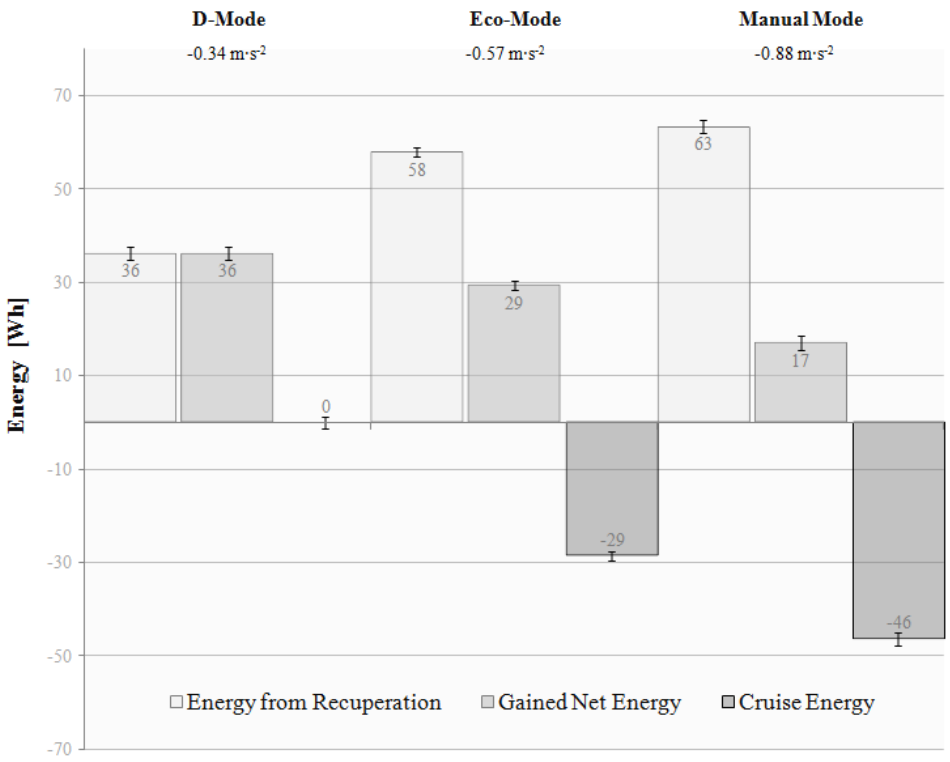

Figure 5-7: Energy recovered during deceleration, cruise and total (net energy) during the series of three decelerations from 70km/h to 0km/h.

As mentioned above it was of interests to know which of the three different vehicle loadings controlled by the RBS settings results in the motor/controller operating in the ideal region of the efficiency map. Figure 5-8 shows the measured and calculated variables overlaid onto a scaled section of a Nissan Leafs traction efficiency map. Note that this map is indicative only since Nissan's official efficiency map for recuperation could not be obtained due to issues of intellectual property. However, investigations on motor and controller efficiency from other research projects showed that efficiency properties for traction and recuperation are relatively

similar [168] and it was assumed that the efficiency for the Nissan Leaf is similar for traction and for recuperation. Figure 5-8 shows how in Manual mode (full recuperation) at high rpm the torque rises steeply into efficient regions of the motor/controller, but never reaches full efficiency of 96%. The maximum measured efficiency was 94% over a short rpm range of around 4500rpm to 4200rpm. Slowing down in Eco-mode or D-mode reduces the motor recuperation torque significantly. As a consequence, the motor/controller operates in a less efficient region.

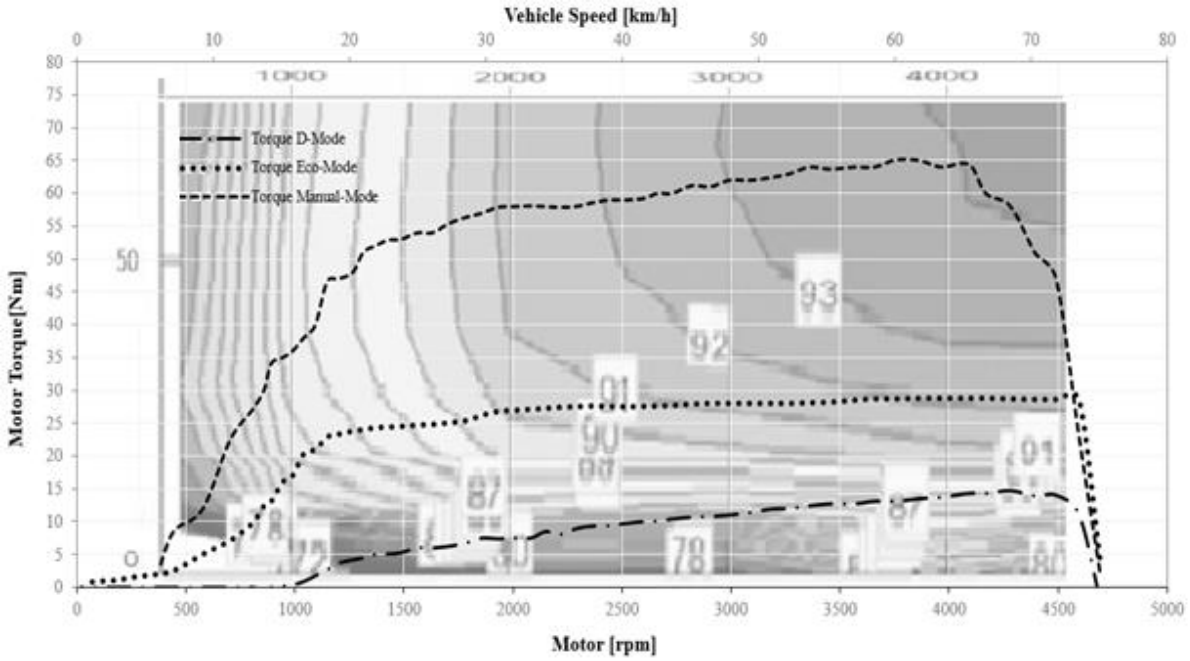

Figure 5-8: Measured data from deceleration tests overlayed onto a section of the Nissan Leafs motor and controller efficiency map during the three deceleration scenarios (Background reproduced with permission from Oak Ridge National Laboratory [32])

5.3.2 *Effect of battery temperature*

Temperature can affect the internal resistance of the traction battery and thus affect efficiency. To ensure this did not affect the results, in particular during test drives with high acceleration rates, temperature was logged over acceleration/decelerations test drives. Figure 5-9 shows the average battery temperature, ambient temperature and motor power as a function of time

taken from a test drive with a moderate acceleration rate (0.49m·s^{-2}, to 1.26m·s^{-2}). The data shows that the ambient temperature remained stable and fluctuated less than 0.5°C. After around 45minutes of moderate driving, shortly after the full load sections of the experiment, where the vehicle accelerated under full power, the temperature started to rise. Measurement in the cells' core was not possible and the thermal lag from the battery core to the sensors is noticeable on the delayed temperature rise.

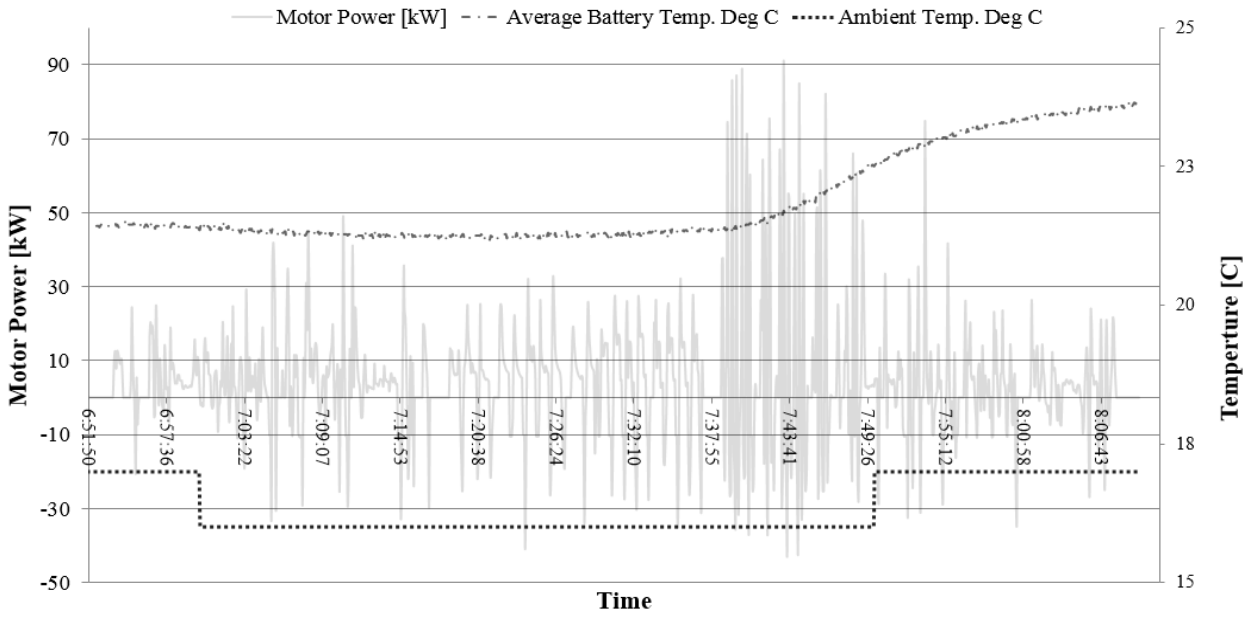

Figure 5-9: Battery temperature, ambient temperature and motor power as a function of time taken from a test drive

5.4 Discussion

The aim was to accelerate and decelerate a vehicle at predefined rates from 0 to 70 km/h and 70km/h back to 0 km/h respectively. The required data was acquired from the vehicle's CAN bus, streamed and logged to a computer system.

The acceleration experiment showed a maximum motor/controller efficiency of 94% occurred, over a short rpm range, at an acceleration rate of 1.26 m.s^{-2}. Due to the low rpm's involved in the experiments, the maximum efficiency of 96% was never achieved. The increased loading of the EV from 0.49m.s^{-2} to 0.67m.s^{-2} reduced the total energy consumption

from -178Wh to -153Wh by 14%. To complete the same distance for acceleration rates higher than 0.49m.s^{-2}, additional cruise energy was required to overcome friction from tyres, bearings and gears, as well as wind loading. As a consequence, when increasing the acceleration rate of 0.67m.s^{-2} to 0.93m.s^{-2}, the additional cruise energy starts to outweigh the benefits of efficient loading. Due to the required additional cruise energy, the overall (total) energy increases gradually from the best energy consumption of -153Wh to the worst of -184Wh.

Focusing on energy for acceleration only, the increased vehicle loading reduced the energy consumption for the acceleration continuously until an acceleration rate of 1.26m.s^{-2} (Figure 5-5). Despite a high loading of the motor/controller at an acceleration rate of 2.78m.s^{-2} the energy required for acceleration increases by 8Wh from -126Wh to -134Wh, as compared to a lower acceleration rate of 1.26m.s^{-2}. According to the efficiency map (Figure 5-6), the motor/controller efficiency between 4,000rpm and 5,000rpm under the high loads associated with accelerating at 2.78m.s^{-2} should further increase. Since the opposite trend was observed, it is assumed that certain losses in the power train increase under full acceleration. This assumption is supported by the results in Figure 5-6. The torque trace under full load passes over the rated torque. As described in the method section, the torque was calculated from the motor's rotational speed and battery power, so the torque is proportional to the measured power. During fast acceleration rates, the logged maximum battery power peaked to 91kWs (Figure 5-9). Assuming the motor controller limits the vehicle's rated nominal power at 80kW, then 11 kWs are lost in heat. Potential losses include cabling losses, increased friction in the mechanical power train and slight wheel slip. In addition, the traction batteries' internal resistance induces loss. Assuming an internal resistance of 80mΩ [169], and a current of 220A under full acceleration, it would induce a voltage drop across the battery of 18V or around 4 kW. Over each of the full load acceleration trails for 7 seconds from 0 to 70km/h, the heat loss in the traction battery would accumulate to 28kW, equally 8Wh. The temperature recordings in Figure 5-9 support this assumption. While the ambient temperature remained stable, a rising temperature in the traction battery under full load was noticeable, this is an indication of losses dissipated in heat.

The data from the acceleration experiments with a Nissan Leaf EV suggest that under an ideal stop-and-go scenario, a faster acceleration rate than the one in the speed profile of the EUDC driving cycles improves motor/controller efficiency. However, above 1.26m·s^{-2} at a high level loading, losses are induced that outweigh the benefits from *"smart acceleration"*.

The recuperation experiment with varying deceleration rates showed an increased energy recovery rate under high RBS settings for the distance from 70 km/h to 0 km/h, from 36Wh to 63Wh (up by to 43%). A disadvantage of the high RBS setting is the shorter distance until the vehicle comes to a full stop. To cover the same distance as slowing down the vehicle in the lowest RBS settings, driving with a higher RBS setting has to be compensated by cruising to arrive at the same distance, which requires energy. The added cruising energy outweighs the benefits of an increased recovery rate. The recovered net energy reduced from 36Wh to 17Wh (reduction by 47%). Not only does the energy compensation for cruising reduce energy efficiency, but it also induces the inherent losses induced by the energy conversion systems. Depending on the stop-and-go pattern and provided the traffic situation allows for it, it is more efficient to immediately use the kinetic energy to overcome resistance from tyres, bearings, gears and wind loading, rather than convert it and store it in the battery. A disadvantage of the suggested declaration rate is the reduced average speed and hence a slight delay in arrival time at the destination.

The improvements in motor/controller efficiency due to smart acceleration and braking are limited to stop-and-go driving scenarios. The applied efficient driving techniques do not improve energy efficiencies during constant cruising speed. The findings from this study are limited to a single test car, the Nissan Leaf. Other cars with different sized batteries, vehicle weight, gears, motors and controllers might perform differently. In addition, due to potentially dangerously high acceleration rates, this driving technique may not be suitable for all vehicle types. The accuracy of the results were limited to a relative short sampling rate, potential small changes in the traction battery's internal resistance (SoC and temperature), a short acceleration distance, speed limit at 70km/h and the vehicle's internal instrumentation system and calibration.

To further improve the efficiency of this “smart accelerating/deceleration”, more experiments are needed and should include traffic simulations and investigations into how traffic light information [170] can influence energy consumptions. This information will potentially allow drivers (or drive computers) to choose acceleration/deceleration rates suitable for most efficient driving. Further research might also investigate how a visual or acoustic efficiency meter for the driver (or a drive computer), following the efficient regions on the efficiency map, could further improve acceleration/deceleration efficiencies.

5.5 Conclusions

Over the last decade, efficiencies, energy storage, recharge technologies and range for plug-in EVs have increased significantly. To further reduce energy consumption and to increase range, efficient operation of EVs remains an important factor. This study investigated whether loading the motor/controller in the ideal region of the car's efficiency map can improve overall efficiency in a stop-and-go scenario. Under real road conditions the vehicle was subjected to a series of various acceleration/deceleration rates. The experiments have shown that increasing the load of the motor/controller to its efficient region improves efficiency and energy consumption. However, this heavily depends on the driving pattern. Under certain scenarios the required cruise energy outweighs the benefits from fast acceleration rates. Under full load acceleration, the motor/controller is expected to operate in highly efficient regions, however, increased losses in the power train may outweigh the benefits of operating the motor/controller in the most efficient region. The recuperation experiment showed an increased energy recovery rate under high deceleration rate, but inherent energy conversion losses and required cruise energy for distance compensation outweighed the benefit of high deceleration rates. For this particular study, the data suggest strong but not full acceleration and soft decelerations of the EV to be the most efficient stop-and-go driving technique. The findings from this study are limited to a stop-and-go driving and do not improve efficiency under steady cruising speeds. Also, investigations on the efficiency impact of traffic light information via V2I communication (vehicle to infrastructure) to the vehicle or automated driving systems could be conducted.

Chapter 6

Battery Cell Balance of Electric Vehicles under Fast-DC Charging

6.1 Introduction

In an electric vehicle (EV) or plug-in hybrid electric vehicle (PHEV), individual battery cells are connected in series to form a battery at the desired voltage. The major types of rechargeable EV batteries are: lead-acid (Pb-acid), nickel-cadmium (NiCd), nickel-metal-hydride (NiMH), lithium-ion (Li-ion), lithium-polymer (Li-poly), sodium-sulfur (NaS) and zinc-air (Zn-Air)[171, 172]. In the early days of EVs the most popular choice for EVs were lead-acid batteries since they were relatively cheap, could be designed for high power, were safe to operate and had a recycling industry in place. A further benefit was its simple charging procedure where individual cells do not require a complex BMS. However, lead-acid batteries take a long time to recharge and have a short calendar and cycle life. Furthermore lead-acid batteries have a low specific energy density and in contrast to automotive distillate, which has a specific energy of around 12000 Wh/kg [173], a lead-acid battery contains just 50 Wh/kg [172]. Even though internal combustion engine (ICE) cars have much lower energy conversion efficiency than EVs, the high specific energy in automotive distillate allows ICE cars a short refuel time and large drivable range.

The energy storage (and hence the drivable range) and the time to recharge an EV are still amongst the most important factors in deciding whether EV technology can become a large-scale feasible alternative to motor vehicles that run on fossil fuels[6, 174-176].

The introduction of lithium-ion batteries has improved the situation. Lithium-ion batteries can store around 170Wh/kg [172], have high specific power, can be fast charged and have a much longer calendar and cycle life than lead-acid batteries. However, their drawbacks are the relatively high costs and the requirement of a complex BMS to balance individual cells and manage complex recharging techniques. To prevent overcharging, overheating and permanent damage, lithium-ion cells require complex charging algorithms[177] and smart chargers that communicate with the EV to ensure a safe and efficient charging procedure.

Currently, the most popular charging methods for EVs are home charging (level-1) and public charging stations (level-2, AC or fast-DC following Combo-CCS or CHAdeMO). Depending on the state of charge (SoC), the size of the onboard battery charger and the available electricity source, recharging of a standard EV traction battery can take more than 10 hours. The long charging time is a result of the low level-1 charge rate (a maximum of 2.4 kW in Australia) and the time required to balance the cells.

Fast-DC charging for EVs is a new technology that provides a charge rate of up to 120 kW[178]. As a result, a standard EV traction battery can be charged to 80% of its battery capacity within as little as 20 minutes. The short recharge time enables EV drivers to drive large distances with acceptable recharge and travelling times. However, this also means that EV drivers may have to forfeit the 20% of their EV's charge capacity and consequently driving range, as fast-DC charging cannot deliver energy for the remaining 20% at an equal speed to the first 80%. If fast-DC charging stations are installed along highways between remote towns, this technology has the potential to make EV driving feasible in areas of low population density where EV driving is currently very limited due to the lack of recharging infrastructure between and within remote towns. In the south west region of rural Western Australia (WA), for example, a number of fast DC charging stations are being installed in country towns that are popular with tourists to form an 'electric highway' that will join the city of Perth to these towns[179, 180] When installation is complete, this will be Australia's first large-scale EV charging network.

While fast-DC charging can significantly reduce the time to recharge, it presents a challenge to the BMSs currently used by EVs. The main task of a BMS is to equalise the individual lithium-ion cells (up to 7000 cells [181]) in an EV traction battery. Cell equalisation is a complex and important task to maintain cell voltage balance and utilise full battery capacity. The cell voltage is proportional to the cell's charge capacity and hence the batteries' capacity is limited to the capacity of the lowest cell voltage of the battery. A BMS measures individual cell voltages and interacts to balance the individual cells. Sophisticated BMSprotect the battery not just from over-charging but also under-charging or temperature related issues and can also report battery health and charge status[182-187].

A wide variety of BMSs are implemented for a large number of lithium-ion battery applications. The simplest form of BMS are cell shunt regulators (dissipation type), for example as implemented in a custom converted Lotus Elise "REV Racer" and Hyundai Getz "REV Eco" by the University of Western Australia (UWA) [188-190]. A simple electronic circuit monitors the cell voltage and as soon as a preset voltage level is detected, the shunt becomes an active load and dissipates excessive energy into heat. Although these systems are cheap and comparatively reliable they are inefficient and on large battery banks produce relatively large amounts of heat. Another drawback is that its balancing power is limited to the maximum heat dissipation of the shunt. Hence the balancing is slow and becomes an issue for fast-DC charging applications. More advanced and complex BMS are capable of transferring excessive energy between cells. Each cell is equipped with a micro controller, which communicates to the main BMS controller. The controller monitors individual cells and decides which cell needs be corrected. In contrast to a shunt regulator, excessive energy is not dissipated into heat but stored in an inductive or capacitive energy storage device and transferred between the cells. Such a system ensures that the cells are balanced even when an EV is at the beginning of a charge, driving or just parked. This balancing of individual cells 'on the fly' results in higher charge efficiencies and reduced balancing time toward the end of charging[174, 182-185, 191]. However, even active BMS have limitations and might not be able to complete cell balancing under fast-DC charging. As a consequence if the voltage of a battery cell drifts low and is out of balance with the rest of the cells over time, the overall battery capacity and range is reduced and an efficient utilisation of the battery capacity cannot be maintained.

Although at least one fast-DC charge study has been undertaken (and shown a negative impact on cell capacity[192]) and studies have been published on the design and implementation of BMS and cell equalisation methods[182-186], there is little information on realistic fast-DC charging of commercially available EVs. In this chapter we are not looking at deterioration of battery cells through fast-DC charging (which very well may be a secondary effect), but we will concentrate on the interaction and impact of realistic fast-DC charging on BMS and battery cell balance and hence on the efficient utilisation of the given battery capacity. The aim of this study is to assess the fast-DC charging impact on the traction battery cell balance and if a BMS can maintain battery capacity and vehicle range under a series of continuous realistic fast-DC charge scenarios on commercially available EVs.

In this project we will investigate the effect of fast-DC charging on cell balance within an EV's battery pack. Cell balance for an EV is essential, as an EV has to stop driving when any cell drops below a certain threshold charge value and likewise has to stop charging once any cell exceeds another threshold charge value. Since fast-DC charging happens in much shorter time than e.g. home-AC charging (typically 20min. vs. 8 hours), there will be significantly less time for the EV's BMS to achieve an active cell balance through redirecting current-flow during charging. In this chapter we investigate the impact of fast-DC charging under different conditions and with two OEM[1]-built EVs.

Please note that this chapter does not address any potential long-term battery degradation effects due to high-powered DC charging. The scope of this work is on the short-term charge imbalance of individual cells, which can typically happen on a single longer EV trip with some short stops for fast-DC charging, such as on the WA 'electric highway'. These imbalances are generally reversible, e.g. by conducting a slow-AC charge, giving the BMS more time to balance cells, but they may have a detrimental effect on vehicle range when driving a long distance highway route.

[1] Original equipment manufacturer

6.2 Materials and Methods

To observe the impact of fast-DC charging on the cell balance in EV batteries, two factory-built EVs were used and their traction batteries were exposed to a series of discharge and fast-DC charge cycles. The test cars used in this study were a pre-used Nissan Leaf (24,000 km) and a pre-used Mitsubishi i-MiEV (5,100 km), depicted in Figure 6-1. The Leaf is manufactured with a 24 kWh battery and the i-MiEV contains a 16 kWh battery. However, in both cases, not all of the nominal battery energy can be used since the BMS protects the batteries from permanent damage due to deep discharge. At a very low battery level the Leaf's and i-MiEV'sBMSs force the cars into "limp mode". In "limp mode" the control system reduces the vehicles' maximum drivable speed significantly, allowing the cars to be driven to a safe location before coming to a full stop[193, 194]. According to Nissan's specifications, under laboratory conditions the Leaf has a drivable range of up to 199 km [195] on full charge, while the i-MiEV claims a range between 150 km [196] and 160 km [197].

Figure 6-1 Test cars Nissan Leaf (left) and Mitsubishi i-MiEV (right) used for the experiments.

A series of eighteen discharge and fast-DC charge cycles were carried out on the Nissan Leaf, and eight cycles on the Mitsubishi i-MiEV. For a uniform discharge rate and a uniform state of charge (SoC), the vehicle batteries were discharged using the cars' internal loads such as the heater or AC system, head lights, demister and fans. As stated previously, the scope of this chapter concentrates on short-term imbalance of battery cells, such as experienced on a drive on a long distance highway (e.g. the WA electric highway) and thus a limited series of discharge and charge cycles were carried out. There were also practical reasons that limited

the number of cycles including the fact that the EVs were borrowed, which limited the time that the vehicles were available and prevented the authors from sacrificing the batteries through continual degradation over a large number of cycles.

A lithium-ion battery cannot be fully discharged, which means that in a real-world driving scenario, the vehicle cannot be driven to the end of its charge capacity. To prevent the vehicles from the "limp mode", where the vehicle cannot be driven further, a safety margin was included. For the Leaf with the larger battery, minimum SoCs of 30% and then 20% were used, while for the i-MiEV a minimum SoC of 30% was used. Up to four discharge/charge cycles were conducted per day with the vehicles being re-charged using a Veefil fast-DC charger, a 50 kW charger that is installed at the University of Western Australia (UWA). The Combo CCS [198] and CHAdeMO standards [199] provide a suitable charging interface to the Leaf and i-MiEV.

To monitor the energy consumption and the charging of the batteries, the following variables were read from the vehicle controller area network (CAN) bus during the experiment: battery capacity (Ah), system voltage (V), individual cell voltages (V), charge and discharge power (W), and current (A). In addition, the Leaf gave an indication of battery health status (%). The CAN bus was accessible via an on board diagnostic connector (OBD2) [200, 201]. For the hardware interface, a commercially available scan tool was used and the data from the scanner was transmitted via a Bluetooth terminal to an android computer system.

The recharged energy was averaged over the charge cycles and the uncertainty was estimated by the associated standard deviation. The calibration and accuracy of all instrumentation used in the experiments was limited to the manufacturing standards of the EVs and the fast-DC charging station.

6.3 Results

During all discharge-charge cycles on the Nissan Leaf and i-MiEV the traction battery charge capacity and cell balance were recorded.

The total applied charge energy to the Leaf over eighteen charges was 159 kWh. Assuming an energy consumption of 150 Wh/km [195] this is equivalent to over 1,000 km of real road driving. The total applied charge energy to the i-MiEV over eight charges was 62.7 kWh,

which is equivalent to over 500 km of road driving, assuming an energy consumption of 125 Wh/km [197].

For the Leaf's first series of discharges to 30% SoC, the average remaining energy in the traction battery was 5.3 kWh. Assuming a New European Driving Cycle NEDC [202] energy consumption of 150 Wh/km [195] the remaining range would be 35 km before the system would switch into "limp mode", which is a reasonably large safety margin compared to the range of "up to 199 km" published by Nissan for the Leaf [195]. However, independent road testing performed at UWA has shown that when driving under realistic highway conditions energy consumptions on both cars can exceed 250Wh/km and driving at higher speeds with an assumed energy consumption of 250 Wh/km reduces the safety margin to 21 km. For the second series of discharges down to 20% SoC, the average remaining energy in the traction battery was 3.2 kWh. Based on the energy consumptions of 150 Wh/km and 250 Wh/km assumed above, this corresponds to remaining drivable distances of 21.2 km and 12.8 km, respectively.

A similar scenario was observed on the i-MiEV. Discharging to 20% SoC, the average remaining energy in the traction battery was 4.6 kWh and, based on anenergy consumption of 125Wh/km reported by Mistsubishi [197] above, the remaining drivable distance before the vehicle enters "limp mode" would be 36.8 km. Compared to a range of 150 km for the i-MiEV published by Mitsubishi [196] this is also a relatively large safety margin. However, assuming continuous, real road driving on a highway at a speed of 110km/h and an assumed energy consumption of 250 Wh/km the safety margin reduces to just 18.4 km.

Figure 6-2a and Figure 6-2b show the stored and usable (recharged) energy over the eighteen discharge-recharge cycles for the Nissan Leaf and the eight cycles for the i-MiEV, respectively. For the Nissan Leaf, Figure 6-2a clearly shows that the stored and usable energy remain stable over all cycles. By recharging the battery from a SoC of 30% the average usable energy was 7,628 ± 109 Wh. By recharging the battery from a SoC of 20%, the average usable energy was 9,790 ± 99 Wh. For both combined recharge scenarios, SoC 20% and SoC 30%, the average energy stored in the battery after the charge was 13,300 ± 58 Wh. Similarly, the data in Figure 6-2b shows that the battery energy remained stable over the eight discharges and fast-DC charges applied to the i-MiEV. By recharging the battery from a SoC

of 30%, the average recharged energy was 7,837 ± 68 Wh. The average energy stored in the battery after the charge was 12,261 Wh.

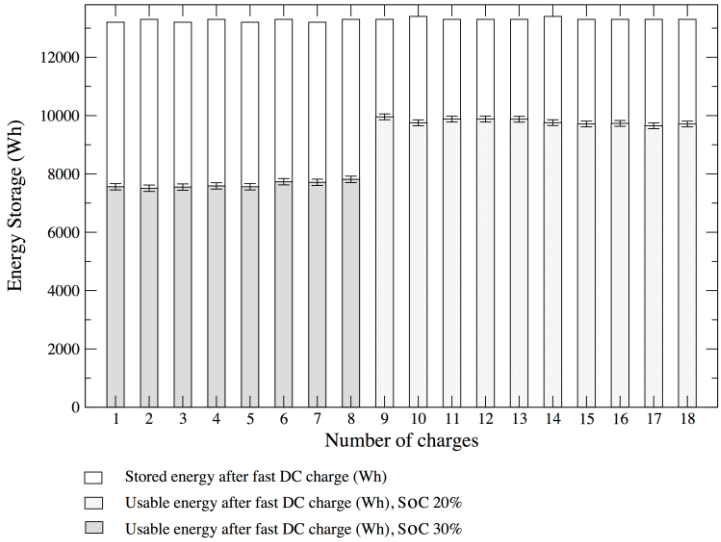

a)

b)

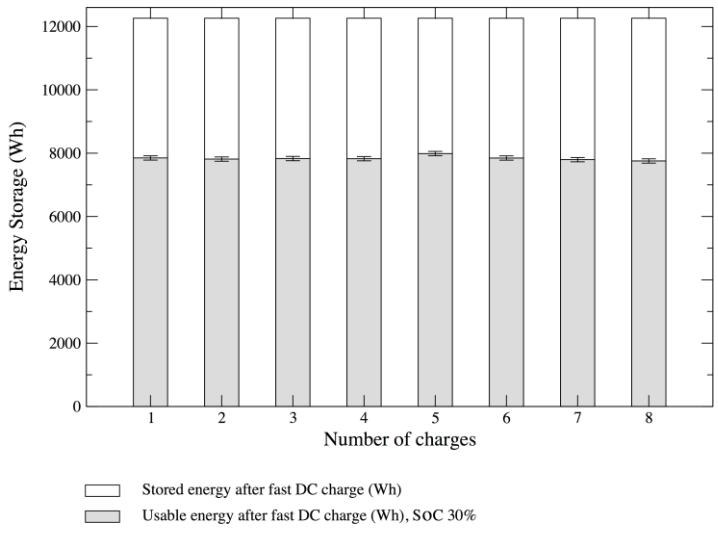

Figure 6-2 Stored and usable energy during a series of fast-DC charges. a) Nissan Leaf stored and usable energy. b) MiEV stored and usable energy over the charge cycles.

For both EVs, the amount of usable energy did not change significantly over the recharge cycles. This is likely to be a result of well-performing BMSs and the findings indicate that the BMSs were capable of efficiently balancing the charge across individual cells. This is supported by the trends of the chart shown in Figure 6-3 that show the activity of the Leaf's BMS during the discharge at a SoC of 68%. The light grey on the individual columns indicates an active shunt and transferring of energy between traction battery cells. Such an active BMS ensures balanced cells all the time, i.e. during both discharge and charge and not just at the end of a charge as on a simple shunt BMS. During all charges and discharges, a very low cell voltage deviation was observed (maximum of ±25 mV).

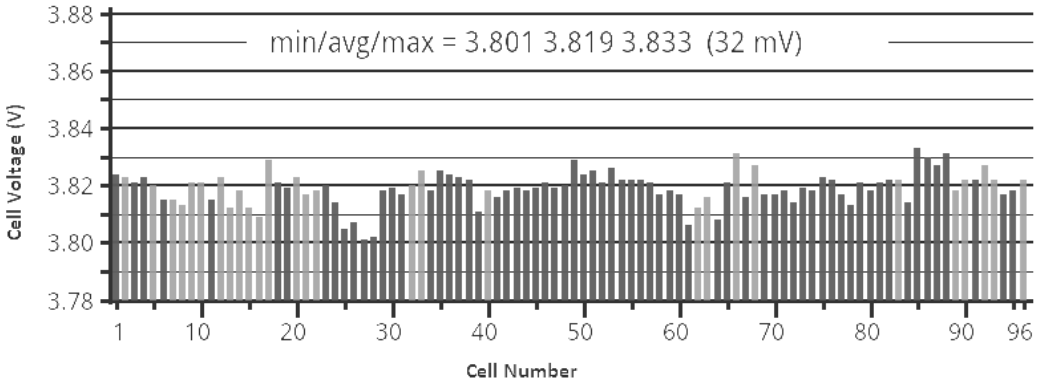

Figure 6-3 An interactive BMS during a discharge of a Leaf traction battery

6.4 Discussion of Results

Assuming an energy consumption of 150 Wh/km as reported by Nissan [195] and an average usable energy from Figure 6-2a of 9,790 Wh (20% SoC), the theoretical drivable range of the Leaf is 65.2 km. From the experiment results, 9,790 Wh of usableenergy corresponds to only 40% of the nominal battery capacity of 24 kWh. This suggests a very inefficient utilisation of the built-in battery capacity.In the case of recharging a battery with remaining 30% SoC, the usable energy is 7, 628 Wh, the theoretical driving range is 50.8 km and the usable energy is 32% of nominal battery capacity.

Assuming an energy consumption of 125 Wh/km as reported by Mitsubishi [197], and an average usable energy from the experiment of 7,837 Wh (30% SoC) , the theoretical drivable range of the i-MiEV is 62.7 km. The average usable energy of 7,837 Wh is also very low. This value is just 49% of the built-in capacity of 16 kWh and could also be considered an inefficient utilisation of the battery's capacity since around half of its full battery capacity is not used but still contributes significantly to the vehicle's weight[203]. Despite the Leaf having a much larger nominal battery capacity, comparison of results for same safety margin of 20% SoC, indicate that the Leaf actually has a shorter driving range than the i-MiEV due to a higher energy consumption [196, 197] and lower battery capacity utilisation.
Although the drivable range on both vehicles remained stable, EV drivers and electric highway designers should be aware that under fast-DC charging, batteries can be charged only to 80% of full capacity. Furthermore, under realistic conditions, EVs being driven between towns cannot fully discharge batteries as this will drive the cars into "limp mode", which will consequently lead to system shutdown. The process of discharging thus requires a safety margin so that not all the nominal stored energy can be taken from the battery. The combination of a reduced charge level of 80% and a safety margin reduces the usable energy from traction batteries significantly and hence a vehicle's drivable range appears to be markedly lower than that published by the car manufacturer.

The fast-DC charging experiments on the Leaf and i-MiEV have shown that continuous discharge and fast-DC charge did not influence the cell balance. The BMS of both cars efficiently prevented a cell voltage drift and balanced each individual cell regardless of charging or discharging. The level of stored energy was relatively low but did not change significantly over time. The findings suggest that, even during a long distance drive with several discharge-recharge cycles per day, the charge capacity and drivable range remain stable. In regards to cell balance and charge capacity, fast-DC charging technology is a feasible option for EVs to travel larger distances. EV drivers and electric highway designers, however, should be aware of the lower drivable range associated with realistic real road scenarios and fast-DC charging.

6.5 Conclusion

Drivable range and recharge time are amongst the largest barriers to the adoption of EVs, particularly in remote areas. Not much is known about the impact on battery cell balance and thus the drivable range of commercial EVs undergoing non-laboratory, realistic fast-DC charging. The aim of this study was to investigate the impact of fast-DC charging on EVs' traction battery cell balance and vehicle drivable range. For the two commercial EVs investigated no short-term negative impact on traction battery cell balance was observed during the fast-DC charging experiments. The vehicles were subjected to a series of continuous battery discharge-charges cycles using fast-DC charging. The results found unchanged traction battery charge capacities and the level of usable energy from the battery (and hence the drivable range) remained stable over time in the short-term scenario of a long drive on an electric highway. EV drivers and electric highway designers, however, should be aware that fast-DC charging to 80% on EV traction battery results in reduced charge capacity and hence reduced drivable range than what is currently stated by EV manufacturers. Further research is required to investigate the impact of fast-DC charging on EV energy consumption and drivable range at higher speeds.

Chapter 7

Driving electric vehicles at highway speeds: The effect of higher driving speeds on energy consumption and driving range for electric vehicles in Australia

7.1 Introduction

Although EV sales are increasing globally, even in a large market like the U.S., EVs still make up less than one percent of all new vehicles sold [204]. To date, limited driving range, limited charging infrastructure and long recharging times have hindered EV technology's attempt to become a large-scale feasible alternative to motor vehicles run on fossil fuels. One promising innovation is the relatively new fast-DC charging technology, which reduces recharge time significantly. An EV traction battery can be fast-DC recharged to 80% of its capacity in around 20 minutes and makes long distance travelling with relatively short recharge stops feasible [178]. Innovative entrepreneurs are currently implementing fast-DC charging stations along highways interconnecting major cities [178]. An 'electric highway' is

planned for the south west region of rural Western Australia, joining the city of Perth to some of the country towns popular with locals and tourists alike [179, 180].

Apart from recharge time, range is a major factor affecting peoples' willingness to adopt EV technology. The drivable range of an EV is determined by the type of car and the capacity of the batteries as well as the vehicles' efficient design and use. Many factors such as charge level, efficient battery capacity utilisation, driving style, vehicle mass, cross-sectional frontal area, drag coefficient, auxiliary loads, driving pattern, vehicle speed and tyre rolling resistance have the potential to decrease EVs' efficiency. All these factors can be influenced by the EV driver and have a significant impact on energy consumption and hence drivable range.

Manufacturers measure their EVs' energy consumption and range based on data collected during chassis dynamometer testing using a standardised driving pattern such as, for example, the New European Driving Cycle (NEDC). Testing under ideal conditions, with minimum auxiliary loads, and with the aid of the vehicle's regenerative braking system (RBS), EV manufacturers achieve low energy consumption values and long drivable ranges. This idealised testing is very different from the scenario where a vehicle is driven over a long distance at high speeds, such as driving a vehicle between cities across remote areas. The difference between lab conditions and real world conditions impacts much more on the energy consumption and drivable range for EVs than for cars with combustion engines. This is because even small changes in parameters such as the vehicle's weight, auxiliary load (AC and heating) or speed have a large impact on the drivable range on EVs, but not so much in combustion engine cars due to their much bigger and denser energy storage device, the fuel tank.

Thus, using the energy consumption measured under lab conditions is likely to overestimate the drivable range for EVs. Although modern EVs have factory-installed RBS, when driving at steady speed, such as on a highway, the recovered energy from slowing down is minimal compared to a city driving stop-and-go scenario. Therefore, in the absence of an RBS by driving at a steady speed and using large auxiliary loads such as an AC and a heater, the vehicle's energy consumption will be much higher than stated by the manufacturer.

Energy consumption will further increase under continuous high speeds, and with the increased mass and increased cross-frontal area that a roof rack adds to a vehicle. As a consequence the vehicle's range reduces significantly and a further reduction in drivable

range can be expected since not all the nominal stored energy from a battery can be accessed and used. To avoid deep discharge and potential permanent damage to battery cells, some energy needs to remain in the battery. For battery protection, factory EVs (e.g. the Nissan Leaf and Mitsubishi i-MiEV) contain a battery control system that monitors the battery charge status and at a critical low battery level switches the vehicles to a 'limp-home mode'. In this mode, the control system reduces the vehicle's maximum speed significantly to just allow the car to be driven off the road to a safe location before the car comes to a complete stop [193, 194]. In addition, similar to driving a combustion engine car to the next fuel station not all fuel or energy can be used. To prevent being stranded, an extra safety margin in the battery charge needs to be included in the planning of a trip and cannot be used.

The combination of a limited fast-DC charge level of 80% capacity, increased energy consumption at highway speeds, large auxiliary loads such as air conditioning and a battery discharge safety margin would be expected to reduce the vehicle's drivable range. To address such issues and improve EVs usability and drivability on highways, several studies have been conducted on drive system optimization, charger selection algorithms, the impact from environmental and auxiliary loads on batteries, energy consumption and drivable range [56, 205-208]. Whilst several studies on pure EV energy consumption feature range tests and simulations conducted under laboratory conditions e.g. [209], with new and fully charged batteries [210-217] and for urban driving with a short highway section [218-221], at the time of this study there is little information available on realistic EV use, energy consumption and vehicle range for travel on an electric highway between cities. In particular, there is a gap in the literature on the interaction of the combination of a limited fast-DC charge level of 80% capacity, increased energy consumption at highway speeds, increased loads due to headwinds, increased aerodynamic drag due to roof racks, additional vehicle weight, the absence of energy recovery and a battery discharge safety margin.

The aim of this study is to investigate the drivable range losses of commercial EVs due to the combination of reduced charge levels from fast-DC charging, increased energy consumption from driving at continuous real-road highway speeds and the limited access to the nominal stored energy in the traction battery. Results are compared with estimations of range by EV manufacturers.

7.2 Methods and Materials

The test cars used in this study were a two year old Nissan Leaf (24,000 km travelled) and a one-year old Mitsubishi i-MiEV (5,100 km travelled), as shown in Figure 7-1. The Leaf accommodates a 24 kWh battery and the i-MiEV contains a 16 kWh battery. According to published data by Nissan, the Leaf has a range of up to 199 km [222] on full charge, while the Mitsubishi's range is stated between 150 km [196] and 160 km [197]. Both cars have factory installed RBS systems.

Figure 7-1 The Mitsubishi i-MiEV and Nissan Leaf test cars used for the experiments

7.2.1 *Road Tests*

The vehicles were road tested to determine realistic on-road energy consumptions and to collect data for calculating a realistic drivable range for both vehicles. The driving experiments were conducted on a flat freeway section in Perth, Western Australia at speeds of 60km/h, 70km/h, 80km/h, 90km/h, 100km/h and 110km/h (legal speed limit in Western Australia). To minimise the impact on headwinds, the test drive was conducted in both directions, from north to south and vice versa and the energy consumption values recorded and averaged.

During driving, the onboard speedometer reading was compared to the measurement from a Suunto GPS device on regular intervals and the vehicle speed adjusted accordingly. For the test drives all auxiliary loads such as head lights, heaters and AC were switched off. To determine the available energy from the car's traction batteries the cars were recharged on a 50 kW 'Veefil' fast-DC charging station installed at The University of Western Australia (UWA) as part of the Renewable Energy Vehicle Project (REV). Note that the same type of fast-DC charging stations have been proposed for long distance highway driving, including

the electric highway planned for Western Australia [178-180]. To measure the vehicle's energy consumption, the available energy in the batteries and other battery related data is available on the vehicles controller area network (CAN) bus and accessible via the vehicle's on-board diagnostic connector (OBD2) as commonly implemented in modern cars [200, 201]. The data from the commercially available OBD2 scan tool was transmitted via a Bluetooth terminal to an android computer system. Since the energy consumption of individual auxiliary loads such as headlights, heater system, AC system and demisters are critical for the overall energy consumption these parameters were measured and logged separately on stationary vehicles. The calibration and accuracy of all instrumentation used in the experiments was limited to the manufacturer standards of the EVs and the fast-DC charging station.

The drivable range was calculated based on the energy consumption and the available and accessible energy from the traction battery. Vehicle ranges were calculated based on the available energy from an 80% capacity fast-DC charged battery that discharges to a level that leaves a realistic safety margin for the driver to get to the next charging station. In energy terms this safety margin was assumed to be 2 kWh. An additional scenario was modeled in which the range was calculated based on the available energy from an 80% capacity fast-DC charged battery that discharges until the vehicle reduces its power in 'limp-home mode'.

7.2.2 *Vehicle Mathematical Modelling*

The speed limit in Western Australia is 110km/h. To simulate higher speed limits or strong headwinds, or large auxiliary loads, the various components of traction power demand on the cars' batteries were modelled mathematically and the energy consumption of the cars were calculated to estimate the drivable range at these high speeds and loads. Hayes et al. [100] conducted research on a simplified power train model for various new and existing production vehicles. The results showed a strong agreement with published energy consumptions [197, 222]. However, Hayes et al. calculated the range based on a new and fully charged battery with a state of charge (SoC) of 100% and no headwinds or other real-road driving factors influencing the energy consumptions. Furthermore, the battery in an EV will degrade over time resulting in a reduced charge capacity. Real world driving with a degraded battery and fast-DC charging up to just 80% would further negatively impact an EV's range. In addition,

some vehicle-specific parameters such as tyre rolling resistance vary between vehicles and influence energy consumption and range.

In this project the output of the model was compared with results from real-road driving on the two specific vehicles and the parameters calibrated accordingly. The model thus permitted the very accurate estimation of increased energy demands by changes to parameters such as vehicle weight, cross-frontal area due to a roof rack, and strong headwinds.

The traction power demand was calculated using Equation (7-1) [223]

$$P_{Tractive} = \sum_{i=1}^{i=N} \left[mgC_{RR} + \frac{1}{2}\rho\, C_D A_F \left(\frac{V_i + V_{i-1}}{2}\right)^2 + mr\left(\frac{V_i - V_{i-1}}{t_{inc}}\right) + mg(\sin\theta) \right] * \left[\frac{V_i + V_{i-1}}{2}\right] \quad (7\text{-}1)$$

The first term in Equation (7-1) is the power required to maintain a given speed (i.e. the power to overcome rolling resistance) and is given by the gravitational force (g = 9.81 ms^{-2}), vehicle's mass and rolling resistance coefficient of the tires used (C_{RR}). This term will change for the different driving scenarios by altering the vehicle's mass, tyres or tyre pressure. The second term describes the power required to overcome the aerodynamic resistance, which is the drag force that acts on the vehicle as it moves through air. The aerodynamic resistance thus depends on the vehicle's shape and frontal area, captured by the variables C_D and A_F and the density of surrounding air (ρ =1.2 kgm^{-3}). This term increases with increasing vehicle speed as a result of increased friction between air and the vehicle surface. In addition, this term will also be affected by changes in the projected frontal area caused by the addition of a roof rack. The third and fourth terms in Equation (7-1) are related to the inertial resistance; the first of the inertial terms models power needed to overcome power lost in acceleration while the second inertial term models the power needed to overcome losses due to road gradients. Power lost in rotary power also needs to be considered and this has been taken into consideration by increasing the first inertial term by a compensation factor of 3%. This compensation factor is described as the rotational inertia compensation factor, r. Finally there are drive train losses including battery discharge losses, cabling, inverter, motor and gears. Overall drive train energy losses change with vehicle loads but also between different types of cars and manufacturers. Obtaining these values from manufacturers is difficult [100] and is out of the scope of this project. Therefore these parameters were adjusted (calibrated) until the

model agreed with the energy requirements measured on the real-road energy consumption tests. The experiment assumes a flat surface and constant speeds. Hence there are no energy requirements from road gradients, no energy recovery from deceleration and therefore no interaction of RBS or inertia and rotary power compensation factor.

Table 7-1 shows vehicle specific parameters in Eq. 1 used for the calculations of traction power demand. A powertrain efficiency factor of 0.8 was assumed and multiplied by the calculated traction power demand. Besides the traction power, the vehicle requires energy for system power such as computer control units, relays and displays. These demands were measured and added to the calculated traction power.

Table 7-1 vehicle specific parameters used for the calculations [197, 222, 224]

Model	*m*	C_{RR}	C_D	A_F
Leaf	1521kg	0.012-	0.29-	2.27m^2
i-MiEV	1085kg	0.012-	0.33-	2.14m^2

7.2.3 *Modelling of Different Load Scenarios*

For both cars the energy consumption and drivable range were modelled for three different driving scenarios. The scenarios were chosen to reflect conditions of overland driving in low-population density areas often encountered for drivers leaving cities for recreation.

1. Scenario 0 is identical to the real-road driving energy consumption test as discussed above. It included a single driver, no ascent or decent, one passenger (80kg) and no headwind. The auxiliary loads were limited to the system loads. There is assumed to be no battery charge safety margin.
2. Scenario 1 is identical to Scenario 0 but with a battery charge safety margin.

3. Scenario 2 included also a battery charge safety margin, no road ascent or decent, two passengers (160kg), baggage of 50kg and no headwind. The auxiliary loads included switching on an AC system with a time-based duty cycle of 50%.
4. Scenario 3 has the same conditions as Scenario 1 and 2 but with an assumed headwind of 20 km/h and the model accounted also for the cars to carry a small roof rack caring a surfboard or Skis (assumed cross sectional area of 0.25m^2). The resulting decline in aerodynamic efficiency from carrying the roof rack was ignored for this study.

Before calculating energy consumption and range for these four scenarios, the model was assessed using a new European drive cycle (NEDC) speed profile. The energy consumption and recovery calculated by the model was compared with EV manufacturers' NEDC energy consumption data. To validate the results from the model, the predicted energy consumptions were compared with data obtained from real-road driving and specific parameters calibrated accordingly.

7.3 Results and Discussion

The energy consumption for each vehicle was determined using a real-road test consisting of a freeway (highway) section without ascents or descents and driving speeds of 60, 70, 80, 90, 100 and 110km/h. Prior to real-road tests the vehicles were charged on a fast-DC charger to 80% charge capacity. The energy consumptions for auxiliary loads and the battery charge level corresponding to the vehicles switching to 'limp-home mode' were measured on stationary vehicles. To estimate the energy consumption and range under higher speeds and vehicle loads, the available energy in the battery was determined and the vehicles were modeled and their energy demands calculated. The aim was to observe the increased energy consumption under continuous real-road highway speeds and the impact on drivable range under the combination of reduction to 80% capacity due to fast-DC charging, increased energy consumption and the limited access to the nominal stored energy in the traction battery.

Fast-DC charging the Leaf from 'limp-home mode' (SoC 3%) to SoC 80% required 13,544 Wh whilst fast-DC charging the MiEV from 'limp-home mode' (SoC 3%) to SoC 80% required 12,261 Wh. This constitutes an effective capacity of only 56.4% for the Leaf and 76.6% for the i-MiEV. Fast-DC recharging, including a driver's safety margin of 2 kWh in order to not get stranded, reduces the average available charging energy for the Leaf to 11,544 Wh (48%) and of the i-MiEV to 10,261 Wh (64%). Just less than half of the Leaf's full battery weight is not used yet still contributes significantly to the vehicle's weight. To verify the low usable energy of the car's batteries, the Leaf and the i-MiEV were recharged, from the same SoC, eighteen and eight times, respectively. The significant difference between the nominal capacity and the rechargeable (and hence usable) energy is due to a combination of the 80% charge level limit of fast-DC charging, battery aging and battery safety margins.

Auxiliary loads influence the energy consumption of an EV and hence its drivable range.

Table 7-2 shows the major auxiliary loads measured on a stationary i-MiEV and Leaf. On both cars the headlights and rear demister require a continuous supply of 200 W. The heater constitutes the largest auxiliary electrical load and draws 2300 W for the Leaf and 2000 W for the i-MiEV. The second largest auxiliary loads are the AC system with a demand of 1400 W and 1200 W for the Leaf and i-MiEV, respectively.

Heaters and air-conditioning systems operate on a duty cycle. Depending on the ambient temperature and solar radiation the duty cycles may vary significantly. For the following energy consumption and range estimation in this project an air conditioning time-based duty cycle of 50% was assumed.

Table 7-2 Auxiliary loads measured on a stationary Nissan Leaf and i-MiEV

Type of load	*i-MiEV*	*Leaf*
	Watts (continuous)	*Watts (continuous)*
Headlights	200	200
Rear demister	200	200
Air conditioner	1200	1400
Heater	2000	2300

7.3.1 *Energy consumption and drivable range for real-road driving*

Table 7-3 shows the measured energy consumptions for the Leaf and i-MiEV for real-road driving under Scenario 1 on a Perth freeway section.

Due to the speed limit the real-road testing was limited to 110km/h and thus the energy consumption for driving at speeds above 110 km/h, which occurs in other Australian States and countries, was modelled. The model is based on the underlying physics that describes the movement of a vehicle along the road at a given speed (given by Eq 7-1). As outlined in section 3.2.2, the equation contains variables that are either specific to the vehicle (such as

mass, rolling resistance, drag coefficient and cross frontal area) or depend on the environment under which the experimental data is collected (e.g. temperature and air pressure), making the model semi-empirical. Consequently, these variables need to be calibrated for a given application. This was achieved by using our experimental data from Table 7-1 and adjusting the model input parameters (such as mechanical and electrical drive train losses, roll resistance and density of air) such that the model output described by Eq. 1 agreed with the measured energy consumption. Thus the specific model used in this study is predictive only for the two vehicles used in this study. However, this model is easily transferable to other vehicles and can become predictive for any given vehicle and/or road condition simply by recalibrating the model.

The model was assessed by comparing the energy consumption for an NEDC driving test calculated by the model to the manufacturer's published data. Overall, the results of measured energy consumption and drivable range from the model showed good agreement with the published NEDC data. For the Nissan Leaf NEDC, the model predicted an energy consumption of 165 Wh/km, 10% greater than the published value of 150 Wh/km [25]. For the iMiEV, the model predicted an energy consumption of 125 Wh/km, which was exactly the same as the published value from the manufacturer. The modelling revealed that the final energy demand is very sensitive to the input parameters in Eq. 1 and the exact energy consumption of 150 Wh/km published by Nissan [222] can easily be reproduced by adjusting the values of these parameters. For example, using different tyre resistance values with a range given by tyre manufacturers (0.006 to 0.0013 [225]) results in final NEDC energy demands ranging from 121 Wh/km to 157 Wh/km for the Nissan Leaf. However the aim of the modelling was not to achieve the exact energy consumption published by a manufacturer but to calculate trends in energy consumption for driving at higher speeds, increased vehicle weight or larger auxiliary loads as expected for the conditions in the three different scenarios. Thus, rather than setting the parameters for tyre resistance and other parameters to values that reproduce the exact energy consumption published by Nissan or Mitsubishi, the parameters were calibrated using the data from real-road testing from the vehicle used in the experiment.
Figure 7-2 shows the measured energy consumptions obtained from the OBD2 scan tool (black markers) for the vehicle speeds listed in Table 7-3 and the calculated (dotted lines) energy consumption values after model calibration versus speed for the Leaf and i-MiEV. The

mean unsigned error between the measured and calculated values over the six measured speeds of Figure 7-2 was 3.2% for the Leaf and 3.4% for the i-MiEV. This agreement is expected since the model was calibrated until a high level of agreement was achieved between the model output and the measured energy consumption. The value of the Figure is that it allows prediction of energy consumption for speeds above 110 km/h, the limit of the speeds in the road-testing. The same calibrated parameters were used to calculate the EVs theoretical drivable range under the different scenarios and situations.

Table 7-3 The measured energy consumptions at various speeds from Nissan Leaf and i-MiEV

Vehicle Speed (km/h)	*i-MiEV (Wh/km)*	*Leaf (Wh/km)*
60	98	128
70	110	133
80	112	152
90	134	163
100	151	181
110	181	220

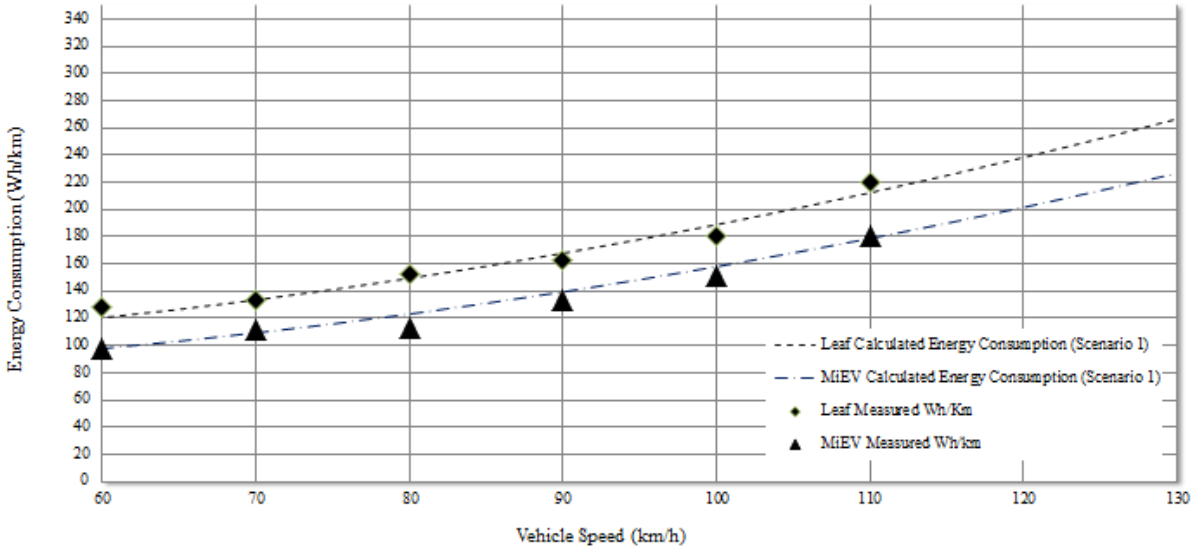

Figure 7-2 Measured and extrapolated energy consumption over a speed range of 60 to 130 km/h.

7.3.2 *Energy consumptions and drivable ranges*

Figure 7-3 shows the simulation for the Leaf (Figure 7-3A) and i-MiEV (Figure 7-3B) and the way in which drivable range reduces under higher speeds and loads. Scenario 1 shows calculated energy consumptions from the calibrated model and hence the output is identical to the real road energy consumption tests. Scenario 2 shows how the calculated range reduces by increasing the overall weight parameter in the model by assuming extra luggage and an extra passenger. The model suggests a much larger impact on reduced range by changing the model input by an assumed increased head wind speed of 20 km/h and an increased cross sectional area from a small roof rack carrying e.g. skis or a surfboard. Although the model parameter inputs for Scenario 0 (no safety margin) are the same as for Scenarios 1, the range for Scenario 0 is due to the extra theoretical available energy much larger than that for Scenarios 1, 2 and 3. Since under realistic road driving a vehicle cannot be fully discharged (no safety margin) the unrealistic range in Scenario 0 is difficult to achieve and therefore is not further discussed. Table 7-4 and Table 7-5 show the calculated range of the Leaf and i-MiEV under the three scenarios. Travelling at a speed of 110 km/h, the model suggests that the Leaf achieves a range of 54 km under Scenario 1, a range of 52 km under Scenario 2 and a range of

only 38 km for Scenario 3. Reducing the speed to 80km/h would drive the Leaf 77 km, 72 km and 53 km for Scenario 1, 2 and 3, respectively. The drivable range under a speed of 50 km/h for the Leaf would be 104 km (Scenario 1), 91 km (Scenario 2) and 71 km (Scenario 3).

Table 7-5 shows the simulation of an i-MiEV, travelling at speeds of 110 km/h, 80 km/h and 50 km/h. The higher speed of 110 km/h would reduce the range to 57 km under Scenario 1, a range of 55 km in Scenario 2 and a range of only 40 km for Scenario 3. Simulating the range for 80 km/h the model suggests a range of 83 km, 76 km and 56 km for Scenarios 1, 2 and 3, respectively. Finally, the speed reduction to 50 km/h would drive the i-MiEV to 115km (Scenario 1), 96 km (Scenario 2) and 75km (Scenario 3).

Under all three scenarios, with increased vehicle speed, mass, increased cross-frontal area, extra auxiliary loads and headwind, the energy consumption consistently increases and hence the range significantly reduces. Based on the model and calculations it can be assumed that with further increase of loads, in particular speed and headwind the range will further reduce. This assumption is supported by the trend of declining range on the curves for Scenarios 1, 2, and 3 in Figure 7-3A and Figure 7-3B.

A

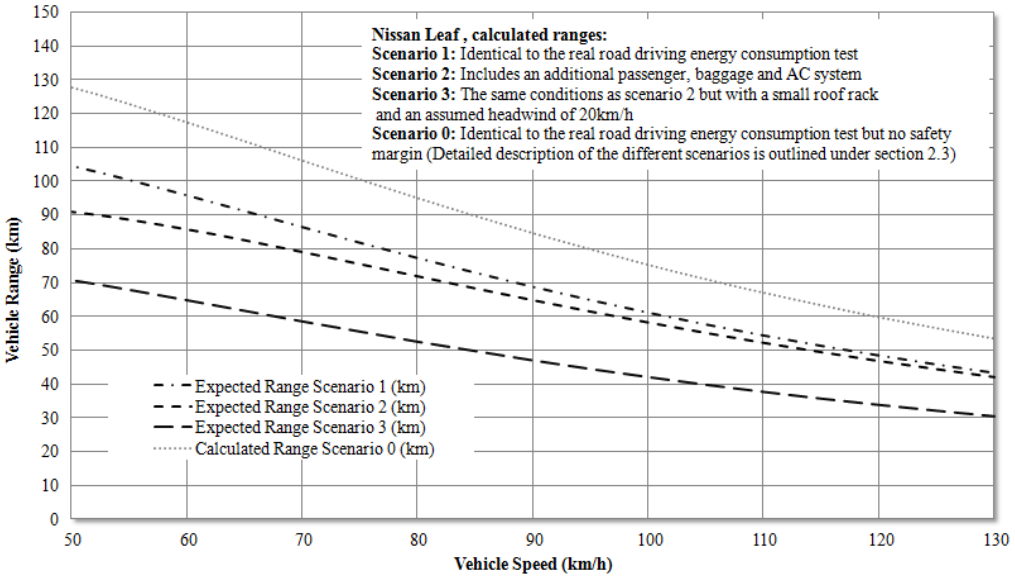

B

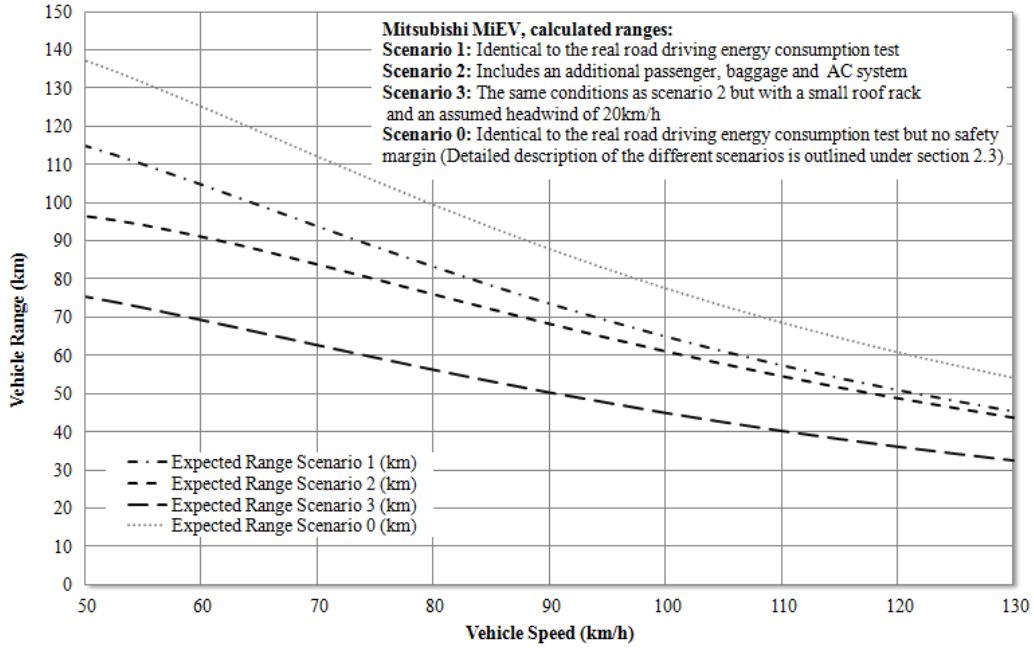

Figure 7-3 Leaf (A) and MiEV's (B) significant decline in drivable range due to an assumed battery discharge safety margin of 2 kWh, increased speed, mass and loads

Table 7-4 Leaf's drivable range (km) under different loads and travelling speeds including a discharge safety margin

Speed (km/h)	*Scenario 0 (km)*	*Scenario 1 (km)*	*Scenario 2 (km)*	*Scenario 3 (km)*
50	128	104	91	71
80	95	77	72	53
110	67	54	52	38

Table 7-5 i-MiEV drivable range (km) under different loads and travelling speeds including a discharge safety margin

Speed (km/h)	*Scenario 0 (km)*	*Scenario 1 (km)*	*Scenario 2 (km)*	*Scenario 3 (km)*
50	137	115	96	75
80	100	83	76	56
110	69	57	55	40

7.4 Comparisons with EV Manufacturers' Range Data

Nissan publishes a drivable range of up to 199 km [222] on an NEDC test driving cycle. Based on the published energy consumption data of 150 Wh/km it would be difficult to

achieve this range on an NEDC driving pattern. Even assuming that all of the 24 kWh battery can be used the maximum drivable range would be 160km. In contrast, the predicted real road-range simulation in under Scenario 3 was just 38 km or only 19% of the published range. A similar much smaller range was observed on the i-MiEV with its 16 kWh battery. Mitsubishi states an energy consumption of 125 Wh/km and a range of 150 km [196]. To achieve such a range a battery with an accessible energy capacity of 20 kWh would be required.

It is worth emphasising that Scenario 3 is not a worst-case scenario. In some situations the safety margin would be required to be larger than just 2 kWh as assumed in the experiment. As a consequence the range would reduce further. Furthermore, there will be situations where there are speed limits higher than 110 km/h, headwinds stronger than 20 km/h, roof racks that reduce aerodynamic efficiency (C_d), changes in rolling resistance (C_{rr}), higher air conditioning or heating demand, climate impacts on traction batteries [226], battery conditioning issues, uphill driving slopes and vehicles loaded to their full capacity. Highway driving under these kinds of conditions would increase the Leaf's and i-MiEV's energy consumption and hence reduce the drivable range even further.

This research showed that real-road driving energy consumptions can be well predicted by a vehicle mathematical model. It was possible to predict the Leaf's and i-MiEV's drivable range under various loads. The simulation showed how significantly energy consumption increases and range reduces under relative high speeds, strong headwinds, increased vehicle weight, auxiliary loads and cross sectional area, the absence of energy recovery by an RBS, limited charge level from fast-DC charging, and limited access to the stored energy due to the requirement for a discharge safety margin. The experiments have shown significant differences between manufacturers published range and simulated scenarios based on data from real-road driving.

The simulations focused on the range impact of driving speeds and increased loads. Further studies could include sensitivity analyses of the different parameters in the model.

Fast-DC charging technology is a potential solution to be implemented along a highway to drive an electric vehicle over a long distance and is also a feasible option for frequently driven cars in cities. This research, however, found that inherent battery aging, discharge safety margins and fast-DC charging to a SoC of just 80% leads to inefficient battery capacity utilisation and a significant reduction in the vehicle's drivable range. These findings are very

important for EV drivers and the efficient design of an electric highway between remote towns or an extended fast-DC charging network in cities. For them it is critical to understand how EV energy and recharging demands change under different driving patterns.

Based on the findings from this study, it appears that manufacturers overestimate their vehicles' range. Since EV drivers have some options to reduce EV energy consumption, e.g. reduce speed or shed unnecessary loads, EV manufacturers should communicate and increase EV drivers' and EV infrastructure planners' awareness. Too many fast-DC stations along a highway increases costs and might be considered financially inefficient. In contrast, by designing an electric highway according to manufacturers' published ranges and without driver awareness some EVs are likely to get stranded in rural areas. As a consequence, EV technology might suffer a poor reputation and negatively influence EV sales uptake.

7.5 Conclusions

Drivable range and recharge time are among the biggest hurdles for EV adoption. Little is known about the impact from the combination of fast-DC charging, increased aerodynamic loads, auxiliary loads, reduced battery capacity and high speed driving. In this study we aimed to investigate this impact on EV drivable range for two commercial EVs, a Nissan Leaf and a Mitsubishi i-MiEV. A marked difference between the nominal battery capacity and the usable capacity was observed on both vehicles, reducing their drivable range significantly. A vehicle mathematical model was developed to simulate vehicle traction power and energy demand, which showed good agreement with published energy consumption data from NEDC tests. The results show that driving at higher speeds, with headwinds or increased vehicle cross sectional area (roof racks) and large auxiliary loads reduce an EV's efficiency significantly and hence significantly reduce its drivable range. The key finding from this chapter is that the energy consumption and drivable range figures published by EV manufacturers deviate significantly compared to real road EV driving scenarios and energy demands. EV infrastructure planners should be made aware of the discrepancies to prevent inefficient implementation of charging infrastructures.

Chapter 8

Summary and Outlook

8.1 Main Findings

A shift from the current transportation paradigm is required in order to address increased air pollution with its negative impact on society, our dependency on fossil fuels and their inherent economic vulnerability. EVs have the potential to improve these issues and improve the quality of human life, in particular in large cities. EVs also have the potential to be driven emission free when charged from renewable energy sources. Although the overall efficiency, energy storage capacity, recharge technologies and driving ranges for EVs have increased over the last decade, EVs and recharge technologies require improvements in these areas to overcome the barriers to market growth of the EV sector.

The aim of this thesis was to investigate the potential for improvements in vehicle energy efficiency and recharging as ways to increase the range of EV's and make longer trips possible. Despite the absence of technical and intellectual support from a mainstream automotive manufacturer, it was possible for the candidate and supervisors to address questions in regards to EV recharge technologies, in particular the impact on EVs from fast-DC charging. Further, it was possible to identify inefficiencies and suggest improvements to EV electric highway planners, EV users and even the automotive industry in Europe.

Chapter 3 describes an RBS performance test that used multiple drive-cycle speed profiles and various RBS settings to compare energy recovery performance for a broad range of driving styles. The results show that due to reduced energy consumption, the RBS increased the driving range by 12-22%, depending on RBS settings and the drive-cycle settings on the dynamometer. The results further showed that driving an EV with a RBS uses the friction brakes more efficiently, which will reduce brake pad wear. This has the potential to improve air quality due to reduced brake pad dust as well as to reduce the maintenance costs of the vehicle. The findings were significant since they showed that friction brake time of use, a

parameter neglected in other RBS testing, plays an important part in the efficient operation of an EV.

Chapter 4 describes how an EV converted Ford Focus air conditioning (AC) system was modified, operated solely from kinetic energy and temperature, humidity, and compressor duty cycle data were logged and analysed. The results show that test drives with the Ford Focus with standard AC operation increased the energy consumption by 11.6% compared to the AC off, yet when the vehicle AC system was synchronised with the drive train the energy consumption increased by only 5.8% compared to the AC off, equivalent to an energy saving of 8.1Wh km-1. It was found that in vehicles with an interconnected automatic AC and engine management system data-bus, this energy consumption improvement strategy could be implemented with a software update only.

Chapter 5 investigated whether loading an EV motor and motor controller in the optimal region of the car's efficiency map can improve overall efficiency in a stop-and-go scenario. A Nissan LEAF was instrumented and under real road conditions, the vehicle was subjected to a series of various acceleration/deceleration rates. The experiments showed that increasing the load of the motor and motor controller to its efficient region improves efficiency and energy consumption. However, the degree of improvement heavily depends on the driving pattern. For this particular study, the data suggested strong but not full acceleration and soft decelerations of the EV to be the most efficient stop-and-go driving technique.

Fast-DC charging is a relatively new technology. The study in Chapter 6 tried to discover if it is a feasible option to recharge an EV solely from a fast-DC charge station. It investigated the impact of fast-DC charging on battery cell balance, charge capacity and range for an EV travelling long distances on an "electric-highway". A Mitsubishi MiEV and a Nissan Leaf were exposed to a series of discharge and fast-DC charge cycles to measure cell balance and charge capacity. The vehicles' battery management systems were capable of successfully balancing individual cells and hence maintaining the batteries' charge capacity. Although fast-DC charge levels and discharge safety margins significantly reduced the vehicles' charge capacity and range compared to the car manufacturer, these values remained stable for the test period. In regards to cell balance and charge capacity, our research suggests that fast-DC charging technology is a feasible option for EVs to travel large distances in a day.

Chapter 6 outlined a major drawback from fast-DC charging as being the limited charge capacity of the battery of just 80%. The study in Chapter 7 investigated the impact on drivable

range from the combination of the 80% charge capacity from fast-DC charging with driving EVs at highway speeds, using large auxiliary loads such as heating or AC and discharge safety margins. In this study, the candidate investigated these parameters and their impact on energy consumption and the drivable range of EVs. The results show a significantly reduced range under conditions relevant for highway driving and a significant deviation from driving ranges published by EV manufacturers. The findings from the mathematical models in chapter 3 and 7 are easily transferable to other vehicles and can become predictive for any given vehicle and/or road condition simply by recalibrating the model. Although the results and outcome from the EVs under test are vehicle specific, similar trends for the performance of the RBS, motor and controller efficiencies, energy storage and range can be expected for other EVs on the market.

The results and outcomes of this project are critical for the efficient design and implementation of so called 'Electric Highways'. To prevent stranded cars and a possible negative perception of EVs, drivers and charging infrastructure planners need be aware of how EV energy and recharging demands can significantly change under different loads and driving patterns.

8.2 Recommendations for Future Work

Chapters 3-5 identified energy inefficiencies of EVs and suggested solutions of how to improve efficiency, reduce energy consumption and increase EV range. Chapter 3 investigated RBS systems and discussed its performance and benefits. Although an RBS improves energy consumption and range, market barriers remain due to low electricity prices not being enough of a financial incentive for consumers to purchase and drive an EV. However, low electricity prices combined with the reduced maintenance cost of friction brakes (by driving vehicles with RBS systems) might become a stronger financial incentive for consumers to select an EV. Further, detailed vehicle operating costs studies [125] on friction brake savings due to an RBS on an EV would quantify cost savings on driving an EV compared to an ICE car. The detailed study should also include an in-depth long-term life cycle analysis including the potential major ICE vehicle maintenance and repair costs. These should include replacement of parts, such as timing belts, radiators, water pumps etc. The cost

analysis should provide vehicle operators with an indication on the real costs of running an ICE vehicle. Such a study would build a level playing field and potentially would assess whether EVs can financially compete with ICE cars. The outcome of the suggested study will benefit fleet operators, such as courier firms or government vehicle fleets. In the long term the study would potentiality contribute to a faster market uptake of EVs.

Chapters 4 and 5 discuss strategies on how to reduce energy consumptions and hence increase drivable range. It can be argued that the marginal increased range from driving these strategies could be achieved by simply installing a larger vehicle traction battery. The disadvantages of larger batteries are higher cost and added vehicle weight. It also needs to be emphasized how the suggested strategies will save energy, particularly if applied in a large fleet of EVs. The studies were limited to a single individual vehicle driving on preselected test routes. Since both energy-reducing strategies strongly depend on driving pattern, further investigations on the impact on potentially available traffic light information via V2I communication (vehicle to infrastructure) to the vehicle or automated driving systems could be conducted. A further study could then include implementing these optimized strategies to a large fleet and driving these cars in many different areas and traffic patterns. Such a study would then provide more detailed information on the potential large-scale energy savings.

The studies in Chapters 6 and 7 outline benefits and issues from EV fast-DC charging. The experiments show fast-DC charging is a feasible option. EV fast-DC charge stations have the potential to overcome range anxiety and to contribute to a faster EV market uptake. The study also revealed some issues for long-distance, high-speed travelling in an EV. These issues were in the focus of Chapter 7. Investigations on long-range, high-speed EV driving show that the energy consumption and drivable range data published by EV manufacturers deviate significantly compared to real road EV driving. Consequently, EV drivers might underestimate energy consumption and potentially become stranded before reaching the planned destination. To prevent negative EV reputation and the potential hindering of EV market uptake, EV drivers and EV infrastructure planners should be made aware of significant higher energy consumption and reduced range under high-speed driving.

References

1. American-Lung-Association, *American Lung Association's recent "State of the Air 2017"*. 2017.
2. Monica Crippa, G.J.-M., Frank Dentener, Diego Guizzardi, Katerina Sindelarova, Marilena Muntean, Rita Van Dingenen, and Claire Granier, *Forty years of improvements in European air quality: regional policy-industry interactions with global impacts.* Atmos. Chem. Phys, 2016. **16**: p. 3825–3841.
3. Wards-Auto. *World Vehicle Population Tops 1 Billion Units*. 2011 [cited 2014 19.04.2014]; Available from: http://wardsauto.com/ar/world_vehicle_population_110815.
4. Michal Krzyzanowski, B.K.-D.a.J.S., *Health effects of transport-related air pollution*. 2005: World Health Organization.
5. E., M., *Health effects of particulate air pollution: time for reassessment?* Environ Health Perspect, 1995. **103**(5): p. 472–480.
6. Ehsani, M., Y. Gao, and A. Emadi, *Modern Electric, Hybrid Electric, and Fuel Cell Vehicles : Fundamentals, Theory, and Design, Second Edition*. 2009, Taylor and Francis: Hoboken.
7. Brinkhoff, T. *Major Agglomerations of the World*. 2014 [cited 2014 19-04-14]; Available from: http://www.citypopulation.de/world/Agglomerations.html.
8. Anne Tibbett, N.C., Merched Azzi, John Carras, *The Impact Of Ethanol Blended Fuel On Vehicle Emissions Of Volatile Organic Compounds* D.o.t. Environment, Editor. 2008.
9. Environmental-Protection-Agency, *Automobile Emissions: An Overview*, U.S.E.P. Agency, Editor. August, 1994.
10. Hime, N., C. Cowie, and G. Marks, *Review of the health impacts of emission sources, types and levels of particulate matter air pollution in ambient air in NSW*. 2015, Woolcock Institute of Medical Research, Centre for Air Quality and Health Research and Evaluation (CAR).
11. Organisation, W.W.H., *Health Aspects of Air Pollution with Particulate Matter, Ozone and Nitrogen Dioxide* 2003.
12. Tom Beer, J.C., David Worth, Nick Coplin, *Evaluating the Health Impacts of EthanolBlend Petrol*, D.o.t. Environment, Editor. 2008.
13. Yim, S.H.L. and S.R.H. Barrett, *Public Health Impacts of Combustion Emissions in the United Kingdom.* Environmental Science & Technology, 2012. **46**(8): p. 4291-4296.
14. Scottish-Government, *Reported road casualties in Great Britain: 2011*, D.f. Transport, Editor. 2011: Annual report London, UK: 2012.
15. Pearson, J.F.B.S., C.B.S. Bachireddy, S.M.S. Shyamprasad, A.B.M.D. Goldfine, and J.S.P.H.D. Brownstein, *Association Between Fine Particulate Matter and Diabetes Prevalence in the U.S.* Diabetes Care, 2010. **33**(10): p. 2196-201.

16. Brook, R.D., et al., *Long-Term Fine Particulate Matter Exposure and Mortality From Diabetes in Canada.* Diabetes Care, 2013. **36**(10): p. 3313-3320.
17. Potterton, P., *Health impacts of transport emissions in Australia: Economic costs*. 2005, Bureau of Transport and Regional Economics.
18. Simpson, R., Williams, G., Petroeschevsky, A., Best, T., Morgan, G., Denison, L., Hinwood, A., Neville, G. and Neller, A. , *The short-term effects of air pollution on daily mortality in four Australian cities.* Australian and New Zealand Journal of Public Health, 2005(29): p. 205–212.
19. CSIRO-Orbital, *2009 Evaluating The Health Impacts Of Ethanol Blend Petrol: The Study* 2009.
20. Beer, T., et al., *The Health Impacts of Ethanol Blend Petrol*. Energies, 2011. **4**(2): p. 352-367.
21. Umwelthilfe, D. *Ultrafeine Feinstaubpartikel: Auch neue Benziner brauchen strenge Grenzwerte*. 2011 [cited 2014 21-04]; Available from: http://www.duh.de/uploads/media/Benzinmotoren-Partikel_2011-07-07.pdf.
22. Agency, I.E., *CO2 emissions from fuel combustion*. 2016, International Energy Agency.
23. Kerschner, C., C. Prell, K. Feng, and K. Hubacek, *Economic vulnerability to Peak Oil.* Global Environmental Change, 2013. **23**(6): p. 1424-1433.
24. Toyota-Motor-Corporation. *The Hybrid that Started it All*. 2008 [cited 2017 19-08-17]; Available from: http://www.toyota-global.com/company/toyota_traditions/innovation/nov2008_feb2009_1.html.
25. account, I.E.C.S.i.C., *Electric vehicle conductive charging system - Part 1: General requirements*. 2017.
26. Motors, T. *Road Trips Made Easy*. 2014 [cited 2014 12-09-14]; Available from: http://www.teslamotors.com/supercharger.
27. Electric-Vehicle-News. *German OEMs Plan 350 kW Fast Charging Network Across Europe*. 2016 [cited 2017 21-03]; Available from: http://www.electric-vehiclenews.com/2016/11/german-oems-plan-high-power-charging.html.
28. Fernández, R.Á., F.B. Cilleruelo, and I.V. Martínez, *A new approach to battery powered electric vehicles: A hydrogen fuel-cell-based range extender system.* International Journal of Hydrogen Energy, 2016. **41**(8): p. 4808-4819.
29. Stan, C., *Alternative Antriebe für Automobile*. 2012: Springer.
30. Tehrani, M.G., J. Kelkka, J. Sopanen, A. Mikkola, and K. Kerkkänen. *Transmission configuration effect on total efficiency of Electric Vehicle powertrain*. in *2014 16th European Conference on Power Electronics and Applications*. 2014.
31. Beretta, J., *Automotive Electricity : Electric Drive*. 2013, Wiley: Hoboken.
32. Burress, T., *Benchmarking State-of-the-Art Technologies*. 2013, Oak Ridge National Laboratory.
33. Husain, I., *Electric And Hybrid Vehicles Design Fundamentals*. 2003: CRC Press.
34. Nissan. *How Far Do You Drive?* 2017 [cited 2017 21-03]; Available from: https://www.nissanusa.com/electric-cars/leaf/charging-range/range/.
35. Terrence Mader, T.B., *Western Australian Electric Vehicle Trial*. 2012.
36. Rauh, N., T. Franke, and J.F. Krems, *Understanding the Impact of Electric Vehicle Driving Experience on Range Anxiety.* Human Factors, 2015. **57**(1): p. 177-187.

37. The Renewable Energy Vehicle (REV) Project. *Fast-charging network trial* 2012 [cited 2012 19 November]; Available from: http://therevproject.com/trials/charging-trial.php.
38. RAC. *The RAC Electric Highway*. 2017 [cited 2017 30-03]; Available from: http://electrichighway.rac.com.au/.
39. The Renewable Energy Vehicle (REV) Project. *Performance*. 2012 [cited 2013 26 August]; Available from: http://therevproject.com/vehicles/performance.php.
40. Walsh, C. and C. Bingham, *Electric drive vehicle deployment in the UK*, in *Hybrid and Fuel Cell Electric Vehicle Symposium*. 2009: Stavanger, Norway.
41. Green Car Congress. *Volvo Car Corporation developing flywheel kinetic energy recovery system; considering broad application*. 2011 [cited 2013 26 August]; Available from: http://www.greencarcongress.com/2011/05/vcc-20110526.html.
42. Wicks, F., J. Maleszweski, C. Wright, and J. Zarybnicky, *Analysis of compressed air regenerative braking and a thermally enhanced option*, in *37th Intersociety Energy Conversion Engineering Conference*. 2002: Washington DC, USA. p. 406-411.
43. Rayess, N. and D. Kleinke, *Elastic regenerative braking system based on superelastic shape memory material: a research focussed ME Capstone design project*, in *American Society for Engineering Education (ASEE) North Central Section Conference*. 2009: Allendale, Michigan, USA.
44. Naseri, F., E. Farjah, and T. Ghanbari, *An Efficient Regenerative Braking System Based on Battery/Supercapacitor for Electric, Hybrid and Plug-In Hybrid Electric Vehicles with BLDC Motor.* IEEE Transactions on Vehicular Technology, 2016. **PP**(99): p. 1-1.
45. Yoong, M.K., Y.H. Gan, G.D. Gan, C.K. Leong, Z.Y. Phuan, B.K. Cheah, and K.W. Chew. *Studies of regenerative braking in electric vehicle*. in *2010 IEEE Conference on Sustainable Utilization and Development in Engineering and Technology*. 2010.
46. Bo, Z., Z. Nong, W. Paul, Z. Xingxing, Z. Wenzhang, W. Yueyuan, and K. Nanji, *Gear shift schedule design for multi-speed pure electric vehicles.* Proceedings of the Institution of Mechanical Engineers, Part D: Journal of Automobile Engineering, 2015. **229**(1): p. 70-82.
47. Maheshwari, P., Y. Tambawala, H.S.V.S.K. Nunna, and S. Doolla. *A review on plug-in electric vehicles charging: Standards and impact on distribution system*. in *2014 IEEE International Conference on Power Electronics, Drives and Energy Systems (PEDES)*. 2014.
48. Montfort, K.v., M. Kooi, G.v.d. Poel, and R.v.d. Hoed. *Which factors influence the success of public charging stations of electric vehicles?* in *6th Hybrid and Electric Vehicles Conference (HEVC 2016)*. 2016.
49. Zhao, T., Y. Li, X. Pan, P. Wang, and J. Zhang, *Real-time Optimal Energy and Reserve Management of Electric Vehicle Fast Charging Station: Hierarchical Game Approach.* IEEE Transactions on Smart Grid, 2017. **PP**(99): p. 1-1.
50. Chen, H., Z. Su, Y. Hui, and H. Hui. *Optimal Approach to Provide Electric Vehicles with Charging Service by Using Mobile Charging Stations in Heterogeneous Networks*. in *2016 IEEE 84th Vehicular Technology Conference (VTC-Fall)*. 2016.
51. Zare, S., P. Najafi, H. Mansuri, and H. Taghiya. *New services of plug-in electric vehicles charging stations*. in *CIRED Workshop 2016*. 2016.

52. Yilmaz, M. and P.T. Krein, *Review of Battery Charger Topologies, Charging Power Levels, and Infrastructure for Plug-In Electric and Hybrid Vehicles.* IEEE Transactions on Power Electronics, 2013. **28**(5): p. 2151-2169.
53. Hong, J., S. Park, and N. Chang. *Accurate remaining range estimation for Electric vehicles*. in *2016 21st Asia and South Pacific Design Automation Conference (ASP-DAC)*. 2016.
54. Hayes, J.G., R.P.R.d. Oliveira, S. Vaughan, and M.G. Egan. *Simplified electric vehicle power train models and range estimation*. in *2011 IEEE Vehicle Power and Propulsion Conference*. 2011.
55. Fechtner, H., T. Teschner, and B. Schmuelling. *Range prediction for electric vehicles: Real-time payload detection by tire pressure monitoring*. in *2015 IEEE Intelligent Vehicles Symposium (IV)*. 2015.
56. R.Farrington and J. Rugh, *Impact of Vehicle Air-Conditioning on Fuel Economy, Tailpipe Emissions, and Electric Vehicle Range*, in *Earth Technologies Forum*. 2000: Washington, D.C.
57. Gass, V., J. Schmidt, and E. Schmid. *Analysis of alternative policy instruments to promote electric vehicles in Austria*. in *World Renewable Energy Congress 2011*. 2011. Linkoping, Sweden.
58. Usher, J., C. Horgan, C. Dunstan, and P. Paevere, *Plugging in: a technical and institutional assessment of electric vehicles and the grid in Australia*, in *Sydney, Australia*. 2011, CSIRO and the Institute for Sustainable Futures, UTS. p. 92.
59. Morrow, K., D. Karner, and J. Francfort, *Plug-in hybrid electric vehicle charging infrastructure review - final report*, in *U.S. Department of Energy vehicle technologies program - advanced vehicle testing activity*. 2008, U.S. Department of Energy: Idaho, USA.
60. Dunstan, C., J. Usher, K. Ross, L. Christie, and P. Paevere, *Supporting electric vehicle adoption in Australia: barriers and policy solutions*. 2011, CSIRO and the Institute for Sustainable Futures, UTS: Sydney, Australia. p. 156.
61. Mullan, J., D. Harries, T. Bräunl, and S. Whitely, *Modelling the impacts of electric vehicle recharging on the Western Australian electricity supply system.* Energy Policy, 2011. **39**(7): p. 4349-4359.
62. Mullan, J., D. Harries, T. Bräunl, and S. Whitely, *The technical, economic and commercial viability of the vehicle-to-grid concept.* Energy Policy, 2012. **48**(Special section: frontiers of sustainability): p. 394-406.
63. McHenry, M.P., M. Schultz, and K. O'Mara, *Wholesale electricity markets and electricity networks: balancing supply reliability, technical governance, and market trading in the context of Western Australian energy disaggregation and marketisation*, in *Advances in Energy Research, Volume 5*, A.R. McAdams, Editor. 2011, Nova Science Publishers: Hauppauge, New York.
64. McHenry, M.P., *Technical and governance considerations for advanced metering infrastructure/smart meters: technology, security, uncertainty, costs, benefits, and risks.* Energy Policy, 2013. **59**: p. 834-842.
65. Bräunl, T., *Synthetic engine noise generation for improving electric vehicle safety.* International Journal of Vehicle Safety, 2012. **6**(1): p. 1-8.
66. Lim, C.S., R. Mamat, and T. Bräunl, *Impact of ambulance dispatch policies on performance of emergency medical services.* IEEE Transactions on Intelligent Transportation Systems, 2011. **12**(2): p. 624-632.

67. Wäger, G., M.P. McHenry, J. Whale, and T. Bräunl, *Testing energy efficiency and driving range of electric vehicles in relation to gear selection.* Renewable Energy, 2014. **62**: p. 303-312.
68. Foley, A., B. Tyther, C. P, and B. Ó Gallachóir, *Impacts of electric vehicle charging under electricity market operations.* Applied Energy, 2013. **101**: p. 93-102.
69. Milan, D., *Know all about hybrid vehicles*. 2012, Delhi, India: English Press.
70. U.S. Department of Energy. *One million electric vehicles by 2015: February 2011 status report* 2011 [cited 2012 29 January]; Available from: http://www1.eere.energy.gov/vehiclesandfuels/pdfs/1_million_electric_vehicles_rpt.pdf.
71. Lund, H. and W. Kempton, *Integration of renewable energy into the transport and electricity sectors through V2G.* Energy Policy, 2008. **36**: p. 3578-3587.
72. Saarenpää, J., M. Kolehmainen, and H. Niska, *Geodemographic analysis and estimation of early plug-in hybrid electric vehicle adoption.* Applied Energy, 2013. **107**: p. 456-464.
73. Doucette, R.T. and M.D. McCulloch, *Modeling the prospects of plug-in hybrid electric vehicles to reduce CO_2 emissions.* Applied Energy, 2011. **88**: p. 2315-2323.
74. Kelly, J.C., J.S. MacDonald, and G.A. Keoleian, *Time-dependent plug-in hybrid electric vehicle charging based on national driving patterns and demographics.* Applied Energy, 2012. **94**: p. 395-405.
75. Katrašnik, T., *Impact of vehicle propulsion electrification on well-to-wheel CO_2 emissions of a medium duty truck.* Applied Energy, 2013. **108**: p. 236-247.
76. Tie, S.F. and C.W. Tan, *A review of energy sources and energy management system in electric vehicles.* Renewable and Sustainable Energy Reviews, 2013. **20**: p. 82-102.
77. Boretti, A., *Comparison of fuel economies of high efficiency diesel and hydrogen engines powering a compact car with a flywheel based kinetic energy recovery systems.* International Journal of Hydrogen Energy, 2010. **35**: p. 8417-8424.
78. Marco, J. and N.D. Vaughan, *A classical control approach to the power management of al all-electric hybrid vehicle.* International Journal of Vehicle Systems Modelling and Testing, 2009. **4**(1-2): p. 55-78.
79. Formula1.com. *Kinetic energy recovery systems (KERS)*. 2013 [cited 2013 2 September]; Available from: http://www.formula1.com/inside_f1/understanding_the_sport/8763.html.
80. Boretti, A.A., *Improvements of vehicle fuel economy using mechanical regenerative braking.* International Journal of Vehicle Design, 2011. **55**(1): p. 35-48.
81. Midgley, W.J. and D. Cebon, *Comparison of regenerative braking technologies for heavy goods vehicles in urban environments.* Proceedings of the Institution of Mechanical Engineers, Part D: Journal of Automobile Engineering, 2012. **226**(7): p. 957-970.
82. Walsh, C. and C. Bingham. *Electric drive vehicle deployment in the UK*. 2009 [cited 2013 29 January]; Available from: http://www.cenex.co.uk/LinkClick.aspx?fileticket=VTnvk0HUiPE%3D&tab.
83. Bayar, K., R. Biasini, S. Onori, G. Rizzoni, and *Modelling and control of a brake system for an extended range electric vehicle equipped with axle motors.* International Journal of Vehicle Design, 2012. **58**(2/3/4): p. 399-426.

84. Zhou, Z., C. Mi, and G. Zhang, *Integrated control of electromechanical braking and regenerative braking in plug-in hybrid electric vehicles.* International Journal of Vehicle Design, 2012. **58**(2/3/4): p. 223-239.
85. Fuhs, A.E., *Hybrid vehicles and the future of personal transport*. 2009, Boca Raton, Florida, USA: CRC Press.
86. López-López, A.J., R.R. Pecharromán, A. Fernández-Cardador, and P. Cucala, *Assessment of energy-saving techniques in direct-current-electrified mass transit systems.* Transportation Research Part C, 2014. **38**: p. 85-100.
87. Lv, C., J. Zhang, Y. Li, and Y. Yuan, *Mode-switching-based active control of a powertrain system with non-linear backlash and flexibility for an electric vehicle during regenerative deceleration.* Proceedings of the Institution of Mechanical Engineers, Part D: Journal of Automobile Engineering, 2015. **229**(11): p. 1429-1442.
88. Lv, C., J. Zhang, and Y. Li, *Extended-Kalman-filter-based regenerative and friction blended braking control for electric vehicle equipped with axle motor considering damping and elastic properties of electric powertrain.* Vehicle System Dynamics, 2014. **52**(11): p. 1372-1388.
89. Zhang, J., D. Kong, L. Chen, and X. Chen, *Optimization of control strategy for regenerative braking of an electrified bus equipped with an anti-lock braking system.* Proceedings of the Institution of Mechanical Engineers, Part D: Journal of Automobile Engineering, 2012. **226**(4): p. 494-506.
90. Peng, D., Y. Zhang, C.-L. Yin, and J.-W. Zhang, *Combined control of a regenerative braking and antilock braking system for hybrid electric vehicles.* International Journal of Automotive Technology, 2008. **9**(6): p. 749-757.
91. Kumar, C.N. and S.C. Subramanian, *Cooperative control of regenerative braking and friction braking for a hybrid electric vehicle.* Proceedings of the Institution of Mechanical Engineers, Part D: Journal of Automobile Engineering, 2016. **230**(1): p. 103-116.
92. Thackeray, M.M., C. Wolverton, and E.D. Isaacs, *Electrical energy storage for transportation - approaching the limits of, and going beyond, lithium-ion batteries.* Energy & Environmental Science, 2012. **5**: p. 7854-7863.
93. Manzie, C., H. Watson, and S. Halgamuge, *Fuel economy improvements for urban driving: hybrid vs. intelligent vehicles.* Transportation Research Part C, 2007. **15**: p. 1-16.
94. Wäger, G., T. Bräunl, J. Whale, and M.P. McHenry, *Enhanced EV and ICE vehicle energy efficiency through drive cycle synchronisation of deferred auxiliary loads.* Journal International Journal of Electric and Hybrid Vehicles, 2014. **6**(3): p. 179-194.
95. Faris, W.F., H.A. Rakha, R.I. Kafafy, M. Idres, and S. Elmoselhy, *Vehicle fuel consumption and emission modelling: an in-depth literature review.* International Journal of Vehicle Systems Modelling and Testing, 2011. **6**(3/4): p. 318-392.
96. Zhang, J., X. Lu, J. Xue, and B. Li, *Regenerative braking system for series hybrid electric city bus.* The World Electric Vehicle Journal, 2008. **2**(4): p. 128-134.
97. Alvarez, R., A. López, and N. De la Torre, *Evaluating the effect of a driver's behaviour on the range of a battery electric vehicle.* Proceedings of the Institution of Mechanical Engineers, Part D: Journal of Automobile Engineering, 2015. **229**(10): p. 1379-1391.

98. Walker, A.M., M.U. Lamperty, and S. Wilkins, *Enhancing Road Vehicle Efficiency By Regenerative Braking*, in *Braking 2002. From The Driver To The Road. Papers From The International Conference*. 2002: Leeds , United Kingdom. p. p. 197-207.
99. Ye, M., Z.-F. Bai, and B.-G. Cao, *Energy recovery for battery electric vehicles.* Proceedings of the Institution of Mechanical Engineers, Part D: Journal of Automobile Engineering, 2008. **222**(10): p. 1827-1839.
100. Hayes, J.G. and K. Davis. *Simplified electric vehicle powertrain model for range and energy consumption based on EPA coast-down parameters and test validation by Argonne National Lab data on the Nissan Leaf*. in *Transportation Electrification Conference and Expo (ITEC), 2014 IEEE*. 2014.
101. Safoutin, M. *Modeling Methodology*. 2009 [cited 2017 15-05]; Available from: http://www.virtual-car.org/wheels/hybrid_road_load_model.html.
102. Lv, C., J. Zhang, Y. Li, and Y. Yuan, *Mechanism analysis and evaluation methodology of regenerative braking contribution to energy efficiency improvement of electrified vehicles.* Energy Conversion and Management, 2015. **92**: p. 469-482.
103. Zhang, J., C. Lv, J. Gou, and D. Kong, *Cooperative control of regenerative braking and hydraulic braking of an electrified passenger car.* Proceedings of the Institution of Mechanical Engineers, Part D: Journal of Automobile Engineering, 2012. **226**(10): p. 1289-1302.
104. Mitsubishi. *How to Drive the i for best Economy*. 2011 [cited 2017 14-05]; Available from: http://www.imiev411.com/c/how-drive-i-best-economy.
105. Yuasa, *Drive cycle development and realworld data in the United States*, in *Working Party on Pollution and Energy (GRPE), informal working group on Worldwide Harmonized Light Vehicles Test Procedure (WLTP)*. 2009, U.S. Environmental Protection Agency,: Geneva, Switzerland.
106. Delphi. *Passenger cars and light duty vehicles*. Worldwide emissions standards 2010 [cited 2012 18 November]; Available from: http://www.delphi.com/pdf/emissions/Delphi_PC.pdf.
107. National Instruments Corporation *NI USB-6008/6009 user guide and specifications*. 2012.
108. National-Instruments, *What Is LabVIEW*. 2017.
109. Mitsubishi-Motors. *MiEV Specifications*. n.d. [cited 2017 06.05.]; Available from: http://www.mitsubishi-motors.com/en/showroom/i-miev/specifications/.
110. Mitsubishi. *2012 Mitsubishi i-MiEV Product Brief*. n.d. [cited 2017 14.05]; Available from: http://manitobaev.ca/wp-content/uploads/2011/11/i-Miev-product-brief.pdf.
111. International-Regulation, *Uniform Provisions Concerning the Approval of: Vehicles of Categories M, N and O with Regards to Braking., Regulation No. 13-11*. 2017.
112. INL-Idaho-National_labarotory, *BEV Battery Testing Results*. 2014.
113. Yuasa, *Industrial Lithium-Ion Batteries LIM50E Module*. 2016.
114. United Nations. *Addendum 100: Regulation No. 101, revision 2. Uniform provisions concerning the approval of passenger cars powered by an internal combustion engine only, or powered by a hybrid electric power train with regard to the measurement of the emission of carbon dioxide and fuel consumption and/or the measurement of electric energy consumption and electric range, and of categories M1 and N1 vehicles powered by an electric power train only with regard to the measurement of electric energy consumption and electric range.* 2005 [cited 2012 2 February]; Available from: http://www.unece.org/fileadmin/DAM/trans/main/wp29/wp29regs/r101r2e.pdf.

115. U.S. Environmental Protection Agency. *Dynamometer drive schedules*. 2013 [cited 2013 26 August]; Available from: http://www.epa.gov/nvfel/testing/dynamometer.htm.
116. Australian Government. *Fuel consumption label*. 2008 [cited 2012 19 November]; Available from: http://www.environment.gov.au/settlements/transport/fuelguide/label.html.
117. Mitsubishi-Motors. *Plug in to the future today with i-MiEV*. n.d. [cited 2012 04.06.]; Available from: http://www.mitsubishi-motors.com.au/vehicles/cars/i-miev.
118. Mader, T. and T. Bräunl, *Western Australian electric vehicle trial 2010 - 2012, final report*. 2013, University of Western Australia: Perth, Western Australia.
119. Perricone, G., M. Alemani, I. Metinöz, V. Matějka, J. Wahlström, and U. Olofsson, *Towards the ranking of airborne particle emissions from car brakes – a system approach.* Proceedings of the Institution of Mechanical Engineers, Part D: Journal of Automobile Engineering, 2016.
120. Wahlström, J. and U. Olofsson, *A field study of airborne particle emissions from automotive disc brakes.* Proceedings of the Institution of Mechanical Engineers, Part D: Journal of Automobile Engineering, 2015. **229**(6): p. 747-757.
121. Adamiec, E., E. Jarosz-Krzeminska, and R. Wieszala, *Heavy metals from non-exhaust vehicle emissions in urban and motorway road dusts.* Environmental Monitoring and Assessment, 2016. **188**(6).
122. Gailis, M. and D. Berjoza, *On Prediction Of Motor Vehicle Brake Pad Wearout*, in *11th International Scientific Conference on Engineering for Rural Development, Vol 11*, L. Malinovska and V. Osadcuks, Editors. 2012. p. 349-354.
123. Bohoris, G.A., A. Desai, and D.J. Edge, *MODELING RAIL VEHICLE BRAKE PAD WEAROUT AND REPLACEMENT.* Quality and Reliability Engineering International, 1995. **11**(2): p. 129-137.
124. Duboka C., T.J., Arsenic Z., *Preventive Maintenance of Units Subject to Two Kinds of Wear Failure.* Yugoslav Journal of Operations Research, 1996. **6**: p. 85-100.
125. Australian-Transport-Assessment-and-Planning-(ATAP)-Guidelines, *PV2 Road Parameter Values*. 2016. https://atap.gov.au/parameter-values/road-transport/files/pv2_road_parameter_values.pdf
126. Auto-Service-Cost. *The Complete Brake Pads Cost Guide*. n.d. [cited 2016 12.1.]; Available from: https://autoservicecosts.com/brake-pad-replacement-cost/.
127. Opila, D.F., X. Wang, R. McGee, J.A. Cook, and J.W. Grizzle, *Performance comparison of hybrid vehicle energy management controllers on real-world drive cycle data*, in *2009 American Control Conference*. 2009: St Louis, USA.
128. Walsh, C., S. Carroll, A. Eastlake, and P. Blythe. *Electric vehicle driving style and duty variation performance study*. 2010 [cited 2013 29 January]; Available from: http://www.cenex.co.uk/LinkClick.aspx?fileticket=yALcN9hPtbo%3D&tabid=119&mid=695.
129. Mi, C., F.Z. Peng, K.J. Kelly, M. O'Keefe, and V. Hassani, *Topology, design, analysis and thermal management of power electronics for hybrid electric vehicle applications.* International Journal of Electric and Hybrid Vehicles, 2008. **1**(3): p. 276-294.
130. Bouvy, C., T. Lichius, and P. Jeck, *On the influence of the thermal demand on the overall efficiency of future drive train architectures for passenger cars.* International Journal of Electric and Hybrid Vehicles, 2011. **3**(3): p. 293-307.

131. Bennion, K. and M. Thornton, *Integrated vehicle thermal management for advanced vehicle propulsion technologies*, in *SAE 2010 World Congress* 2010: Detroit, Michigan, USA.
132. Hellgren, J. and J. Groot, *Energy storage system optimisation of a plug-in HEV.* International Journal of Electric and Hybrid Vehicles, 2008. **1**(3): p. 319-331.
133. Francfort, J.E., R.B. Carlson, M.L. Kirkpatrick, M.G. Shirk, J.G. Smart, and S.E. White, *Plug-in hybrid electric vehicle fuel use reporting methods and results* 2009, U.S. Department of Energy: Idaho Falls, USA.
134. Zhang, H., L. Dai, G. Xu, Y. Li, W. Chen, and W.-Q. Tao, *Studies of air-flow and temperature fields inside a passenger compartment for improving thermal comfort and saving energy. Part I: Test/numerical model and validation.* Applied Thermal Engineering, 2009. **29**(10): p. 2022-2027.
135. Nam, E., *Drive cycle development and realworld data in the United States*, in *Working Party on Pollution and Energy (GRPE), informal working group on Worldwide Harmonized Light Vehicles Test Procedure (WLTP)*. 2009, U.S. Environmental Protection Agency,: Geneva, Switzerland.
136. Zhang, H., E. Arens, C. Huizenga, and T. Han, *Thermal sensation and comfort models for non-uniform and transient environments: Part III: whole-body sensation and comfort*. 2009, Center for the Built Environment, UC Berkeley: Berkeley, California, USA.
137. ASHRAE, *Thermal environmental conditions for human occupancy*, in *ANSI/ASHRAE Standard 55-2013. (Supersedes ANSI/ASHRAE Standard 55-2010), includes ANSI/ASHRAE addenda listed in Appendix M*. 2013, ANSI/ASHRAE: Atlanta, Geogia, USA. p. 58.
138. International Organization for Standardization, *Ergonomics of the thermal environment -- analytical determination and interpretation of thermal comfort using calculation of the PMV and PPD indices and local thermal comfort criteria. Edition 3, Stage 90.93 (2004-04-08)*, in *ISO 7730:2005*. 2005, International Organization for Standardization,: Geneva, Switzerland. p. 52.
139. Wyon, D., S. Larsson, B. Forsgren, and I. Lundgren, *Standard procedures for assessing vehicle climate with a thermal manikin*, in *SAE technical paper 890049*. 1989, SAE International: Warrendale, Pennsylvania, USA.
140. Rugh, J.P. and D. Bharathan, *Predicting human thermal comfort in automobiles*, in *Vehicle Thermal Management Systems Conference and Exhibition*. 2005: Toronto, Canada.
141. Spanoudakis, P., N.C. Tsourveloudis, G. Koumartzakis, A. Krahtoudis, T. Karpouzis, and I. Tsinaris. *Evaluation of a 2-speed transmission on electric vehicle's energy consumption*. in *2014 IEEE International Electric Vehicle Conference (IEVC)*. 2014.
142. Everitt, M. *On-road testing of new multi-speed transmission for EVs from Oerlikon Graziano/Vocis begins; potential for increased range or reduced pack size*. 2011 [cited 2017 17.02.17]; Available from: http://www.greencarcongress.com/2011/09/vocis-20110905.html.
143. Mike Knowles, H.S., David Baglee, *The effect of driving style on electric vehicle performance, economy and perception.* International Journal of Electric and Hybrid Vehicles 2012 **Vol. 4** (No.3): p. pp. 228 - 247.
144. Wang, H., X. Zhang, and M. Ouyang, *Energy consumption of electric vehicles based on real-world driving patterns: A case study of Beijing*. Vol. 157. 2015.

145. Felipe, J., J.C. Amarillo, J.E. Naranjo, F. Serradilla, and A. Díaz. *Energy Consumption Estimation in Electric Vehicles Considering Driving Style*. in *2015 IEEE 18th International Conference on Intelligent Transportation Systems*. 2015.
146. Yi, Z. and P.H. Bauer, *Effects of environmental factors on electric vehicle energy consumption: a sensitivity analysis.* IET Electrical Systems in Transportation, 2017. **7**(1): p. 3-13.
147. Shankar, R. and J. Marco, *Method for estimating the energy consumption of electric vehicles and plug-in hybrid electric vehicles under real-world driving conditions.* IET Intelligent Transport Systems, 2013. **7**(1): p. 138-150.
148. Abousleiman, R. and O. Rawashdeh. *Energy consumption model of an electric vehicle*. in *2015 IEEE Transportation Electrification Conference and Expo (ITEC)*. 2015.
149. Nijmeijer, J.W.I.B.H., *Battery electric vehicle energy consumption modelling for range estimation.* Int. J. of Electric and Hybrid Vehicles, 2017. **Vol. 9**(2): p. 79-102.
150. Srinivasa Rao Gorantla, G.K.R., S. Siva Naga Raju, Ravindranath Tagore, Ravi Sankar Pentyala, Jayanth Kumar Reddy, *Design and implementation of automated regenerative braking of electric/hybrid electric vehicle.* International Journal of Electric and Hybrid Vehicles 2012 **Vol. 4** (No.1): p. pp. 1 - 11.
151. Barys Shyrokau, D.W., Dzmitry Savitski, Valentin Ivanov, *Vehicle dynamics control with energy recuperation based on control allocation for independent wheel motors and brake system.* International Journal of Powertrains 2013 **Vol. 2** (No.2/3): p. pp. 153 - 181.
152. Huangfu, M.Y.Y., *Power electronics design and application for the energy recovery controller of a battery electric vehicle.* Int. J. of Electric and Hybrid Vehicles 2014 **Vol.6** (No.4): p. pp.315 - 334.
153. Guo, J., *Development of regenerative braking for electric vehicles in China: a review.* Int. J. of Electric and Hybrid Vehicles, 2015. **Vol.7**(2): p. 120-138.
154. Stratton;, A.J. and J.B. Heywood, *Impact of regenerative braking on hybrid vehicle fuel economy.* Int. J. of Vehicle Design, 2016. **Vol. 72,** (4): p. 285 - 304.
155. Montero, C., D. Marcos, C. Bordons, M. A. Ridao, E. Camacho, E. Gonzalez, and A. Oliva, *Modeling and torque control for a 4-wheel-drive electric vehicle*. Vol. 2015. 2015. 2650-2655.
156. Subathra, D.G.N.M.K.R.S.S.B., *Optimal fractional controller design methodology for electric drive train.* Int. J. of Electric and Hybrid Vehicles 2016 **Vol.8**(No.4): p. pp.335 - 350.
157. Minghui Hu, H.X., Chunyun Fu, *Study on EV transmission system parameter design based on vehicle dynamic performance.* International Journal of Electric and Hybrid Vehicles 2014 **Vol. 6** (No.2): p. pp. 133 - 151.
158. Küçükay, B.C.I.L.S.H.S.F., *Conceptual design of battery electric vehicle powertrains.* Conceptual design of battery electric vehicle powertrains, 2015. **Vol.67**(2): p. 137-156.
159. Shetty, P. and S. Dawnee. *Modeling and simulation of the complete electric power train of a hybrid electric vehicle*. in *2014 Annual International Conference on Emerging Research Areas: Magnetics, Machines and Drives (AICERA/iCMMD)*. 2014.

160. Yoon, T.F.R.J.E.G.J.M.H.-S., *Effect of an electric vehicle mode in a plug-in hybrid electric vehicle with a post-transmission electric motor.* Int. J. of Electric and Hybrid Vehicles, 2016. **Vol.8**(No.4): p. pp.302 - 320.
161. Seo, D.H. and J.N. Bae. *Development of simulation model of driving motor and controller for electric vehicle*. in *2014 International Conference on Information Science, Electronics and Electrical Engineering*. 2014.
162. Wojciech Gis, A., *Testing Of The Electric Vehicle In Driving Cycles.* Journal of KONES Powertrain and Transport,, 2012. **Vol. 19**(No. 4): p. 207-221.
163. Instrument, N., *LabVIEW System Design Software*. 2017.
164. Vaz, W.S., A.K. Nandi, and U.O. Koylu, *A Multiobjective Approach to Find Optimal Electric-Vehicle Acceleration: Simultaneous Minimization of Acceleration Duration and Energy Consumption.* IEEE Transactions on Vehicular Technology, 2016. **65**(6): p. 4633-4644.
165. Tseng, C.-M., W. Zhou, M.A. Hashmi, C.-K. Chau, S.G. Song, and E. Wilhelm, *Data extraction from electric vehicles through OBD and application of carbon footprint evaluation*, in *Proceedings of the Workshop on Electric Vehicle Systems, Data, and Applications*. 2016, ACM: Waterloo, Ontario, Canada. p. 1-6.
166. Electronics, E., *ELM327 OBD to RS232 Interpreter*. 2017.
167. Qstarts-International. *eXtreme 66-Channel Performance for fast acquisition and reacquisition* 2013 [cited 2017 25.02.]; Available from: http://www.qstarz.com/Products/GPS%20Products/BT-Q818X-F.htm.
168. Wang, X.H., Hongwen; Sun, Fengchun; Zhang, Jieli, *"Application Study on the Dynamic Programming Algorithm for Energy Management of Plug-in Hybrid Electric Vehicles.* Energies 8, 2015. **4**.
169. Jun, W., *Lithium-ion Battery Data Sheet, Battery Model: LIR14500*. 2006.
170. Matthew Ginsberg, D.P. *Traffic Light Data & Predictions* 2016 [cited 2017 25.02.]; Available from: https://connectedsignals.com/.
171. Manzetti, S. and F. Mariasiu, *Electric vehicle battery technologies: From present state to future systems.* Renewable and Sustainable Energy Reviews, 2015. **51**: p. 1004-1012.
172. Husain, I., *Electric and Hybrid Vehicles: Design Fundamentals*. 2003, CRC Press: Hoboken.
173. Energy, A.I.o. *Energy Value and Greenhouse Emission Factor of Selected Fuels*. [cited 2015 12-05]; Available from: http://www.aie.org.au/AIE/Energy_Info/Energy_Value.aspx.
174. Lukic, S., *Charging ahead.* Industrial Electronics Magazine, IEEE, 2008. **2**(4): p. 22-31.
175. Heyvaert, S., T. Coosemans;, J.V. Mierlo;, and C. Macharis, *Electric vehicle attitudes and purchase intention: a Flemish case study.* J. of Electric and Hybrid Vehicles, 2015. **Vol.7**(No.1): p. pp.83 - 100.
176. Lebeau, K., J.V. Mierlo;, P. Lebeau;, O. Mairesse;, and C. Macharis, *Consumer attitudes towards battery electric vehicles: a large-scale survey.* Int. J. of Electric and Hybrid Vehicles, 2013. **Vol.5**(No.1): p. pp.28 - 41.
177. Hussein, H.A.H. and I. Batarseh, *A Review of Charging Algorithms for Nickel and Lithium Battery Chargers.* Vehicular Technology, IEEE Transactions on, 2011. **60**(3): p. 830-838.
178. Motors, T. *Super Charger*. 2015 [cited 2015 10-03].

179. Moodie, C., *WA hoping to win race to build Australia's first electric car network*, in *ABC*. 2015.
180. Project, T.R. *Electric Highway* n.d. [cited 2015 10-03]; Available from: http://revproject.com/trials/highway.php.
181. Wiki, T.M. *Battery Pack*. 2014 [cited 2015 12.03]; Available from: http://www.teslamotors.wiki/wiki/Battery_Pack.
182. Stuart, T.A. and W. Zhu, *Modularized battery management for large lithium ion cells.* J. Power Sources, (1): p. 458-464.
183. Chatzakis, J., K. Kalaitzakis, N.C. Voulgaris, and S.N. Manias, *Designing a new generalized battery management system.* Industrial Electronics, IEEE Transactions on, 2003. **50**(5): p. 990-999.
184. Bowkett, M., K. Thanapalan, T. Stockley, M. Hathway, and J. Williams. *Design and implementation of an optimal battery management system for hybrid electric vehicles*. in *Automation and Computing (ICAC), 2013 19th International Conference on*. 2013.
185. Chol-Ho, K., K. Moon-Young, and M. Gun-Woo, *A Modularized Charge Equalizer Using a Battery Monitoring IC for Series-Connected Li-Ion Battery Strings in Electric Vehicles.* Power Electronics, IEEE Transactions on, 2013. **28**(8): p. 3779-3787.
186. Bonfiglio, C. and W. Roessler. *A cost optimized battery management system with active cell balancing for lithium ion battery stacks*. in *Vehicle Power and Propulsion Conference, 2009. VPPC '09. IEEE*. 2009.
187. Zhou, J. and X. Zhang, *Power battery SOC estimation with combination method based on UKF and open circuit voltage.* Int. J. of Electric and Hybrid Vehicles, 2015. **Vol.6**(No.3): p. pp.215 - 226.
188. Dilkes, R., *LiFePO4 BMS.* EV Power, 2014.
189. TYLER, M., *REV Performance Vehicle Instrumentation*, in *School of Electrical, Electronic and Computer Engineering, University of Western Australia*. 2011, University Of Western Australia.
190. University-of-Western-Australia. *The REV Project*. n.d. [cited 2015 20-03]; Available from: http://revproject.com/vehicles/performance.php.
191. Moore, S.a.S., P., *A Review of Cell Equalization Methods for Lithium Ion and Lithium Polymer Battery Systems.* SAE Technical Paper, 2001.
192. Boesenberg, U., M. Falk, C.G. Ryan, R. Kirkham, M. Menzel, J. Janek, M. Fröba, G. Falkenberg, and U.E.A. Fittschen, *Correlation between Chemical and Morphological Heterogeneities in LiNi0.5Mn1.5O4 Spinel Composite Electrodes for Lithium-Ion Batteries Determined by Micro-X-ray Fluorescence Analysis.* Chemistry of Materials, 2015. **27**(7): p. 2525-2531.
193. Nissan, *2013 Leaf Owners Manual*. 2013.
194. Mitsubishi, *Mitsubishi i-MiEV - Owner's Handbook*. 2015.
195. Nissan. *Nissan Leaf*. 2013; Available from: http://www.nissan.co.uk/content/dam/services/gb/brochure/New%20LEAF%20Tech%20Spec%20and%20Pricesv2.pdf.
196. Mitsubishi. *i-MiEV FEATURES*. 2015 [cited 2015 12-03]; Available from: http://www.mitsubishi-motors.com.au/vehicles/i-miev.
197. Mitsubishi. *MiEV Specifications*. n.d [cited 2015 13.03]; Available from: http://www.mitsubishi-motors.com/en/showroom/i-miev/specifications/.
198. SAE, *SAE Electric Vehicle and Plug in Hybrid Electric Vehicle Conductive Charge Coupler*. 2012.

199. CHAdeMO. *CHAdeMO fast Charging Stations in the Worls*. 2015 [cited 2015 04-05]; Available from: http://www.chademo.com/wp/.
200. John Allande, P.T., Eric Woodruff, *Nissan Leaf On Board Diagnostic Bluetooth Utility*. 2013.
201. Bart Benders, K.W., Christian Kolf, *Methodology of EV measurements*. 2013.
202. UN-Vehicle-Regulations, *Regulation No. 101*. 2013.
203. Gissing, J., S. Baltzer;, T. Lichius;, P. Jeck;, and L. Eckstein, *Economical approach for sizing a battery in plug-in hybrid electric vehicles considering statistical user behaviour and power demand for climatisation.* Int. J. of Electric and Hybrid Vehicles, 2015. **Vol. 7**(No.1,): p. pp.62 - 82.
204. Agency, I.E., *Global EV Outlook, Understanding the Electric Vehicle Landscape to 2020*. 2013.
205. Moore, T., *Tools and Strategies for Hybrid-Electric Drivesystem Optimization.* SAE Technical Paper 961660, 1996.
206. T.Yuksel and J. J.Michalek, *Effects of Regional Temperature on Electric Vehicle Efficiency, Range, and Emissions in the United States.* Environmental Science and Technology, 2015.
207. González Vayá, M., *Optimizing the electricity demand of electric vehicles: creating value through flexibility*, in *Department of Information Technology and Electrical Engineering* 2015, ETH-Zürich Zurich, Switzerland.
208. Yang, S.-N., W.-S. Cheng, Y.-C. Hsu, C.-H. Gan, and Y.-B. Lin, *Charge scheduling of electric vehicles in highways.* Mathematical and Computer Modelling, 2013. **57**(11–12): p. 2873-2882.
209. United-Nations. *Regulation No. 101* 2005 [cited 2015 21-06]; Available from: http://www.unece.org/fileadmin/DAM/trans/main/wp29/wp29regs/r101r2e.pdf.
210. Thomas Bütler, H.W., Material Science & Technolgy, *Energy consumption of battery electric vehicles (BEV)*. 2012.
211. Mike Duoba, E.R., Mark Meyer, *Advanced Powertrain Research Facility AVTA Nissan Leaf testing and analysis*. 2012.
212. Shankar, R. and J. Marco, *Method for estimating the energy consumption of electric vehicles and plug-in hybrid electric vehicles under real-world driving conditions.* Intelligent Transport Systems, IET, 2013. **7**(1): p. 138-150.
213. Qin, Y., Z. Bei, and M. Kezunovic. *Optimization of electric vehicle movement for efficient energy consumption*. in *North American Power Symposium (NAPS), 2014*. 2014.
214. Kubaisi, R., F. Gauterin, and M. Giessler. *A method to analyze driver influence on the energy consumption and power needs of electric vehicles*. in *Electric Vehicle Conference (IEVC), 2014 IEEE International*. 2014.
215. Birrell, S.A., A. McGordon, and P.A. Jennings. *Defining the accuracy of real-world range estimations of an electric vehicle*. in *Intelligent Transportation Systems (ITSC), 2014 IEEE 17th International Conference on*. 2014.
216. Vaz, W., A.K.R. Nandi, R.G. Landers, and U.O. Koylu, *Electric vehicle range prediction for constant speed trip using multi-objective optimization.* Journal of Power Sources, 2015. **275**(0): p. 435-446.
217. Kambly, K. and T.H. Bradley, *Geographical and temporal differences in electric vehicle range due to cabin conditioning energy consumption.* Journal of Power Sources, 2015. **275**(0): p. 468-475.

218. Enjian, Y., Zhiqiang, Y, Yuanyuan, S, & Ting, Z, *Comparison of Electric Vehicle's Energy Consumption Factors for Different Road Types.* Discrete Dynamics In Nature & Society, 2013: p. pp. 1-7.
219. Bingham, C., C. Walsh, and S. Carroll, *Impact of driving characteristics on electric vehicle energy consumption and range.* Intelligent Transport Systems, IET, 2012. **6**(1): p. 29-35.
220. Maia, R.S., M. Araujo, R. Nunes, U. *Electric vehicle simulator for energy consumption studies in electric mobility systems*. in *Integrated and Sustainable Transportation System (FISTS), 2011 IEEE Forum on*. 2011.
221. Frank, R.C., G. Schmitz, R. Engel, T. *A novel eco-driving application to reduce energy consumption of electric vehicles*. in *Connected Vehicles and Expo (ICCVE), 2013 International Conference on*. 2013.
222. Nissan, *Nissan Leaf*. 2013.
223. Larminie, J. and J. Lowry, *Electric Vehicle Technology Explained*. 2012, Wiley: Hoboken.
224. Roper, D., *Nissan Leaf Range Calculation*. 2012.
225. Ecos, *Passenger Tire Rolling Resistance Measurements From Ecos*. 2011.
226. Yuksel, T. and J.J. Michalek, *Effects of Regional Temperature on Electric Vehicle Efficiency, Range, and Emissions in the United States.* Environmental Science & Technology, 2015.